FRM II
Forschungs-Neutronenquelle
Heinz Maier-Leibnitz

MLZ
Heinz Maier-Leibnitz Zentrum

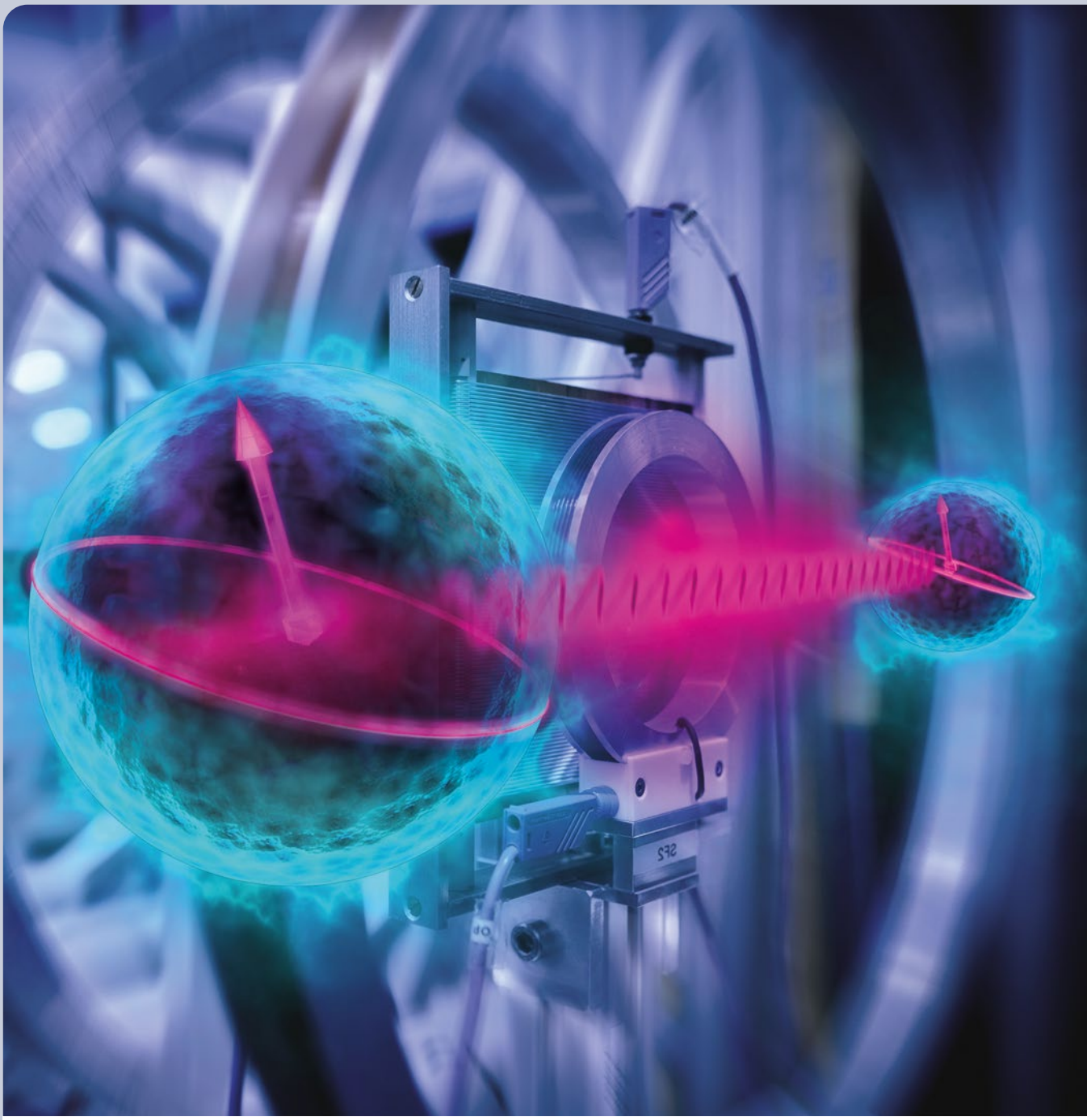

Annual Report 2024

MLZ is a cooperation between:

JÜLICH
Forschungszentrum

Helmholtz-Zentrum
hereon

Technical
University
of Munich

Bavarian State Ministry of Science and the Arts

SPONSORED BY THE

Federal Ministry of Education and Research

The Heinz Maier-Leibnitz Zentrum (MLZ):
The Heinz Maier-Leibnitz Zentrum is a leading centre for cutting-edge research with neutrons and positrons. Operating as a user facility, the MLZ offers a unique suite of high-performance neutron scattering instruments. This cooperation involves the Technische Universität München, the Forschungszentrum Jülich GmbH and the Helmholtz-Zentrum hereon GmbH. The MLZ is funded by the German Federal Ministry of Education and Research, together with the Bavarian State Ministry of Science and the Arts and the partners of the cooperation.

The Forschungs-Neutronenquelle Heinz-Maier-Leibnitz (FRM II):
The Forschungs-Neutronenquelle Heinz-Maier-Leibnitz provides neutron beams for the scientific experiments at the MLZ. The FRM II is operated by the Technische Universität München and is funded by the Bavarian State Ministry of Science and the Arts.

Joint Annual Report 2024

of the MLZ and FRM II

547 media articles

202 scientific journal articles

37 news articles on the web pages

2,671 followers on social media

PUBLICATIONS AND COMMUNICATION

50 Third-Party Funding Projects at MLZ with a total volume of € 8.5 million

€ 4.95 million — Federal Ministry of Education and Research

€ 1.36 million — DFG

€ 1.25 million

€ 0.95 million from other institutions

THIRD-PARTY FUNDING

2024 IN NUMBERS

SCIENTIFIC EVENTS

184 participants at the "Machine Learning Conference for X-Ray and Neutron-Based Experiments"

250 participants at the MLZ User Meeting

50 participants at the MLZ Conference "Neutrons for Energy Storage"

Around **70** experts from science and industry at the 9th TUM Expert Forum (non-destructive testing)

EVENTS FOR THE PUBLIC

80 children and **364** adults participating in FRM II tours at the "Open-Door-Day with the Mouse"

4,069 visitors

More than **200** viewers at the "Science for Everyone" lecture (by Deutsches Museum)

20 Years of FRM II – a busy anniversary 7

Scientific Highlights

Efficient iron scavengers 10
Analysing pores in water cleaning membranes 11
How heat harms Li-ion batteries 12
Towards more efficient batteries 13
Modelling electrolyte transport in porous electrodes 14
Shedding light on dark matter 15
Useful in fuel cells or luminescent materials 16
Unlocking quantum secrets with entangled neutrons 17
Stronger steel bonds for oil pipes 18
Making order visible in crystals 19
Drug cab for insulin 20
Movement in a crowded place 21

Scientific Reports

Materials Science 24
Soft Matter 34
Structure Research 42
Quantum Phenomena 45
Neutron Methods 49

News from the instruments

News from the instruments 62

Reactor & Development

Despite strong head winds – still moving forward 72
Extending capabilities: Full core calculations to support the conversion of FRM II 74

Facts & Figures

The year in pictures 78
Awards 86
Workshops, Conferences and Schools 88
Changing media presence 92
Various activities at the MLZ User Office 96
Organisation, Staff and Budget 98
Publications & Theses 102
Cover pages 104
Committees 105
Partner institutions 110
Imprint 114

20 Years of FRM II – a busy anniversary

On 2 March 2024, the Research Neutron Source Heinz Maier-Leibnitz (FRM II) celebrated its 20th birthday. Since its commissioning in 2004, the FRM II has played a key role nationally and internationally in the supply of neutrons for research, industry and medicine. To date, over 10,000 experiments have generated around 5,000 scientific publications, ranging from materials science, over energy, quantum technologies, climate & environment, health & nutrition to mobility and archaeology and cultural heritage.

Of course, we would have preferred to celebrate this anniversary in a year with a busy user service programme within the framework of the Heinz Maier-Leibnitz Zentrum (MLZ). It is very regrettable that, again, we could not provide any neutrons in 2024. The reason for this is the ongoing replacement of the central channel, which is expected in 2025. Meanwhile, we have made the most of this unfortunate time without neutrons: The periodic inspections due every ten years have been successfully completed. Furthermore, major upgrades and revisions of reactor systems only possible in shut-down conditions were carried out in 2024 as well. By this, our operations division has laid the foundation for the restart of safe operation of our neutron source in the near future.

On 18 June 2024 we received the encouraging decision of the Bavarian Administrative Court that the FRM II is lawfully in operation and may continue to be operated with highly enriched uranium. As a long-term commitment, we are fully engaged in the conversion to low-enriched uranium fuel. An important milestone was the signing of a contract between the FRM II and Framatome for the industrialisation of the production of high-density, low-enriched fuel in April 2024. Funded by the Bavarian government, we are grateful for substantial additional funding from the BMBF and EU, enabling important research on this type of nuclear fuel.

During the last year, major progress has also been made with the Neutron Guide Hall East, finally approaching completion. Several new instruments will open up new fields of research. This includes especially experiments in the field of particle physics at MEPHISTO with the experiment PERC requiring extensive space and a clean magnetic environment offered by the new hall. Geophysics will benefit from two new instruments with extreme pressure and temperature environments, namely SAPHiR and POWTEX, offering extraordinary possibilities for texture analyses on geological samples. Further unique instruments include the thermal time-of-flight spectrometer TOPAS and the triple-axis spin-echo spectrometer TRISP, which has been relocated from its former place in the Experimental Hall. The instrument suite being moved and built up in the Guide Hall East using positrons from the NEPOMUC source will be enlarged, enabling a wide variety of experiments ranging from fundamental physics via solid state and surface physics to applied materials science.

On a different note, in 2024 strong efforts went into the in-depth review of MLZ's scientific portfolio and performance for the years 2018 – 2023. We are grateful to a highly accomplished panel of international experts providing an assessment and advice. The results of the evaluation will form the basis for the continuation and organisation of the scientific use of FRM II.

After 20 years of operation, especially the proposed MORIS instrumentation upgrade programme will lay the foundation to maintain world-class neutron instrumentation at the MLZ. Having also been assessed as part of the MLZ review, MORIS received strong support of the review panel. It essentially pursues three goals: First, a general overhaul of instruments that cannot much longer be operated in their current form. Second, the development of additional scientific fields using new measurement capabilities. And third, the improvement of methods directly related to the neutron experiments, including new sample environment, experimental equipment or better automation technology.

For two decades, FRM II has been at the forefront of outstanding research, enabling ground-breaking discoveries and advancements. Through the further strengthened cooperation between TUM and the Helmholtz partners Forschungszentrum Jülich and Helmholtz-Zentrum Hereon, for the last almost 15 years in the framework of the MLZ, as well as through intense collaborations with the Max Planck Society and university groups, scientists, and industry, we have enabled and promoted innovation across diverse fields.

We as FRM II – with two new directors since 2024, namely Prof. Dr. Christian Pfleiderer as Scientific Director and Dr. Jürgen Neuhaus as Administrative Director – together with the entire team of the MLZ are motivated to provide neutrons again as soon as possible. Together with our user community, we wish to shape the next 20 years of excellent research in Garching.

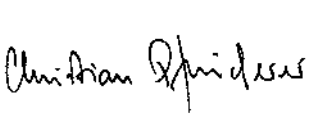

Christian Pfleiderer

Martin Müller

Axel Pichlmaier

Jürgen Neuhaus

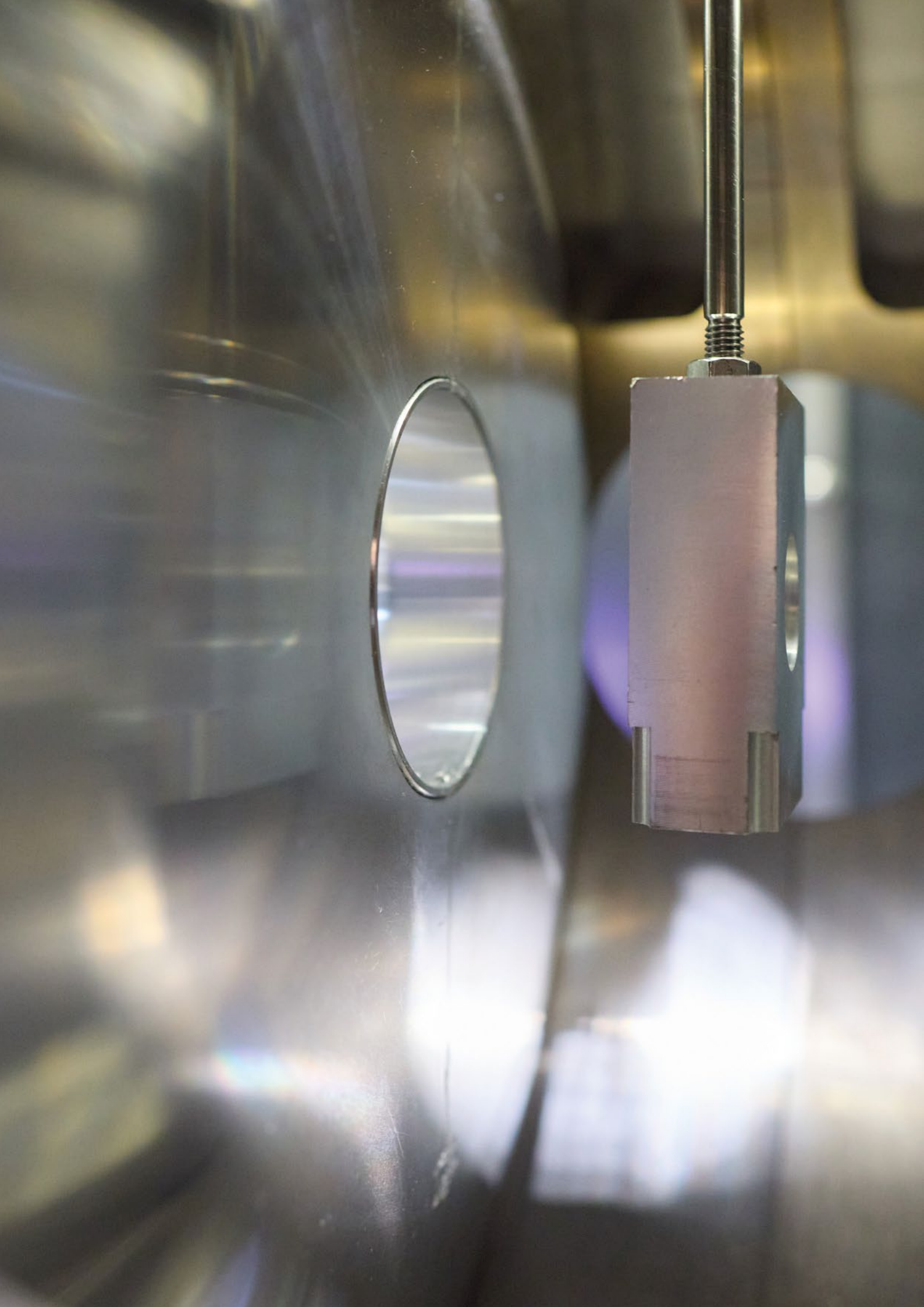

Scientific Highlights

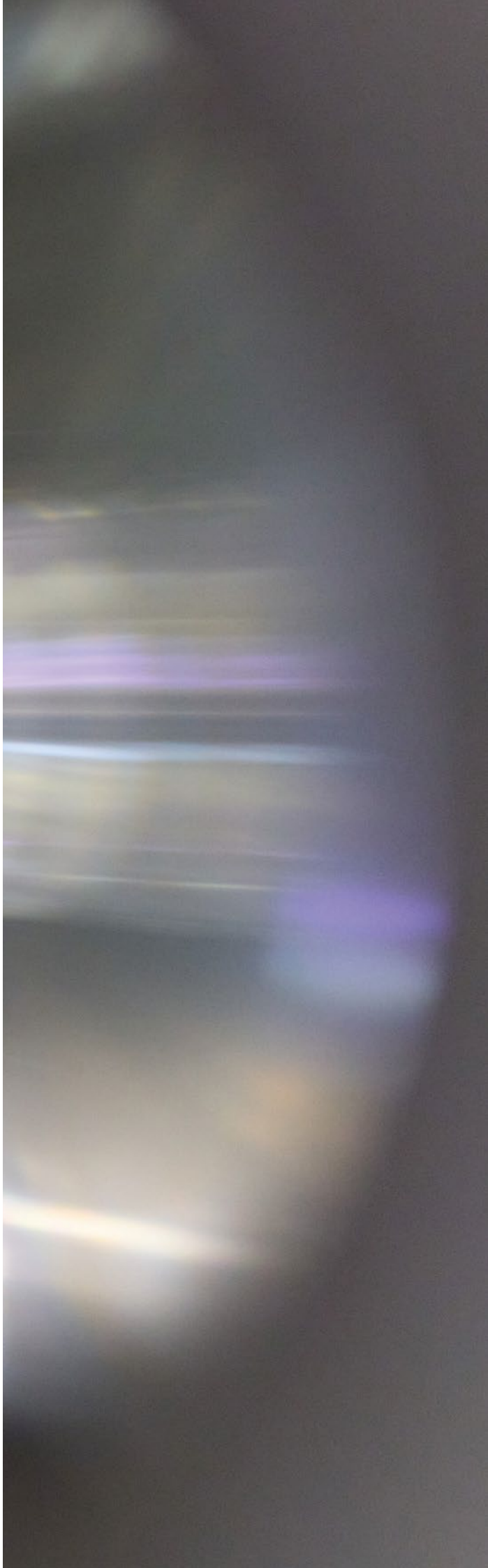

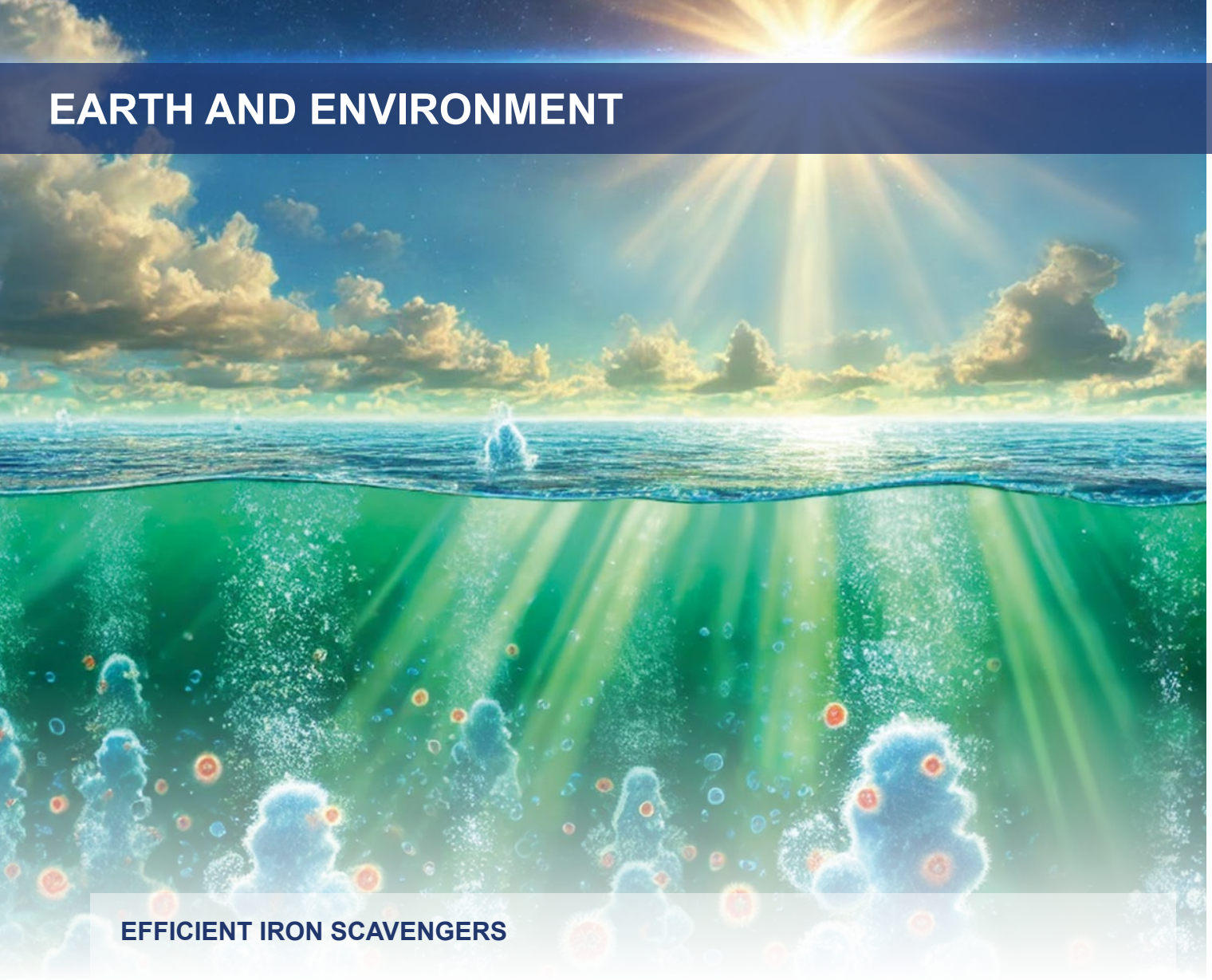

EFFICIENT IRON SCAVENGERS

Prochlorococcus is a photosynthetic bacterium that found a particularly efficient way to absorb and store vital iron. An international team of researchers used neutron and X-ray experiments to visualise an astonishing mechanism for iron binding.

Organisms living in the sea that carry out photosynthesis produce around half of the oxygen on Earth, and they are an important carbon sink in the fight against climate change. As the smallest photosynthetic organism on earth, Prochlorococcus alone produces four gigatons of sequestered carbon per year, which corresponds to the annual net primary production of global agriculture. Its photosynthetic activity, however, depends on iron, which is only available to a limited extent in the ocean.

One protein binds two distinct forms of iron

Most bacteria have two proteins to absorb the two distinct states of iron. However, being small, Prochlorococcus has only got a single protein for iron scavenging. The researchers suspected that this single protein has a dual function, and demonstrated a molecular switch that enables the protein to switch back and forth between binding the two states of iron, this being an important reason for its ecological success.

Neutrons reveal the charge of the iron

"Even the hydrogen atoms in the water were clearly visible," says Rachel Bolton, a doctoral student at the University of Southampton, who carried out experiments with neutrons at MLZ. Being able to see the hydrogen atoms enabled the research team to understand the charge of bound iron, resolving the riddle.

R. Bolton, M. M. Machelett, J. Stubbs, D. Axford, N. Caramello, L. Catapano, M. Malý, Matthew. J. Rodrigues, C. Cordery, G. J. Tizzard, F. MacMillan, S. Engilberge, D. v. Stetten, T. Tosha, H. Sugimoto, J. A. R. Worrall, J. S. Webb, M. Zubkov, S. Coles, E. Mathieu, R. A. Steiner, G. Murshudov, T. E. Schrader, A. M. Orville, A. Royant, G. Evans, M. A. Hough, R. L. Owen, I. Tews, A redox switch allows binding of Fe(II) and Fe(III) ions in the cyanobacterial iron-binding protein FutA from Prochlorococcus
PNAS 121, e2308478121 (2024)
DOI: 10.1073/pnas.2308478121

Experiments were carried out at I24, Diamond Light Source, UK; BL2 EH3, SACLA, Japan and BIODIFF.

ANALYSING PORES IN WATER CLEANING MEMBRANES

Water purification and desalination based on reverse osmosis is widely applied nowadays. The core of the technology is a special membrane. The system of pores in such membranes requires a comprehensive analysis, which is best performed using neutrons.

The conversion of sea- or wastewater into freshwater is essential in arid regions and in a closed biotope, for example a spaceship. Desalination using reverse osmosis membranes (ROMs) of a typical thickness of some 100 µm can provide high quality water in a most energy-efficient way. The process relies on the selective transport of water molecules across a membrane driven by pressure.

Assessing membrane pores with neutrons

The performance of a ROM is largely determined by the structure of its pores and the nature of the ROM material. Using neutrons, an Israeli-German research team was able to gain unique detailed information on the pores in a commercial composite ROM under operation. The trick is to enhance the contrast to visualise the pores by a suitable mixture of light (H_2O) and heavy (D_2O) water feeds.

The complex network of pores

The key findings are related to the pore parameters and its evolution during operation in the top and support layers of the composite ROM. Desalination is mainly achieved by a network of nanometre large pores in the µm thin top layer. Besides this network of open pores adopting a fractal structure, a small fraction of closed nanopores is identified in one of the support layers. During operation the pores' volume fraction diminishes slightly, until an equilibrium is established. This process can take many hours.

With this knowledge at hand, researchers can help to further optimise membranes, increasing their efficiency and thereby reducing the cost of water desalination.

V. Pipich, T. Starc, R. Kasher, W. Petry, Y. Oren, D. Schwahn, The porous system of a reverse osmosis membrane – operando studies with small-angle neutron scattering, Chem. Eng. J. 495, 153304 (2024)
DOI: 10.1016/j.cej.2024.153304

Experiments were carried out at KWS-1 and KWS-3.

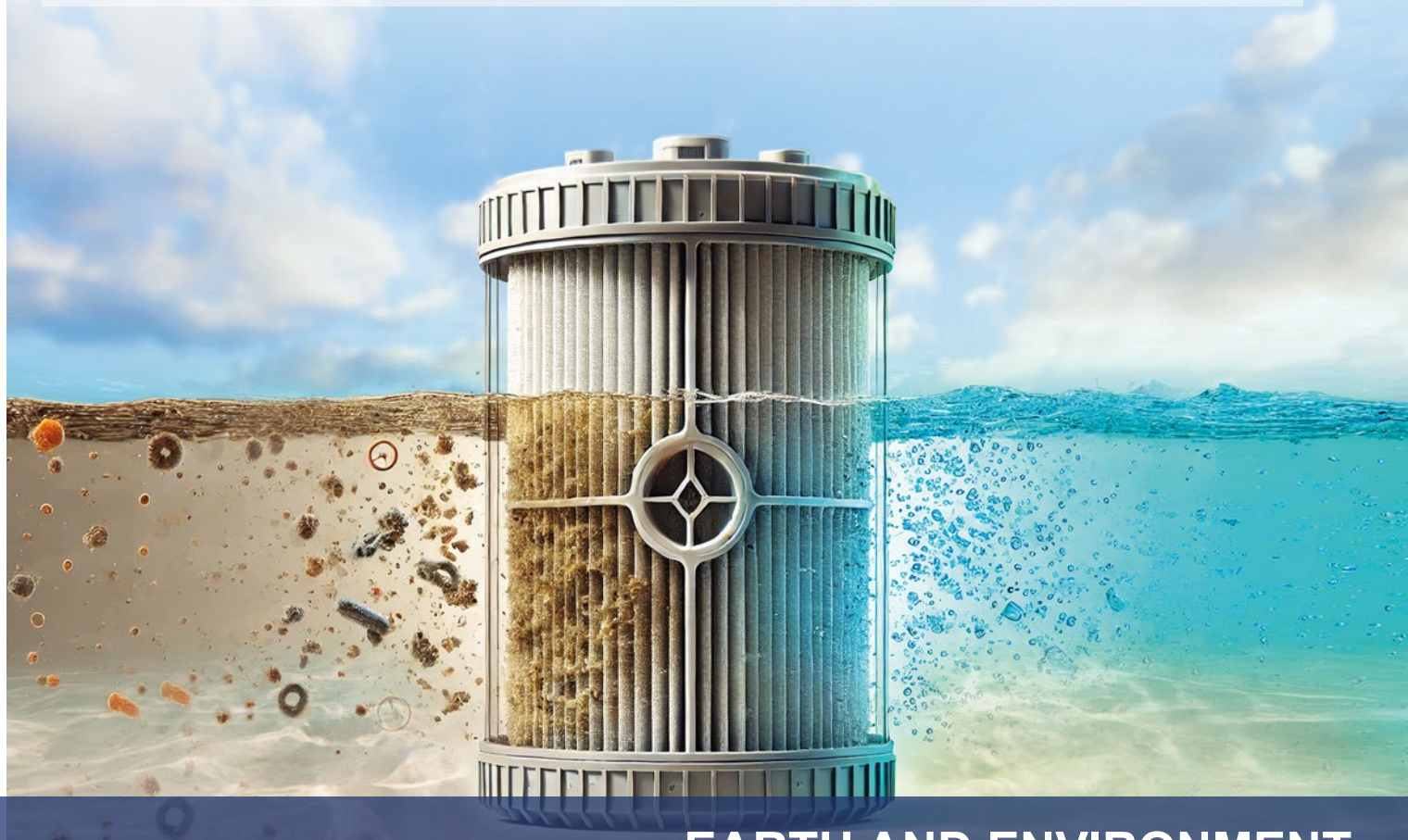

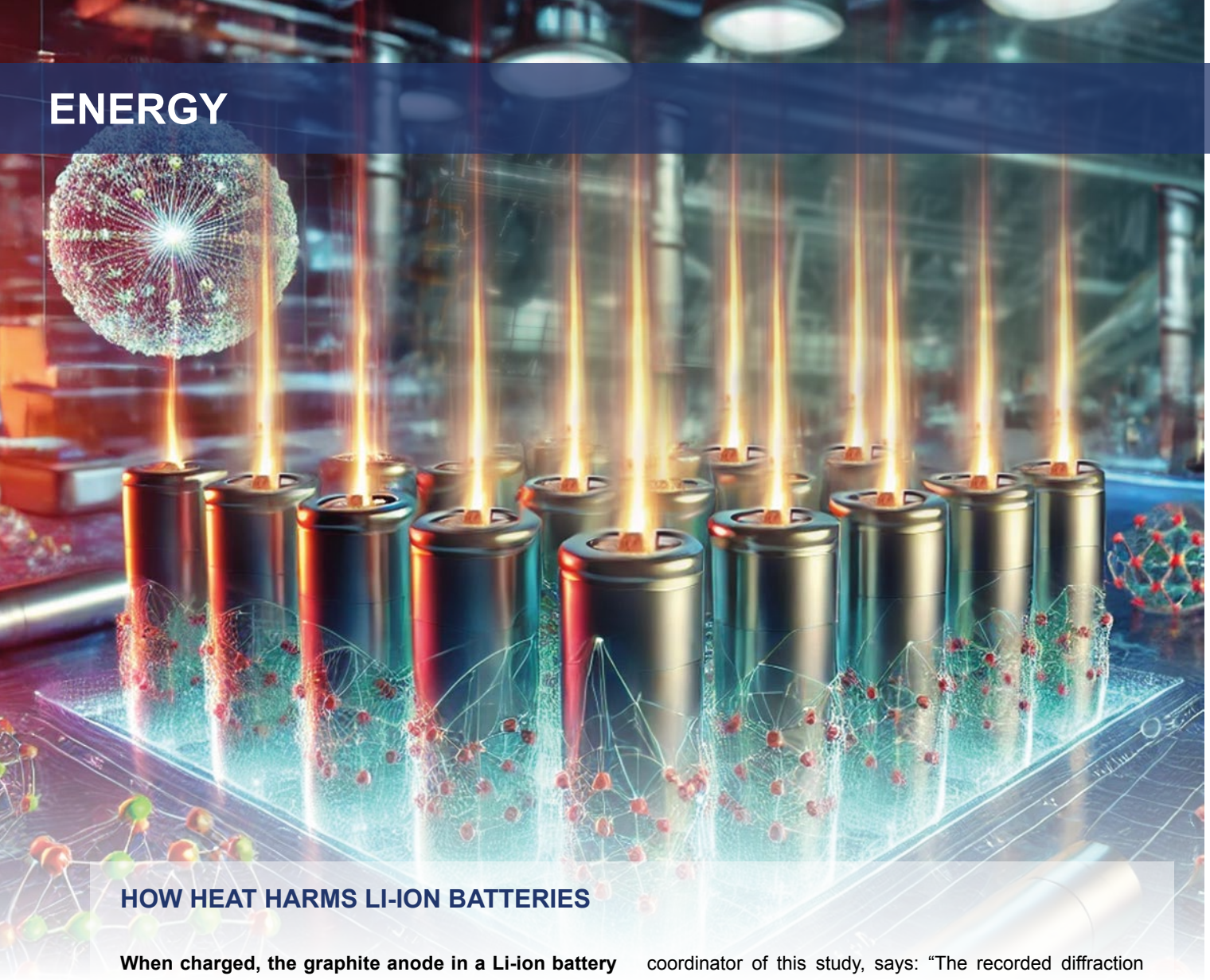

HOW HEAT HARMS LI-ION BATTERIES

When charged, the graphite anode in a Li-ion battery (LIB) can be exposed to temperature-driven changes, causing structural degradation and negatively affecting its performance. X-rays and neutrons help to reveal the underlying processes behind these changes.

The thermal stability of lithiated graphite has been identified as a crucial factor affecting efficiency in LIBs, particularly during fast charging or high discharge rates. Both low and high temperatures induce changes in the behaviour of graphite that impact the overall lifespan and safety of LIBs.

Low-temperature stability

At temperatures below −33°C, no substantial degradation of lithiated graphite was observed. Minor changes in diffraction intensities and the appearance of additional reflections from frozen electrolyte components were detected during in-situ characterisations. However, these changes did not impact the structural stability of the graphite, but did hinder the Li-ion diffusion during operation at low temperatures.

In contrast, overheating the Li intercalated graphite anode leads to irreversible structural changes occurring across the full range of states of charge. Dr. Anatoliy Senyshyn, coordinator of this study, says: “The recorded diffraction patterns unambiguously indicate the formation of various side products upon heating, resulting in the loss of active lithium and harming stable cell operation.”

Side reactions at high temperatures

Calorimetric studies further identified the involvement of the binder and electrolyte residues in the degradation process, which result in the formation of passivation layers on the graphite particle surfaces. Stabilising the electrolyte composition could help mitigate these effects and improve overall battery longevity.

T. Hölderle, M. Monchak, V. Baran, A. Kriele, M. J. Mühlbauer, V. Dyadkin, A. Rabenbauer, A. Schökel, H. Ehrenberg, P. Müller-Buschbaum, A. Senyshyn, Thermal Structural Behaviour of Electrochemically Lithiated Graphite (Li_xC_6) Anodes in Li-ion Batteries, Batteries & Supercaps 7, e202300499 (2024)
DOI: 10.1002/batt.202300499

Experiments were carried out at P02.1, PETRA III/DESY, Germany; SNBL, ESRF, France and SPODI.

TOWARDS MORE EFFICIENT BATTERIES

Using X-ray diffraction tomography aided by machine learning, an international team of researchers screened one of the various degradation processes that occur in battery cathodes.

The rechargeable lithium-ion battery is indisputably a revolutionary technological solution that already provides electric power to many types of mobile devices for a reasonable length of time. Nevertheless, there is room for improvement, including lifetime, safety, and cost.

Cathode loses charge capacity

International researchers pinpointed the exact mechanisms behind the deterioration of the batteries' performance during exploitation. To find out why the commonly used cathodes lose their charge capacity upon continuous operation, characterisation of the cathode material with the desired accuracy, depth, and length scale was required, which led to a highly advanced experimental approach.

Measurements were carried out simultaneously using microfocused X-ray diffraction and fluorescence tomography, supported by neutron powder diffraction. The crucial feature of this approach is the involvement of machine learning in handling and analysing the resulting, extremely large, data sets.

Insights into degradation mechanisms

The team monitored various changes induced by the operation of the cathode for 100 charge/recharge cycles, with an unprecedented 3D spatial resolution of one micrometre. The fine details observed provided unique insights into the elemental composition variations, chemical phase transformations, and morphological altering. This made it possible to define degradation mechanisms specific to the selected cathode material, the role of the carbon matrix and the binder in the battery aging. The conclusions pave the way for tweaking the composite cathode materials towards higher efficiency and sustainability.

W.B. Hua, J.N. Chen, D.F. Sanchez, B. Schwarz, Y. Yang, A. Senyshyn, Z.G. Wu, C.H. Shen, M. Knapp, H. Ehrenberg, S. Indris, X.D. Guo, X.P. Ouyang, Probing Particle-Carbon/Binder Degradation Behavior in Fatigued Layered Cathode Materials through Machine Learning Aided Diffraction Tomography, Angew. Chem. Int. Ed. 63, e202403189 (2024)
DOI: 10.1002/anie.202403189

Experiments were carried out at MSPD, ALBA, Spain; P02.1, PETRA III/DESY, Germany; X05LA, SLS/PSI, Switzerland and SPODI.

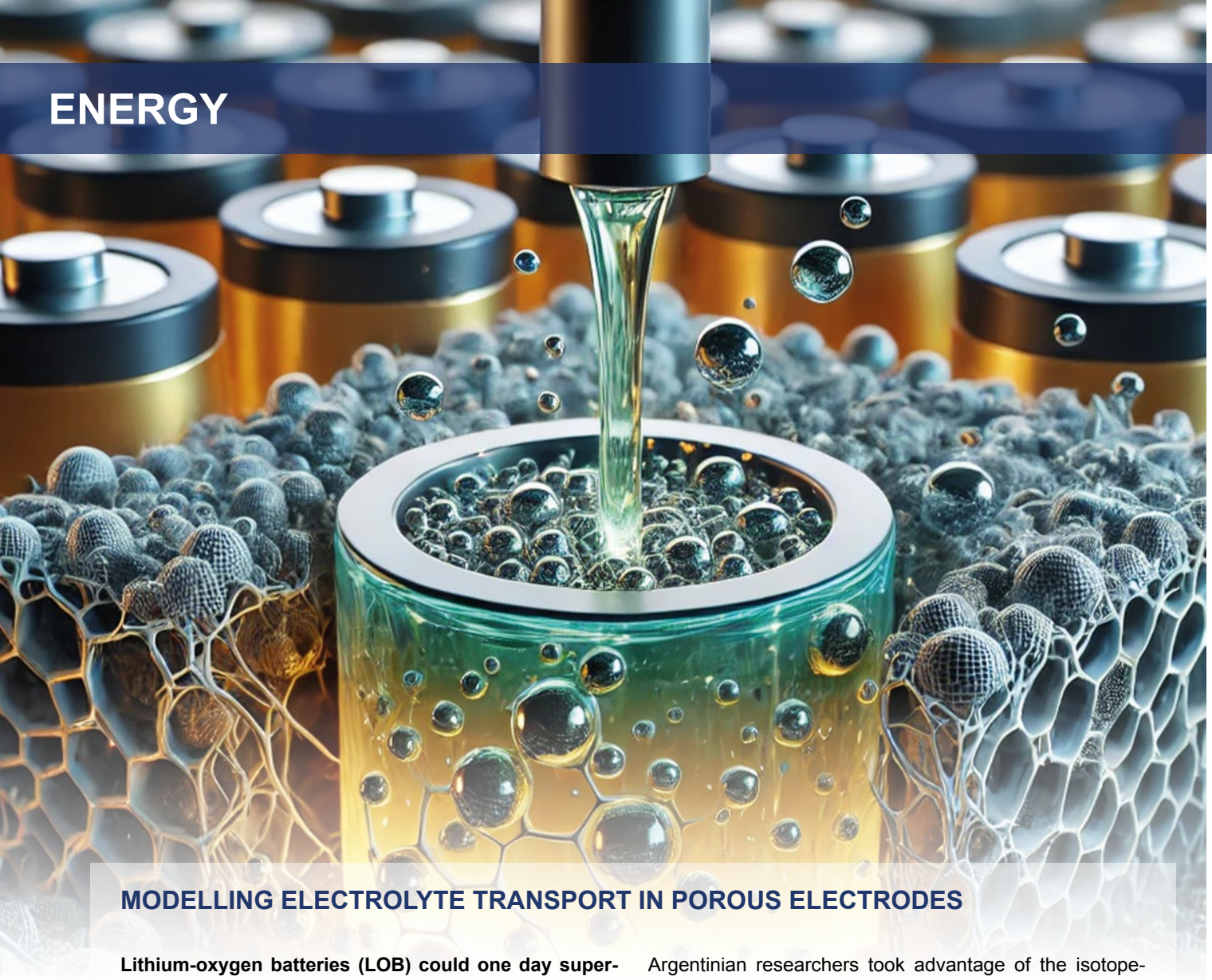

MODELLING ELECTROLYTE TRANSPORT IN POROUS ELECTRODES

Lithium-oxygen batteries (LOB) could one day supersede the widely used lithium-ion batteries because, theoretically, they have 10 times higher energy density. However, the technology of LOBs is not yet ripe for commercial exploitation. Neutron imaging sheds light on possible electrolytes and cathode materials.

Non-flammable and environmentally friendlier

Among promising candidates as an electrolyte in LOBs are aqueous solutions with a high lithium salt content. These so-called water-in-salt (WiS) electrolytes possess useful properties for improved LOB performance. Additionally, they are non-flammable and more environmentally friendly compared to those based on organic solvents.

Mesoporous carbon is a promising material of choice for the cathode in LOBs. Besides electrical conductivity, it has to satisfy many further requirements such as high porosity and specific surface area, while maintaining high accessibility for oxygen and Li^+-ions.

Neutrons for a detailed insight

Understanding the interplay of the electrolyte and the cathode material is crucial for the design of an efficient electrode. Together with German colleagues, a group of Argentinian researchers took advantage of the isotope-specific interaction of neutrons with Li-ions. Applying neutron imaging, they tracked and modelled the transport processes of WiSs in the monolithic mesoporous carbon. “We could see that thanks to the sufficiently strong capillary forces, the uptake of viscous solutions of lithium salts by mesoporous carbon is faster than that of pure water. Also, the interdiffusion of Li^+-ions between the soaked carbon material and the liquid electrolyte phase is surprisingly relatively high”, says Dr. Michael Schulz, a co-author of this study. The findings point to the further development of electrodes for LOBs and supercapacitors.

F.M. Cabello, G. Horwitz, A. Tartaglione, M. Schulz, J.H. Marin, A. Rozenblit, M.A. Trejo Urdaneta, M.S. Bellora, F.A. Viva, H.R. Corti, Wettability, imbibition and interdiffusion of lithium-based water-in-salt electrolytes in nanoporous carbon in relation to energy storage: A neutron radiography study, Carbon 228, 119292 (2024)
DOI: 10.1016/j.carbon.2024.119292

Experiments were carried out at STORNI, Bariloche Atomic Centre (CNEA), Argentina and ANTARES.

SHEDDING LIGHT ON DARK MATTER

Polarised nuclei of the noble gas xenon interact with neutrons in a specific manner. Exact measurement of this interaction promises far-reaching applications, which include particle physics.

Depending on the number of protons and neutrons, a nucleus can possess a non-zero spin. Isotopes of the noble gas xenon, ^{129}Xe and ^{131}Xe, have spins 1/2 and 3/2, respectively. Also, the neutron and ^{3}He isotope possess spin 1/2. Thanks to this feature, these nuclei can behave as small magnets and interact with each other and with external electromagnetic fields. In an ensemble of such nuclei, their magnetic dipoles usually cancel each other statistically. However, this can be changed by external stimuli – one speaks about nuclear polarisation in such a case.

Passing neutrons through the noble gas

An international team of researchers coordinated by Dr. Earl Babcock addressed the interaction of polarised neutron beam with polarised ^{129}Xe and ^{131}Xe isotopes. Depending on the mutual spin orientation, the propagation of neutrons through xenon causes a splitting of the neutron beam into two distinct polarisation states. This results in the so-called birefringence. While referring to ^{3}He for calibration, researchers exploited the neutron spin-echo (NSE) technique to extract specific interaction parameters with high precision for the first time, so that the results can be used further to clarify various fundamental questions.

Search for sources of time reversal violation

For example, polarised xenon isotopes can help in measurements of the electric dipole moments of nuclides and in experiments on quantum entanglements. Polarised ^{131}Xe nuclei could be used in a search for new sources of time reversal violation in neutron-nucleus interactions and help validate the theories beyond the standard model. As a consequence, they might help to shed light on dark matter and its hypothesised elementary particle, the axion.

H. Lu, M. J. Barlow, D. Basler, P. Gutfreund, O. Holderer, A. Ioffe, S. Pasini, P. Pistel, Z. Salhi, K. Zhernenkov, B. M. Goodson, W.M. Snow, E. Babcock, First measurement of neutron birefringence in polarised ^{129}Xe and ^{131}Xe nuclei, Phys. Rev. C 109, L011001 (2024)
DOI: 10.1103/PhysRevC.109.L011001

Experiments were carried out at J-NSE Phoenix.

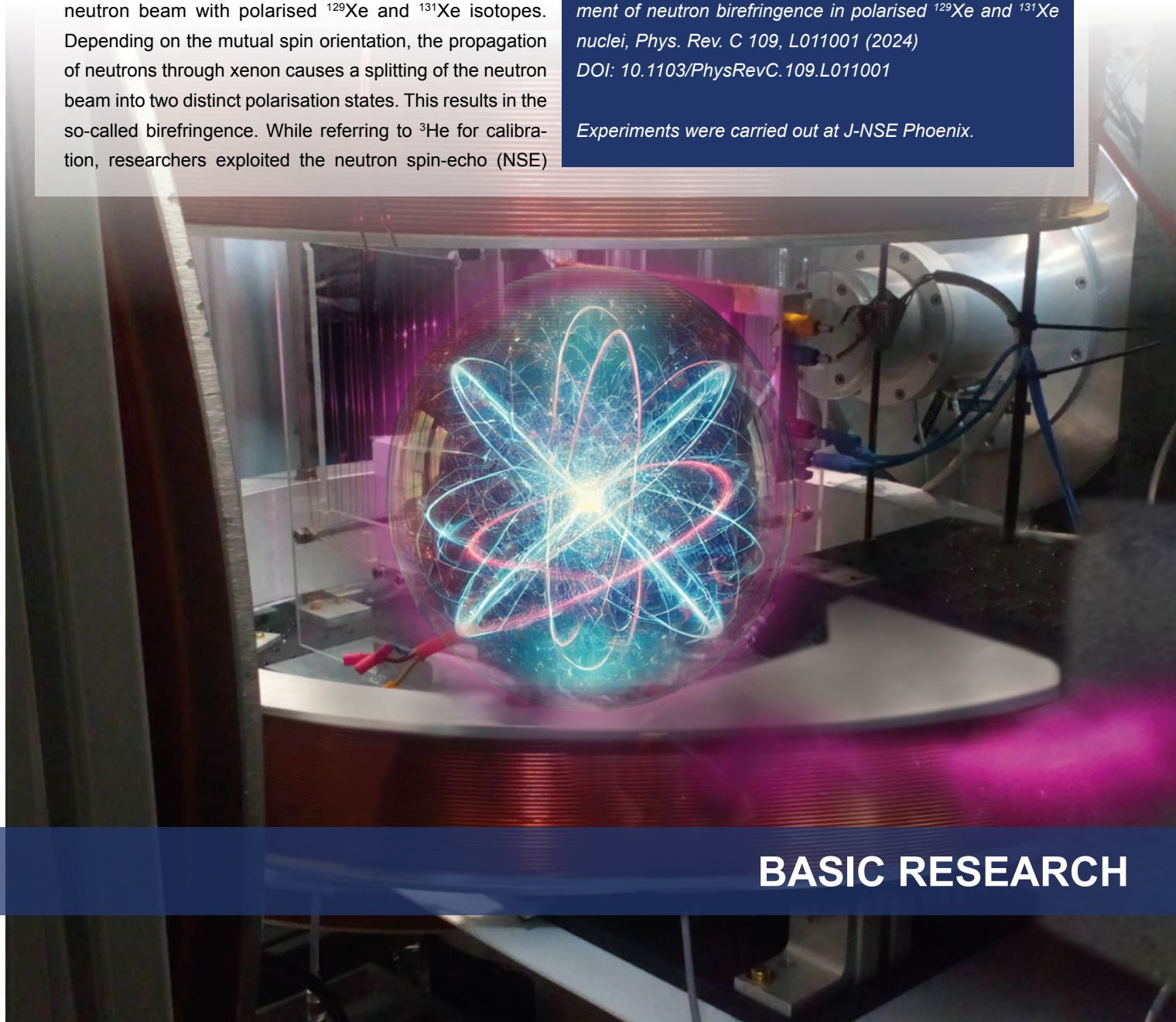

USEFUL IN FUEL CELLS OR LUMINESCENT MATERIALS

An international team has discovered a completely new compound composed of the salt of boric acid and hydrogen and elucidated its structure with the help of neutrons. The borate hydride could lend itself for use in fuel cells, luminescent materials or catalysis in the future.

Application in hydrogen storage

Why did Alexander Mutschke and his colleagues from Australia, Finland, the Czech Republic, Sweden, and Germany go to the trouble of producing and analysing this compound? Dr. Alexander Mutschke, who works as a post-doctoral researcher at the MLZ, enthuses: “This is a rare discovery! There is only one other compound of this kind.” His idea: Combining the practical properties of both negatively charged ions, borate and hydrogen, in one compound. On the one hand, there is the light and often mobile hydrogen, which is important for many catalytic reactions. On the other hand, the unreactive borate, the salt of boric acid, gives the compound a solid and stable framework. To quote Alexander Mutschke “This is interesting with possible applications for hydrogen storage, hydride ion conductors, catalysts or even luminescent materials.”

Structure only resolved with neutrons

However, in order to be able to do anything with the compound, its structure must first be understood. And this is where the most spectacular part of the work comes in, as Alexander Mutschke says: “The most difficult thing is actually to elucidate the structure.” This can and could only be done with the help of neutrons. The team carried this out on the Australian counterpart to the MLZ instrument SPODI. Measurements at the German Electron Synchrotron DESY complemented the investigation. “As soon as the FRM II delivers neutrons again, further measurements are planned at SPODI to investigate the structure of possible daughter compounds,” says Alexander Mutschke.

A. Mutschke, T. Wylezich, P. Beran, T. Holderle, V. Baran, M. Avdeev, A. J. Karttunen, N. Kunkel, The Non-Centrosymmetric Borate Hydride $Sr_4Ba_3(BO_3)_{3.83}H_{2.5}$, Chem. Eur. J., 30, e202403048 (2024),
DOI: 10.1002/chem.202403048

Experiments were carried out at Echidna, ANSTO, Australia and P02.1, PETRA III/DESY, Germany.

UNLOCKING QUANTUM SECRETS WITH ENTANGLED NEUTRONS

Einstein called it 'spooky action at a distance.' Schrödinger deemed it quantum mechanics' most essential trait. For decades, quantum entanglement has captivated the brightest minds – and now, we can create entangled neutrons using a standard neutron scattering instrument.

While quantum entanglement – recognised with the 2022 Nobel Prize in Physics – has paved the way for ultra-secure communications and advanced computing, its significance extends far beyond quantum information technology, reaching deep into the foundations of condensed matter physics and beyond.

Quantum entanglement in condensed matter physics

Quantum spin liquids, for example, possess a quantum entangled ground state – the system's lowest-energy configuration, which it adopts as it approaches absolute zero. However, demonstrating the existence of such a state remains an experimental challenge pursued by researchers worldwide.

Using neutron beams to explore entangled states

Neutron spectroscopy has been a vital tool in this pursuit, enabling researchers to probe a material's excitation spectrum for signs of entanglement. Recently, a global team of researchers demonstrated progress by showing that a neutron resonance spin-echo spectrometer – such as RESEDA at the MLZ – can produce a beam of entangled neutrons. An entangled beam of neutrons opens new possibilities for probing condensed matter systems, providing a powerful tool to explore quantum entanglement.

J. C. Leiner, S. J. Kuhn, S. McKay, J. K. Jochum, F. Li, A. A. M. Irfan, F. Funama, D. Mettus, L. Beddrich, C. Franz, J. Shen, S. R. Parnell, R. M. Dalgliesh, M. Loyd, N. Geerits, G. Ortiz, C. Pfleiderer, R. Pynn. Spin-energy entanglement of a time-focused neutron, Phys. Rev. Applied 22, L031005 (2024), DOI: 10.1103/PhysRevApplied.22.L031005

Experiments were carried out at CG-4B polarised test beamline at HFIR, USA, following initial experiments at RESEDA.

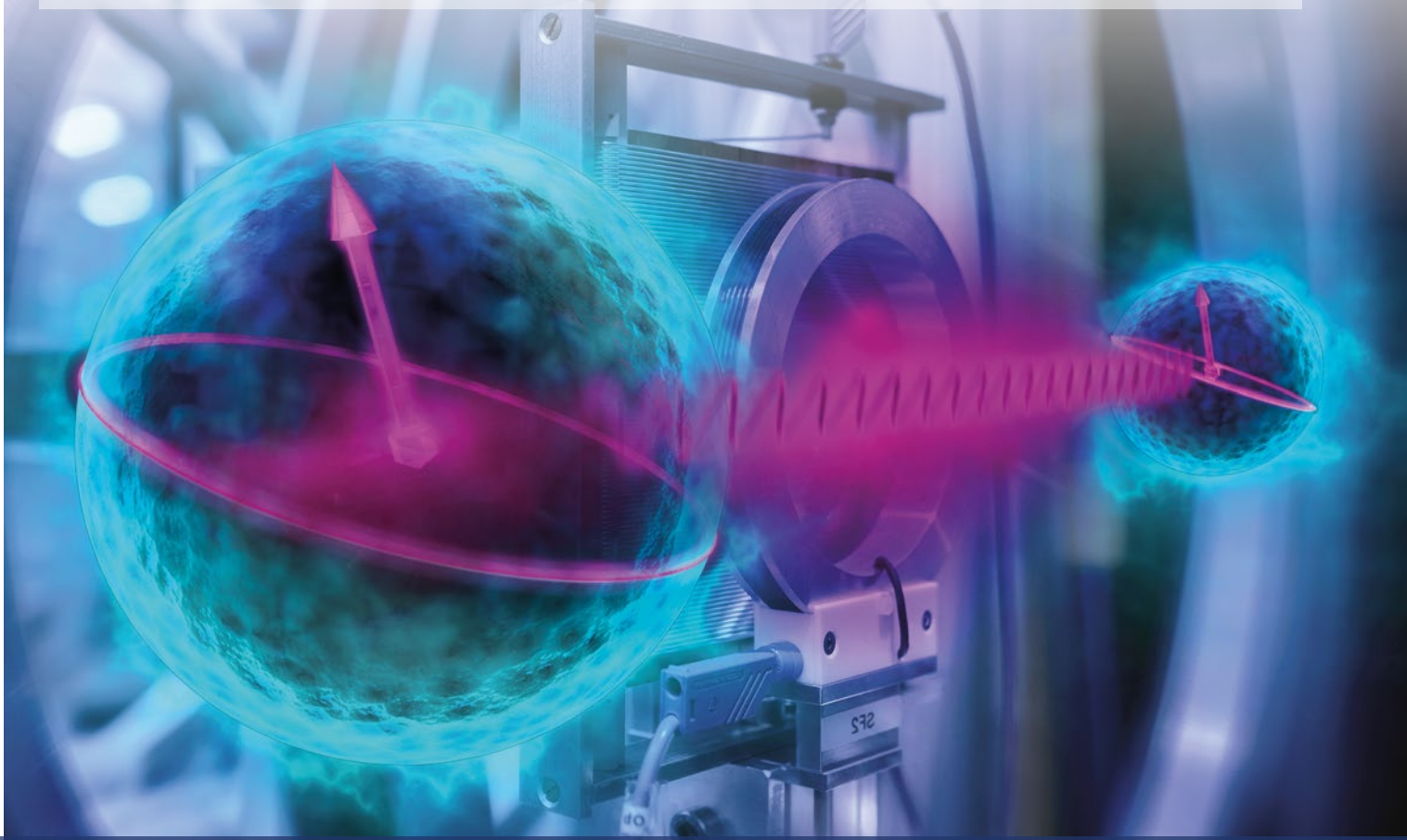

STRONGER STEEL BONDS FOR OIL PIPES

Argentinian researchers have developed a new method for detecting boron in steel using neutron radiography. Their results have significant implications for industries that rely on steel components, such as the oil and gas sector.

New technique with filler material

To join steel components, researchers turned to a method called transient liquid phase bonding (TLPB). This technique uses a special filler material – thin metallic foils made of iron and boron – to bond steel pieces at high temperatures. To make this process work effectively, researchers needed to study and control how the boron spreads throughout the joint.

Peering inside steel bonds

Neutron radiography played a crucial role: the neutron images revealed the diffusion of boron across the joint. This balance was critical – it ensured that the joint remained strong and precluded the formation of brittle compounds that could weaken the bond. With this insight, the researchers confirmed that their process created a connection as strong and ductile as the original steel.

This opens the door to applications: the oil and gas industry still relies on threaded pipes inside the well, flush steel bonds can outperform flush threaded connections.

N. Di Luozzo, M. Schulz, M. Boudard, S. Limandri, G. Garbarino, M. Fontana, Diffusion bonding of steels with a homogeneous microstructure throughout the joint, J. Mater. Sci. 59, 20400 (2024)
DOI: 10.1007/s10853-024-10343-x

Experiments were carried out at the instrument ANTARES.

MAKING ORDER VISIBLE IN CRYSTALS

The crystal structure of a material is the arrangement of the atoms of which it is composed and determines the properties of the material. Many advances in energy storage or manufacturing rely on new materials with desirable properties. An international team has developed methods to better understand the structures behind those properties.

Tiny magnets?

They investigated $CePdAl_3$ crystals. The paper's first author, Dr Michał Stękiel from Forschungszentrum Jülich at MLZ, reports: "We wanted to find out which structural characteristics allow $CePdAl_3$ to develop magnetic order in the first place."

Magnetic order describes the relationship between the magnetic moments of individual atoms. In simple terms, the magnetic moments are tiny magnets and can be thought of as compass needles that indicate the direction of the magnetic fields generated by individual atoms. In ferromagnets, for example, they are aligned in the same direction; in antiferromagnets, every second compass needle adopts the opposite direction; in some other materials, they are even chaotic.

Neutrons reveal magnetic order

Using neutrons, the researchers were able to determine the orientation of the magnetic moments of the atoms in the crystals. "We knew that tetragonal $CePdAl_3$ cannot develop uniform magnetic order. The magnetic structure is frustrated, and the atoms block each other to align their magnetic moments comfortably", explains Michał Stękiel. "However, with the transition to an orthorhombic structure, the magnetic moments are more comfortably aligned and show antiferromagnetic order. Additionally, we have developed a new tool that enables us to better analyse the vast amounts of data we obtain through measurements on spectrometers."

M. Stekiel, P. Čermák, C. Franz, M. Meven, D. Legut, W. Simeth, U. B. Hansen, B. Fåk, S. Weber, R. Schönmann, V. Kumar, K. Nemkovski, H. Deng, A. Bauer, C. Pfleiderer, and A. Schneidewind. Long-range magnetic order in $CePdAl_3$ enabled by orthorhombic deformation, Phys. Rev. Research 6, 023117 (2024)
DOI: 10.1103/PhysRevResearch.6.023117

Experiments were carried out at HeiDi and DNS as well as PANTHER, ILL, France.

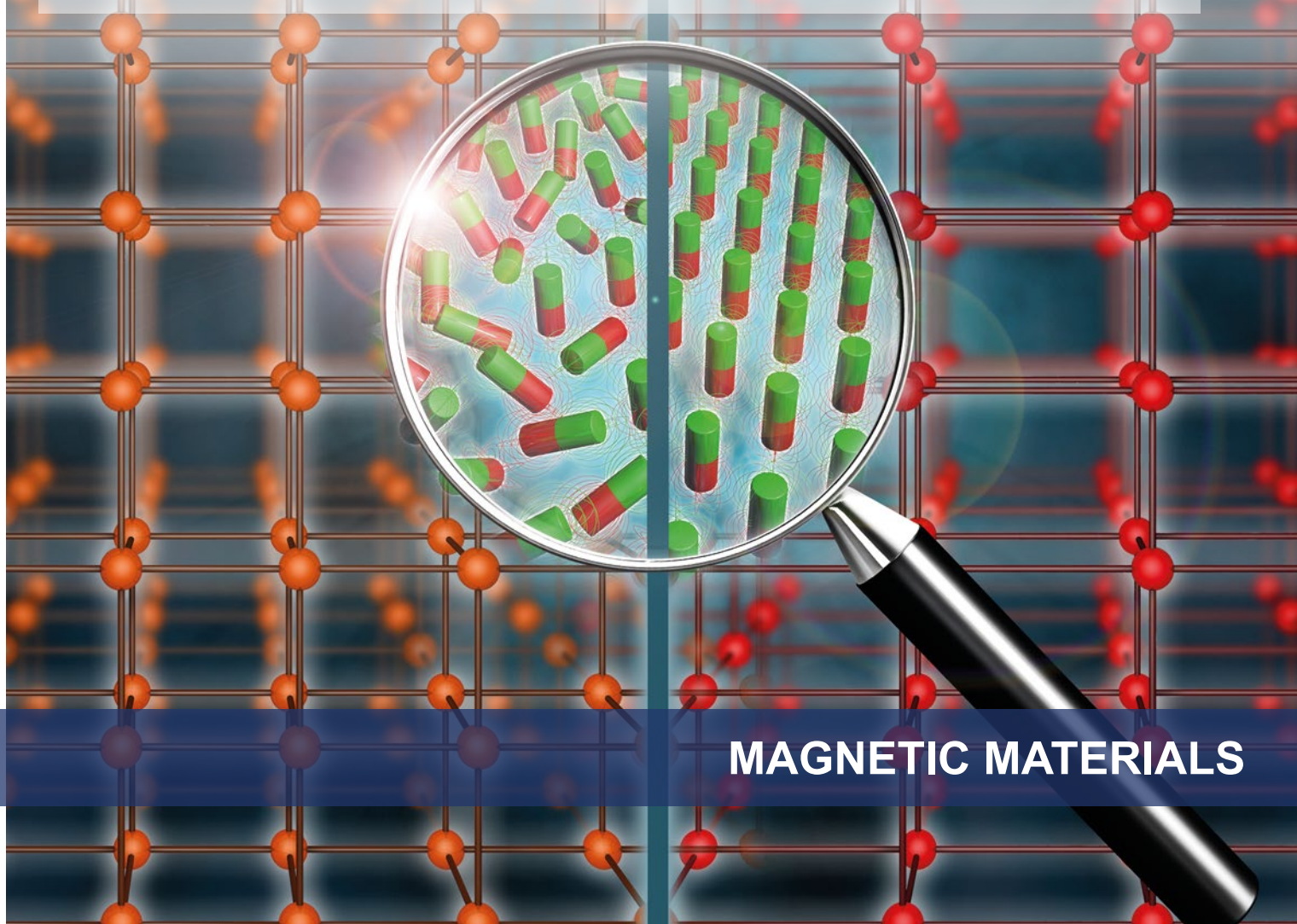

MAGNETIC MATERIALS

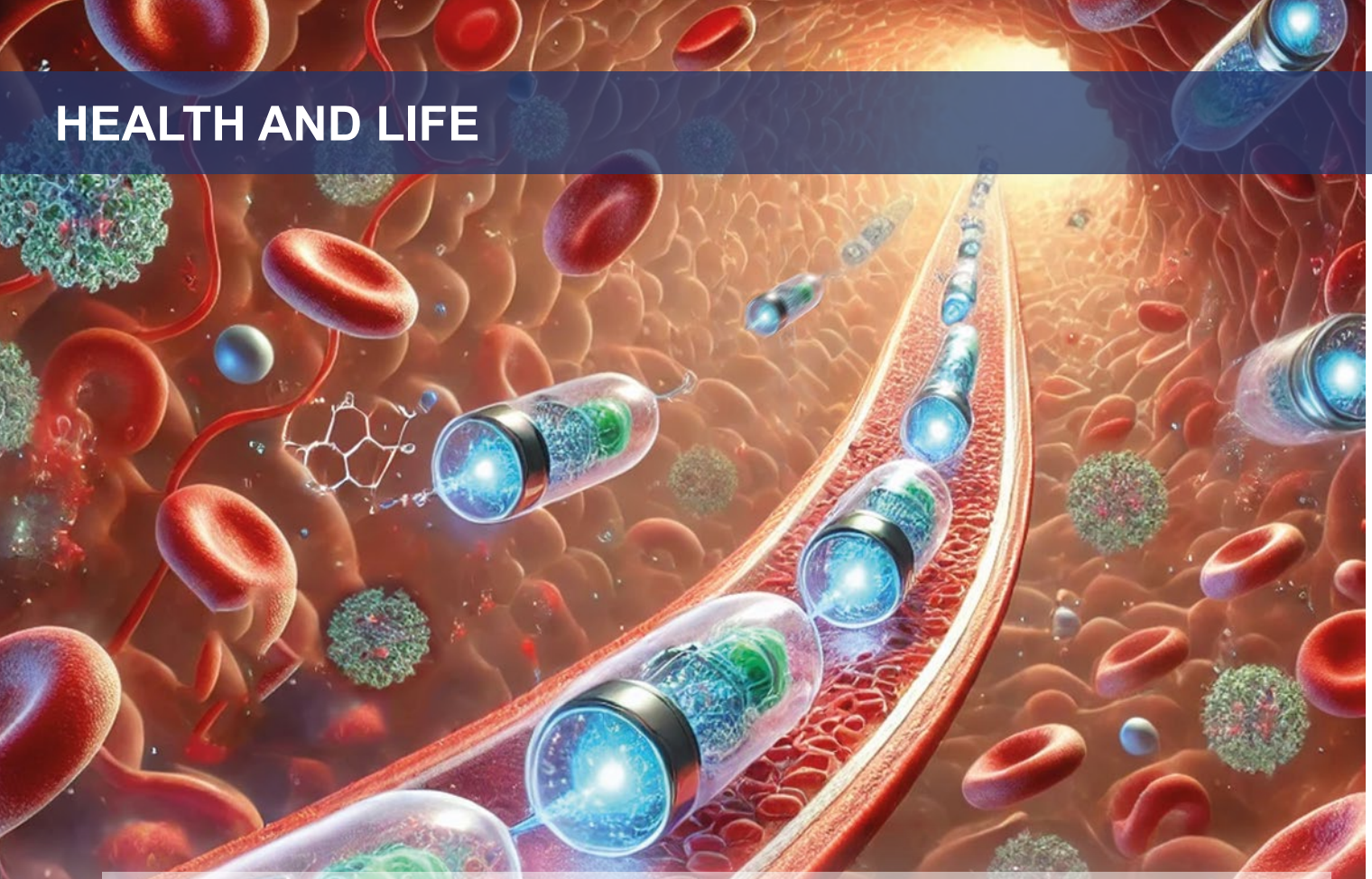

DRUG CAB FOR INSULIN

Up to three percent of people with diabetes have an allergic reaction to insulin. A team of researchers has now investigated a method that could be used to deliver the active ingredient of insulin into the body in a masked form.

An allergy to insulin is rare. The skin around the injection site reddens. The area swells, itches, and hurts. It can even result in an anaphylactic reaction. To optimise therapeutic outcomes and diminish side effects in insulin delivery, related therapies involving pH-responsive nanocarriers should be used. They are optimised for precise control over the kinetics of drug release, allowing for sustained release or triggered release in response to pH variations in the human body.

Targeted drug delivery

"Our idea was to incorporate insulin into targeted drug delivery systems that may protect insulin from enzymatic degradation and thus enhance its stability during storage and transit. To do this we have studied the binding of insulin in protein/polyelectrolyte complexes and investigated their morphology and controlled release potential", says Dr. Anastasiia Murmiliuk, first author of the paper.

The complexes of insulin and polymer molecules combine to form nanoparticles, which are then transported from the blood vessels to the organs. In the slightly alkaline environment of the blood, the two components initially remain firmly bound together. When the pH value in the tissue changes, the insulin and polymer separate.

Useful for cancer drugs

To study the particles, small-angle neutron scattering has proven to be particularly useful. So far, the team has only been able to show in the laboratory that the molecular transporter works, paving the way for future studies in blood and tissue samples. In the future, this could also be used to encapsulate active ingredients that are poorly soluble in water, for example cancer drugs.

A. Murmiliuk, H. Iwase, J.-J. Kang, S. Mohanakumar, M.-S. Appavou, K. Wood, L. Almásy, A. Len, K. Schwärzer, J. Allgaier, M. Dulle, T. Gensch, B. Förster, K. Ito, H. Nakagawa, S. Wiegand, S. Förster A. Radulescu, Polyelectrolyte-protein synergism: pH-responsive polyelectrolyte/insulin complexes as versatile carriers for targeted protein and drug delivery, J. colloid interface sci., 665 801 (2024)
DOI: 10.1016/j.jcis.2024.03.156

Experiments were carried out at Taikan BL-15, J-PARC, Japan; SANS-J, JRR-3, Japan; Yellow-Submarine, BNC, Hungary as well as Quokka, ANSTO, Australia, following initial experiments at KWS-2.

MOVEMENT IN A CROWDED PLACE

Imagine standing in a crowded place and trying to navigate the crowd. The proteins in our cells are constantly faced with this problem. How they move with precision in the densely packed cell has yet to be clarified. A Spanish research team has investigated how the dynamics of mimetic model polymer nanoparticles change depending on their environment.

Proteins are long-chain molecules essential for all biochemical processes in our body. They move around inside the cell and must find the right partners for biochemical processes. The so-called single-chain nanoparticles (SCNPs) are similar in size and structure to intrinsically disordered proteins and served the researchers as a model system for this study.

Neutron spin as an indicator

To model the impact of macromolecular crowding, e. g. of the cell interior, the researchers observed the dynamics of the SCNPs in a dense solution of molecules of different sizes. They used neutron spin echo spectroscopy (NSE). The technique makes it possible to determine the change in velocity that neutrons experience during a scattering process on the sample using the neutron spin, a fundamental property of elementary particles.

Free movement in dense crowds

"Thanks to NSE, the researchers discovered that these particles can still 'twist' and 'turn' in confined environments even under crowding," says Dr. Stefano Pasini from the Jülich Centre for Neutron Science at the MLZ who had conducted the measurements.

An important finding was that the size of the surrounding molecules has no significant influence on the internal movements of the SCNPs. Understanding these dynamics helps to understand cellular processes such as protein folding and molecule recognition, which are essential for the smooth functioning of the cell.

B. Robles-Hernández, P. Malo de Molina, I. Asenjo-Sanz, M. Gonzalez-Burgos, S. Pasini, J. A. Pomposo, A. Arbe, J. Colmenero, Dynamics of Single-Chain Nanoparticles under Crowding: A Neutron Spin Echo Study, Macromolecules, 57, 10, 4706 (2024)
DOI: 10.1021/acs.macromol.4c00182

Experiments were carried out at the instrument J-NSE Phoenix.

Scientific Reports

Monitoring the texture evolution of graphene reinforced copper matrix composites during tension using neutron diffraction

H. L. Shi [1], X. J. Wang [1], W. M. Gan [2], Y. D. Zhang [3], M. Hofmann [4]

[1] Harbin Institute of Technology, Harbin, China; [2] German Engineering Materials Science Centre (GEMS) at MLZ, Helmholtz-Zentrum hereon GmbH, Garching, Germany; [3] University of Lorraine, Metz, France; [4] Heinz Maier-Leibnitz Zentrum (MLZ), Technical University of Munich, Garching, Germany

Neutron diffraction and visco-plastic self-consistent (VPSC) simulation were employed to investigate the texture evolution of graphene nanosheets (GNSs) reinforced copper (Cu) matrix laminated composites. The results suggest that the grains in the GNSs/Cu laminated metal matrix composites (MMCs) deformed independently, without accommodating neighbouring grains in adjacent Cu layers.

Laminated MMCs' structures attract great interest as they offer the possibility of enhancing both strength and ductility simultaneously. In particular, current research focus is on investigating the deformation mechanisms of laminated grain structures within the MMCs. A key focus of the current study was to understand the crystallographic texture evolution of laminated GNSs/Cu composites fabricated through electrophoretic deposition, vacuum hot-press sintering, and hot rolling during tensile deformation. Neutron measurements offering excellent grain statistics and VPSC modelling were used to unravel the hitherto unexplored interactions between neighbouring grains during tension [1]. The final aim of this research was to provide valuable guidance for optimising the mechanical property design of laminated composites.

Texture evolution of GNSs/Cu composites during tension

STRESS-SPEC was used to measure the bulk volume texture of GNSs/Cu composites as well as pure Cu reference samples at specific terminal strains between 0% and 25%. The data obtained were presented in the form of (111) pole figures (see Fig. 1a, b). The texture of the GNSs/Cu composites evolved from almost random to the emergence of a weak partial fibre texture type as the strain increased. Generally, the pure Cu showed a typical work hardening behaviour, while the GNSc/Cu showed a significant increase in yield strength by almost a factor of two compared to Cu and little subsequent work hardening (Fig. 1c).

The deformation mechanisms of GNSs/Cu composites

The neutron diffraction data were used as input for the VPSC texture modelling, and the simulated texture was compared with the experimental results in terms of texture type and intensity, as shown in Fig. 1. The results indicated that the Cu grains of the GNSs/Cu samples deformed independently of strain accommodation by other grains, which is explained by mechanical decoupling across GNS/Cu interfaces. As strain accumulates, the lack of strain accommodation between adjacent Cu layers leads to the nucleation of micro-cracks at the interfaces, resulting in a decrease in the maximum elongation of the GNSs/Cu composites before failure compared to pure Cu.

Our findings provide valuable insights into the texture evolution of laminated GNSs/Cu composites, helping to improve our understanding of the deformation mechanisms in these materials.

[1] H. L. Shi et al., Revealing the deformation behaviour of graphene nanosheets (GNSs) reinforced copper matrix laminated composites via viscoplastic self-consistent (VPSC) modelling, Compos. Commun. 51, 102044 (2024) DOI: 10.1016/j.coco.2024.102044

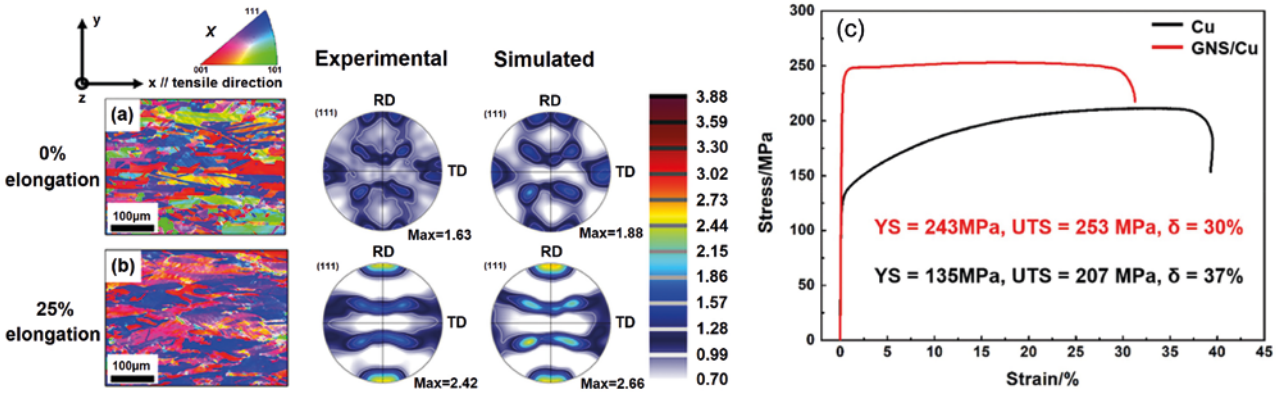

Figure 1: Coloured inverse pole figures (from EBSD), the corresponding neutron and simulated (111) pole figures of the GNSs/Cu composites at elongations of (a) 0%, (b) 25%. (c) shows the engineering stress-strain curve of pure Cu and the laminated GNSs/Cu composites.

Advanced polycrystalline γ′-strengthened CoNiCr-based superalloys

S. Neumeier[1], L. P. Freund[1], A. Bezold[1], M. Köbrich[1], J. Vollhüter[1], D. Hausmann[1], C. Solis[2], A. Stark[3], N. Schell[3], F. Pyczak[3], P. Felfer[1], R. Gilles[4], M. Göken[1]

[1] Department of Materials Science & Engineering, Institute I: General Materials Properties, Friedrich-Alexander-Universität Erlangen-Nürnberg, Erlangen, Germany; [2] German Engineering Materials Science Centre (GEMS) at MLZ, Helmholtz-Zentrum hereon GmbH, Garching, Germany; [3] Institute of Materials Physics, Helmholtz-Zentrum hereon GmbH, Geesthacht, Germany; [4] Heinz Maier-Leibnitz Zentrum (MLZ), Technical University of Munich, Garching, Germany

CoNiCr-based superalloys have been developed, combining high-entropy alloy principles with precipitation strengthening. These novel alloys, featuring a complex concentrated matrix and a high-volume fraction of multicomponent precipitates, exhibit superior creep strength compared to conventional wrought Ni-base superalloys due to altered deformation mechanisms. This research provides guidelines for designing advanced high-temperature superalloys.

Superalloys are essential in applications such as gas turbines, jet engines, and other critical aerospace and industrial components. Based on the discovery of a $Co_3(Al,W)$ compound, multinary, complex concentrated CoNiCr-based superalloys (Fig. 1), called CoWAlloys, have been developed which excel particularly in creep properties. This study investigates seven variants, with varying Al, W, Ti, Ta, Mo, and Nb contents, correlating their thermophysical properties and deformation mechanisms with mechanical strength to inform future superalloy design.

In-depth microstructural characterisation

All CoWAlloys were analysed by advanced characterisation tools, such as SEM, EBSD, TEM, APT, SANS (at SANS-1 beamline at MLZ) and HEXRD (Fig. 1). Their microstructures consist of the fcc solid solution γ matrix, which is strengthened by the multicomponent γ′ (Ni,Co)3(Al,Ti,Ta,W,Nb)-based precipitates. The trimodally distributed precipitates with a very high volume fraction of around 60% are coherently embedded in the matrix with RT lattice misfits of 0.10–0.55%. The alloys have high solidus temperatures above 1300°C and moderate γ′ solvus temperatures between 985°C and 1080°C leading to a large processing window.

Thermophysical, microstructural and mechanical properties

The rising content of γ′-forming elements Ti, Ta, W, and Nb increases the γ/γ′ lattice misfit and the anti-phase boundary energy (APB). In comparison with conventional wrought Ni-base superalloys and $L1_2$-strengthened high-entropy alloys, they have either a larger processing window or a higher yield strength. Regarding the time-dependent deformation at high temperatures, the CoWAlloys exhibit significantly greater resistance to creep (Fig. 1). This is due to their reduced strain rate sensitivity owing to different underlying deformation mechanisms: by increasing the APB energy, a transition to stacking fault shearing and microtwinning occurs.

Implications for alloy design

To achieve enhanced creep resistance in high-temperature applications, the future design of polycrystalline superalloys should (i) optimise the chemical composition to increase the APB energy within γ′, in order to (ii) promote a shift from APB-based to stacking fault shearing of γ′ and (iii) facilitate local phase transformations along stacking faults and microtwin boundaries to achieve ordered χ/η phases.

[1] S. Neumeier et al., Advanced polycrystalline γ'-strengthened CoNiCr-based superalloys, Metall. Mater. Trans. A 55, 1319–1337 (2024)
DOI: 10.1007/s11661-024-07319-6

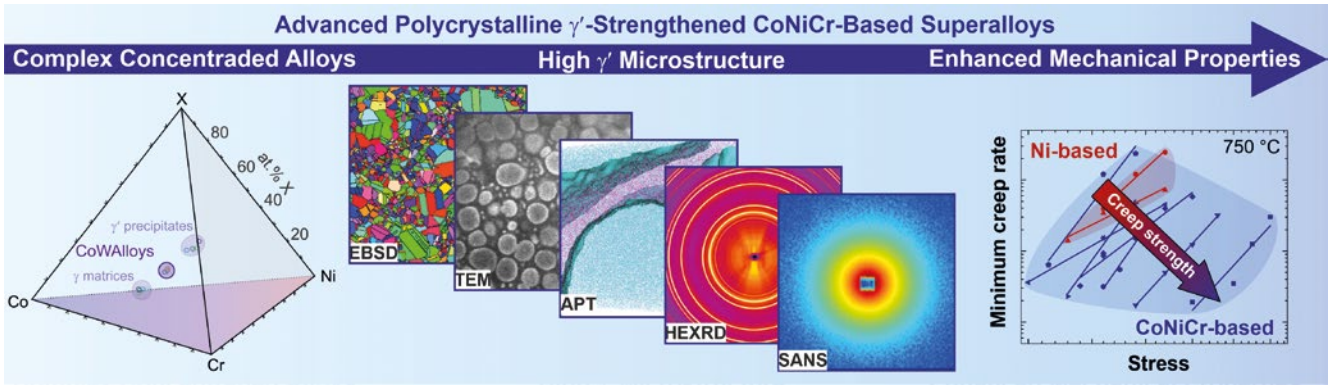

Figure 1: Complex concentrated CoNiCr-based superalloys were developed for high-temperature applications. Various advanced characterisation methods were employed to correlate the microstructure of seven polycrystalline variants with their excellent mechanical properties.

Charging and relaxation mechanisms in silicon-graphite based Li-ion batteries

T. Waldmann [1,2,3], N. Paul [4], R. Gilles [4]

[1] Zentrum für Sonnenenergie- und Wasserstoff-Forschung Baden-Württemberg, Ulm, Germany; [2] Helmholtz Institute for Electrochemical Energy Storage, Ulm, Germany; [3] Institute of Surface Chemistry and Catalysis, Ulm University, Ulm, Germany; [4] Heinz Maier-Leibnitz Zentrum (MLZ), Technical University of Munich, Garching, Germany

In our collaborative study, we investigated the lithiation behaviour and lithium redistribution processes taking place in graphite and silicon-graphite composite electrodes (20.8 wt.-% silicon) via operando X-ray diffraction at MLZ and other complementary physico-chemical analysis methods.

Anodes with high silicon content for high energy batteries

Lithium-ion batteries with silicon-graphite anodes are considered to be a next generation electrochemical energy storage technology in mobile and stationary applications. During the charging of such batteries, lithium is alloyed with the silicon compound and intercalated into graphite. At charging rates of C/2, the kinetic differences of both materials come into play and relaxation processes can be observed. In our collaborative study, we investigated the lithiation behaviour and lithium redistribution processes within graphite and silicon-graphite composite electrodes with 20.8 wt.-% silicon via operando X-ray diffraction (see Fig. 1) at MLZ and by other complementary physico-chemical analysis methods (e.g. in situ optical microscopy at ZSW). The results are additionally used to validate the methods against one another.

Lithium redistribution in silicon-graphite anodes

By operando XRD measurements during the charging of pouch full cells as compared to relaxed cells, a higher lithiation degree in the graphite component of the anode is found during charging compared to the relaxed state, indicating lithium redistribution from the graphite to silicon compound during relaxation. Using optical microscopy measurements, the vanishing of the gold coloured LiC_6 within 24 h after charging was directly observed in the cells containing silicon-graphite. In contrast, the graphite cells exhibited no significant colour change during the 24 h relaxation period. Furthermore, all methods find that the Li redistribution is more pronounced at a higher C-rate of C/2, suggesting a preference for graphite lithiation over silicon alloying.

The findings demonstrate the benefits of integrating complementary physico-chemical analysis methods and provide insights into the lithiation and relaxation behaviour of silicon-graphite anodes in lithium-ion batteries. The charge and lithium redistribution mechanisms within silicon-graphite electrodes were investigated in full cells using bulk-sensitive techniques (in situ and operando XRD), surface-sensitive techniques (ex situ and in situ optical/light microscopy), and 3D microstructure-resolved simulations. The validation of these methods through a comparative analysis of lithium distribution during charging establishes a basis for more precise characterisation.

[1] C. Hogrefe et al., Lithium redistribution mechanism within silicon-graphite electrodes: Multi-method approach and method validation, J. Electrochem. Soc. 171, 070503 (2024)

DOI: 10.1149/1945-7111/ad59c7

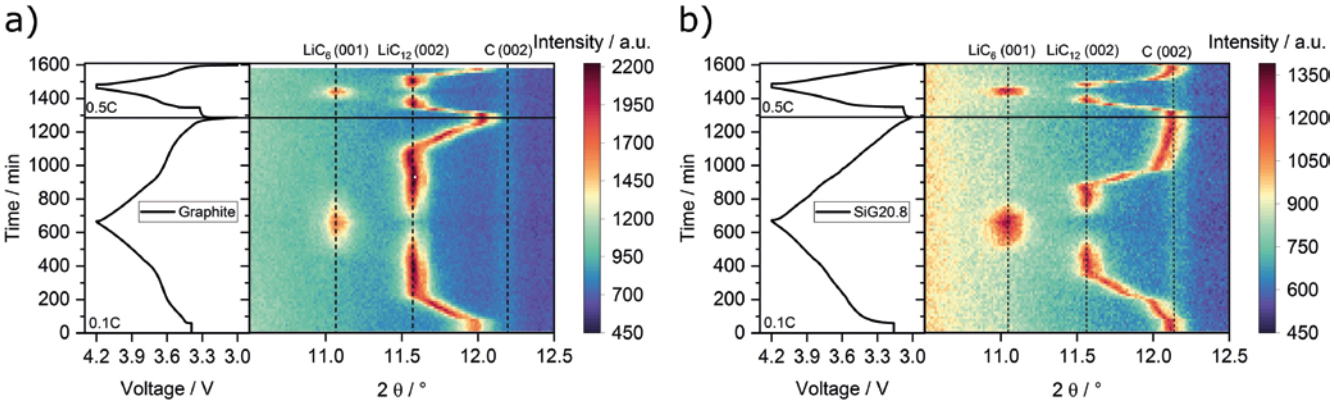

Figure 1: Contour plot representations of the operando XRD measurements for C/10 and C/2 for graphite (a) and silicon-graphite (b) (20.8 wt.-% Si = SiG20.8) pouch full cells. Reproduced with permission from reference [1] (CC-BY).

Workflows for detection of lithium plating in Li-ion batteries

T. Waldmann[1,2,3], I. Pivarníková[4], N. Paul[4], R. Gilles[4]

[1] Zentrum für Sonnenenergie- und Wasserstoff-Forschung Baden-Württemberg, Ulm, Germany; [2] Helmholtz Institute for Electrochemical Energy Storage, Ulm, Germany; [3] Institute of Surface Chemistry and Catalysis, Ulm University, Ulm, Germany; [4] Heinz Maier-Leibnitz Zentrum (MLZ), Technical University of Munich, Garching, Germany

In this collaborative study, we developed effective workflows for detecting, characterising and avoiding the critical aging mechanism of lithium deposition in lithium-ion cells. These workflows are based on complementary validated physico-chemical post-mortem and electrochemical analysis methods and can be applied to commercial cells to increase their cycle life.

The lifetime of lithium-ion batteries is limited by aging mechanisms on the material and electrode level. If the underlying main aging mechanisms are understood, they can be prevented, thereby offering the chance to increase the battery life-time. One critical aging mechanism is the unintended deposition of lithium metal on the anode and subsequent side reactions of electrolyte on the lithium metal surface, leading to capacity decrease and resistance increase.

Effective workflows and the importance of short rest times

In this collaborative study, we developed effective workflows i) for detecting the presence of lithium deposition (see Fig. 1) and ii) the locations of lithium deposition inside the cells, as well as iii) for finding operating conditions under which lithium deposition can be avoided. Regarding these workflows, it is important to bear in mind that deposited lithium can partly re-intercalate into the anode material during long rest times. Therefore the time between the end of an aging test and cell disassembly should be limited to a maximum of two hours. The workflows developed are based on validated complementary physico-chemical analysis methods, such as neutron depth profiling (NDP), glow discharge optical emission spectroscopy (GD-OES), optical microscopy (OM), scanning electron microscopy/energy dispersive X-ray spectroscopy (SEM/EDX) in post-mortem analysis and electrochemical methods. One interesting result is that lithium depositions occur mainly on the anode surface, which was confirmed by NDP carried out at the Nuclear Physics Institute in Rez near Prague, GD-OES depth profiling, in situ optical microscopy, and simulations.

Life-time extension by prevention of lithium plating

Lithium plating can be prevented by favourable combinations of the charging C-rate, end-of-charge-voltage and temperature, as well as by optimised fast-charging protocols. The developed workflows are valuable contributions to increasing the long-term usability, sustainability, and safety of lithium-ion batteries. Increased battery life can furthermore help reduce dependence on critical raw materials such as lithium and cobalt.

[1] T. Waldmann et al., Efficient workflows for detecting Li depositions in lithium-ion batteries, J. Electrochem. Soc. 171, 070526 (2024).
DOI: 10.1149/1945-7111/ad5ef8

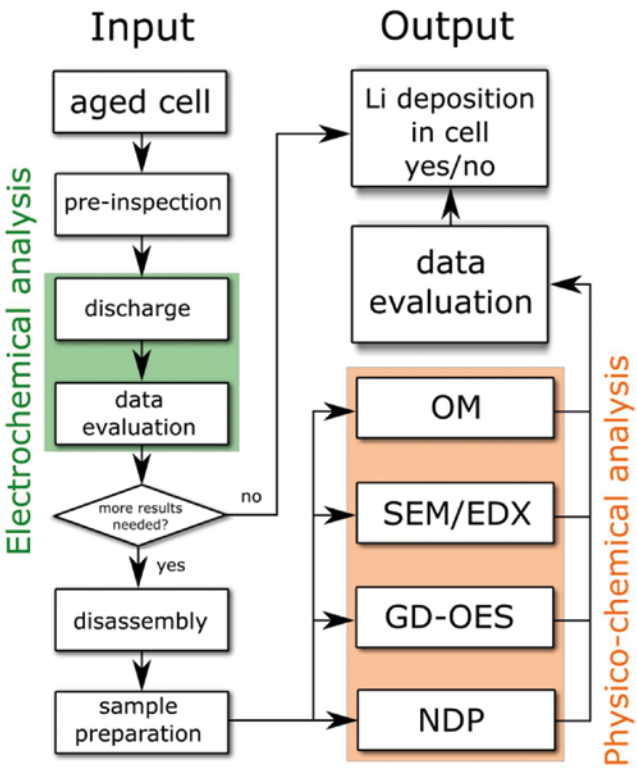

Figure 1: Workflow to address the question of whether Li deposition is present in an aged battery cell. Reproduced with permission from reference [1] (CC-BY).

Lithiation of aluminium anode-based Li-ion batteries and the impact of Al_2O_3 on the β-LiAl formation

T.A. Pham[1], R. Gilles[1]

[1] Heinz Maier-Leibnitz Zentrum (MLZ), Technical University of Munich, Garching, Germany

X-ray diffraction and neutron depth profiling are performed to study Al anodes at different lithiation degrees. The lithiation of Al foil is inhomogeneous as Li accumulates close to the interface between the electrode and separator and decreases towards the bulk. The addition of an Al_2O_3 passivation layer is investigated using high-precision electrochemical microcalorimetry and shows an increase in the nucleation energy.

Metal alloys such as LiAl are being explored as potential anode materials for Li-ion batteries due to their high capacity and cost-effectiveness. Al offers nearly three times the specific capacity (~993 mAh/g) compared to conventional graphite anodes. During lithiation, Al forms a solid solution with Li (α-LiAl phase). When the solubility limit is exceeded, it transitions into the β-LiAl phase.

XRD analysis of LiAl phases

In this study, Al electrodes were electrochemically lithiated in coin cells with Li metal as the counter electrode. Electrodes with 25% and 50% lithiation were compared, where 100% lithiation corresponds to pure β-LiAl. XRD measurements indicate that the 25% lithiated samples contain a greater proportion of α-LiAl. As expected, the fraction of β-LiAl increases with higher lithiation levels.

Lithium distribution study by NDP

Neutron depth profile measurements at NPI CAS Rez were performed to examine Li distribution. For the 50% sample, a concentration shoulder between 2–5 µm, followed by a decline, suggests β-LiAl formation (see Fig. 1). Beyond 5 µm, the concentration decreases more gradually, similar to the 25% sample, but remains higher. In the 25% sample, lithium concentration decreases from surface to bulk, indicating β-LiAl presence. The relatively constant bulk concentration suggests it consists mainly of α-LiAl. Additionally, lithium never reaches zero, confirming full-thickness lithiation. In the 50% sample, β-LiAl extends further into the bulk. Surface peaks indicate possible solid-electrolyte interphase formation, LiOH from the reaction of Li with ambient moisture or Li-Al-O glass formation.

Al_2O_3 at the anode surface

Furthermore, the native passivation layer, Al_2O_3, is thoroughly investigated using high-precision electrochemical microcalorimetry. Adding 25 nm of Al_2O_3 to the surface of the active material increases the nucleation energy barrier by 83% over the native oxide layer always present on the Al surfaces. However, the results indicate that the added Al_2O_3 does not negatively impact the reversibility, suggesting that removing Al_2O_3 is unnecessary for improving the cyclability of Al anode-based lithium-ion batteries.

[1] L. Wells et al., Unravelling the role and impact of alumina on the nucleation and reversibility of β-LiAl in aluminium anode based lithium-ion batteries, ChemElectroChem 11, e202400322 (2024)
DOI: 10.1002/celc.202400322

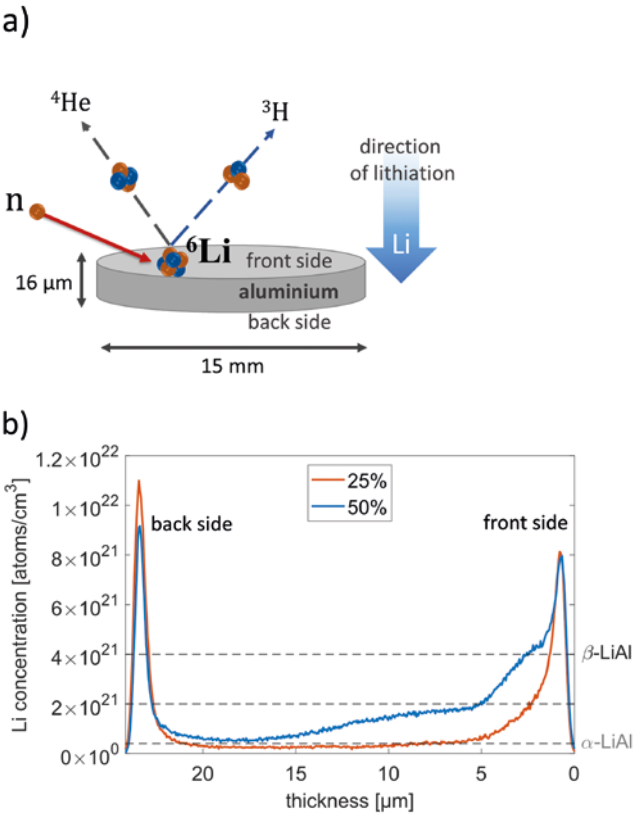

Figure 1: (a) Sketch of the NDP measurements on the lithiated Al electrodes. The Li atoms get activated by the neutrons and emit ^{3}H and ^{4}He particles, from which the Li concentration inside the sample as well as the depth position of the reaction can be deduced. (b) Li depth profile for the 25% and 50% lithiated electrodes.

Control of ion-channel structure for improved chemical stability of polymer electrolyte membranes

Y. Zhao [1], K. Yoshimura [1], J. Chen [1], S. Sawada [1], A. Radulescu [2], Y. Maekawa [1]

[1] Department of Advanced Functional Materials Research, Takasaki Institute for Advanced Quantum Science, National Institutes for Quantum Science and Technology (QST), Takasaki, Japan; [2] Jülich Centre for Neutron Science (JCNS) at MLZ, Forschungszentrum Jülich GmbH, Garching, Germany

This work presents a strategy for controlling the ion-channel structure and the local hydration number (λ_{local}) for improving the chemical stability of graft-type polymer electrolyte membranes, which is the major problem confronting their application in energy conversion devices such as fuel cells and electrolysers. The detailed structure and λ_{local} are determined by the partial scattering function (PSF) analysis using KWS-2 SANS diffractometer @ MLZ.

Radiation-grafted PEMs

Hydrocarbon-based polymer electrolyte membranes (PEMs) prepared using the radiation-induced graft polymerisation technique, which are less expensive and capable of achieving high performance, are a promising alternative for the benchmark material Nafion^R. In this work, we have prepared a series of radiation-grafted PEMs, consisting of poly(styrene sulfonic acid) grafted onto poly(ethylene-*co*-tetrafluoroethylene) (ETFE) base film with ion exchange capacities (IECs) ranging from 0.8 to 2.5 mmol/g, allowing for a significant variation in PEM properties such as conductivity, swelling, and chemical stability. We investigated the effect of ion-channel structure on the chemical durability and conductivity of these PEMs in order to provide structural design rules for preventing the degradation of hydrocarbon PEMs.

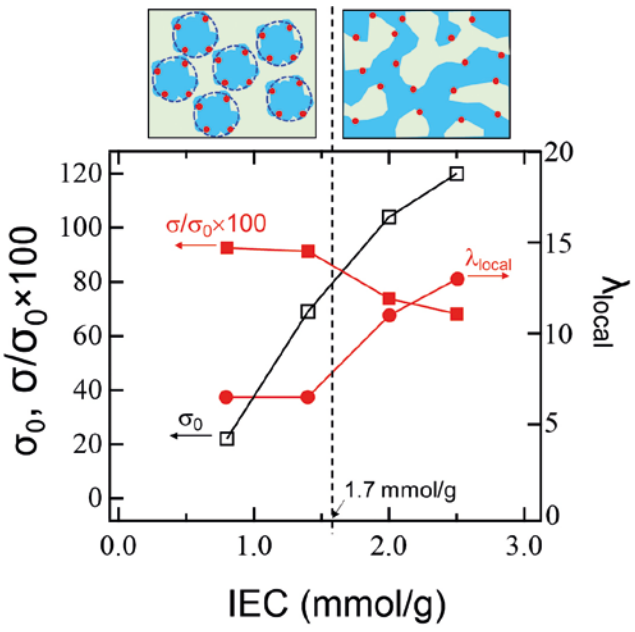

Figure 1: The initial conductivity (σ_0 with the unit of mS/cm, open squares), relative conductivity ($\sigma/\sigma_0 \times 100$ with the unit of %, solid squares) in Fenton test for 24 h, and λ_{local} (solid circles) of PEMs as a function of IEC.

Structure-stability correlation

Using PSF analysis through contrast-variation small angle neutron scattering, we revealed that the detailed ion-channel structure of these PEMs undergoes a morphological transition from a spherical to a bicontinuous structure at IEC of ~1.7 mmol/g (see Fig. 1) [1]. Beyond that, we pointed out that the spherical and bicontinuous ion-channel structures are the origin of low and high λ_{local} (~6.5 and >10) in these PEMs, where λ_{local} is defined as the number of water molecules surrounding ionic groups in ion-channels. We then evaluated the PEM chemical stability that is characterised by conductivity loss in the accelerated Fenton test, and found that stability can be dramatically improved by the control of the ion-channel structure and λ_{local}. That is, good PEM stability can be achieved at IEC < 1.7 mmol/g, with spherical ion-channels and λ_{local} ~6.5, because this structure maintains less water around SO_3H groups and effectively prevents the access of peroxy radicals to both the hydrophobic polystyrene and ETFE base polymer to degrade the PEMs. However, a further increase in IEC results in an increase in λ_{local}, leading to a morphological transition from spherical to bicontinuous-shaped ion-channels and a severe decrease in stability. Therefore, we propose that additional cross-linking in PEMs with high IEC will effectively suppress the membrane hydration level down to λ_{local} ~6.5, thereby achieving good membrane chemical stability while maintaining good conductivity.

The work offers practical guidelines for improving the most important macroscopic (or bulk) properties of PEMs such as conductivity and stability through structural control.

[1] K. Yoshimura et al., Structural factors for the chemical stability of graft-type polymer electrolyte membranes evaluated from the local hydration number, ACS Appl. Polym. Mater. 6, 13585-13593 (2024)
DOI: 10.1021/acsapm.4c02232

In situ positron annihilation spectroscopy during tensile tests on Al alloys

C. Hugenschmidt[1], M. Thalmayr[1], T. Gigl[1]

[1] Heinz Maier-Leibnitz Zentrum (MLZ), Technical University of Munich, Garching, Germany

We present a materials analysis method to enable in situ Doppler broadening spectroscopy (DBS) of the 511 keV annihilation line in matter during tensile tests. This technique permits the correlation between the formation of lattice defects on an atomic scale and the macroscopic physical materials properties stress and strain. In AlMg3 (3.3535) and AlMgSi (3.3206), we observed the onset of plastic deformation through changes in the DBS spectra due to positron trapping in (open-volume) defects formed by applying mechanical load.

The characterisation of the microstructure and the detection of defects in technical alloys during or after mechanical load is crucial for the optimisation of materials in all kinds of engineering applications. Plastic deformation leads to the formation of dislocations and vacancies which efficiently trap thermalised positrons. Doppler-broadening spectroscopy (DBS) of the positron annihilation line is a defect-sensitive analysis technique that provides valuable information about such open-volume lattice defects.

Upgrade of the CDB spectrometer

We designed a tensile-test device (see Fig. 1) which is operated at high sample voltage (for positron acceleration) inside the UHV sample chamber of the CDB spectrometer at NEPOMUC in order to enable in situ DBS on samples during tensile tests. The positron beam is typically implanted with an energy of 30 keV in order to probe bulk properties during deformation of the sample. Compared to conventional experiments “off situ”, the new device offers several advantages: (i) for a single sample, information on stress, strain and defects created on an atomic level are obtained simultaneously, (ii) the time-consuming need to change many samples is avoided, and finally (iii) a large number of data points is recorded without relaxation of the sample.

Correlation of macroscopic properties with atomic-scale defects

To demonstrate the capabilities of this new technique and to observe the formation of lattice defects, we performed exemplary in situ DBS during tensile tests on two technical alloys AlMgSi and AlMg3. The successful operation of in situ DBS was demonstrated by observing the onset of plastic deformation on an atomic level and its correlation to the stress applied.

In DBS the defect density is commonly quantified by the defect-sensitive S parameter. During mechanical load, a significant increase in the S value was observed as a function of applied stress. In particular, the onset of S parameter increase is observed at the same stress level of about 48(4) N/mm^2 for both Al alloys. This observation is consistent with previous (ex situ) studies on deformed Al samples. The (reversible) elastic elongation at very small stress, however, does not lead to changes in DBS spectra, indicating its selective sensitivity to plastic strain.

[1] C. Hugenschmidt et al., In situ positron annihilation spectroscopy during tensile tests on Al alloys, Appl. Phys. A 130, 147 (2024)
DOI: 10.1007/s00339-024-07301-4

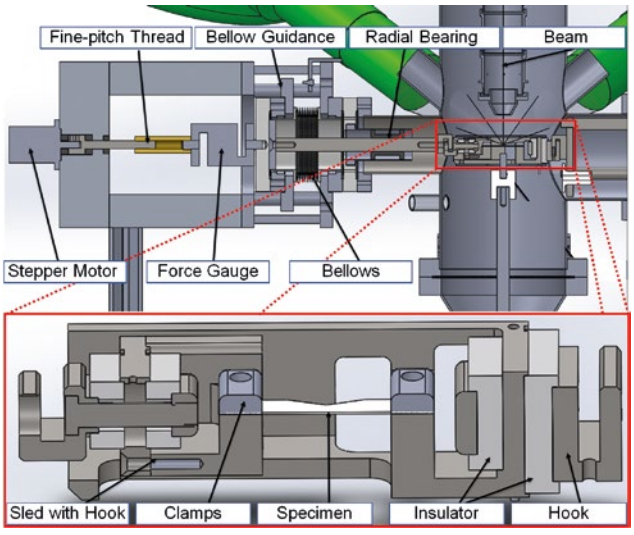

Figure 1: Cross section of the tensile machine: The zoom shows the central part of the device, which can be hooked in its position via the bottom port of the CDBS sample chamber. The sled and the guidance profile offer clamps that grip a flat specimen. The sled and all moving components are pulled/pushed by a stepper-motor powered bolt which screws in/out a counter-thread. The mechanical load is measured by a force gauge mounted air-sided at the blind flange.

Surface and near-surface positron annihilation spectroscopy at very low positron energy

L. Mathes [1,2], M. Suhr [1], V.V. Burwitz [2], D. Russell [1], S. Vohburger [1], C. Hugenschmidt [1]

[1] Heinz Maier-Leibnitz Zentrum (MLZ), Technical University of Munich, Garching, Germany;
[2] Department of Physics, TUM School of Natural Sciences, Technical University of Munich, Garching, Germany

We present a monoenergetic positron beam tailored for (near-) surface positron annihilation spectroscopy. The Setup for LOw-energy Positron Experiments (SLOPE) now allows the use of positron implantation energies ranging from 3 eV to 40 keV. At low energies (< 20 eV), the count rate is ~4400 s^{-1}, and the beam diameter is below (12 ± 3) mm. Exemplary studies on boehmite show that positronium formation peaks at 10 eV, consistent with the hydrogen ionisation energy.

SLOPE key components and design features

We present the Setup for LOw-energy Positron Experiments (SLOPE), a dedicated system for surface and near-surface positron annihilation spectroscopy [1]. An overview of SLOPE is shown in Fig. 1. Designed to meet the growing demand for precise investigations of material surfaces and interfaces, SLOPE offers positron implantation energies ranging from 3 eV to 40 keV. It features a high-activity ^{22}Na source, tungsten moderator, and an adiabatic beam guidance. The experimental setup further includes an ultra-high vacuum system with a separate positron source and sample chamber, two HPGe detectors for coincidence Doppler-broadening spectroscopy (CDBS), and a movable sample holder. The beam guidance system employs adiabatic compression via an Fe pin at the sample position, which reduces the beam diameter to less than (12 ± 3) mm at low energies. The system achieves a count rate of approximately 4400 counts per second independently from the positron implantation energies, supporting fast high-precision measurements.

Benchmark measurements and case studies

Phase space simulations using COMSOL Multiphysics® were conducted to model magnetic and electric fields, optimise beam guidance, and minimise the transverse momentum spread. Measurements show good agreement with the simulations. To showcase SLOPE's capabilities, studies on positronium (Ps) formation at a hydrogen-terminated boehmite surface were conducted. The Ps formation peaks at a kinetic positron energy of 10 eV, corresponding to the hydrogen ionisation energy of 13.6 eV, as predicted by the Ore gap model. Studies on copper demonstrate SLOPE's depth-resolved CDBS capabilities, showing enhanced background suppression through coincidence methods.

SLOPE's future applications include the study of complex surfaces, an understanding of Ps formation mechanisms, and the advance of surface physics. With its combination of precision and versatility, SLOPE offers new opportunities for positron beam experiments in surface and near-surface regions.

[1] L. Mathes et al., Surface and near-surface positron annihilation spectroscopy at very low positron energy, J. Instrum. 19, P11026 (2024)
DOI: 10.1088/1748-0221/19/11/P11026

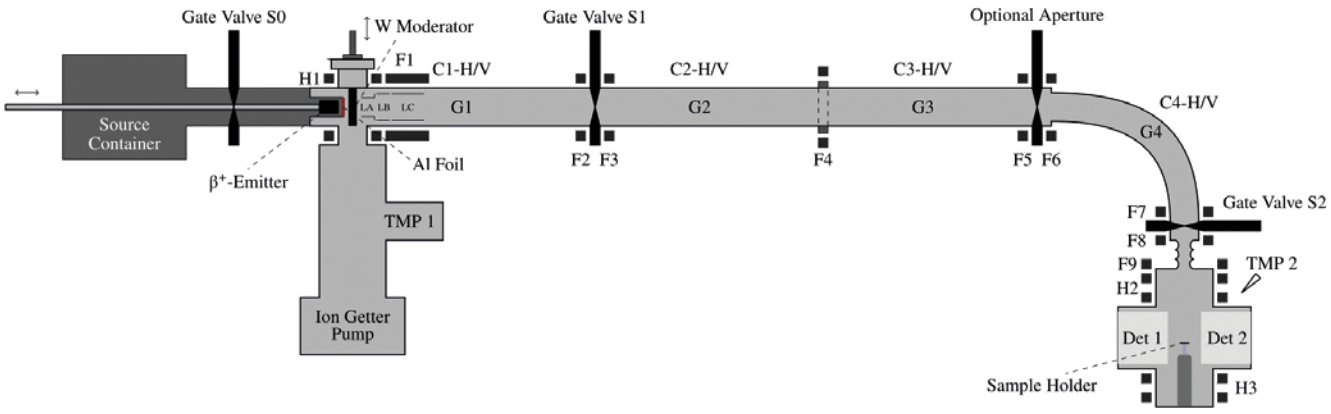

Figure 1: Schematic drawing of SLOPE. LA, LB, and LC denote the cylindrical acceleration and beam formation electrodes. Solenoids, Helmholtz coil pairs, and flange coils for magnetic beam guidance are labelled G, H, and F, respectively. Transverse magnetic fields are applied by saddle coils (CH and CV) to compensate for the earth's magnetic field and the curvature drift. (Lead shielding not shown.)

Proton beam based production of positron emitters by exploiting the $^{27}Al(p,x)^{22}Na$ reaction

L. M. Krug[1], L. Cryssos[1], J. Bundesmann[2], A. Dittwald[2], G. Kourkafas[2], A. Denker[2], C. Hugenschmidt[1]

[1] Heinz Maier-Leibnitz Zentrum (MLZ), Technical University of Munich, Garching, Germany;
[2] Helmholtz-Zentrum Berlin für Materialien und Energie, Proton Therapy, Berlin, Germany

We present the production of positron sources based on the $^{27}Al(p,x)^{22}Na$ reaction by irradiation of Al with a 68 MeV proton beam. A simple target consisting of a stack of Al discs allows the direct use of the discs as positron emitters and the production of multiple sources at the same time. The concept presented here can easily be adapted for the production of stronger ^{22}Na sources by increasing the proton current or/and the irradiation time.

Simulation of ^{22}Na formation

Positron sources are essential for Positron Annihilation Spectroscopy (PAS) used as a non-destructive analysis technique, which is extremely sensitive to lattice defects. A widely used β^+ emitter is ^{22}Na, but the availability is limited. Based on our simulations, we have designed an Al target with which we can produce multiple ^{22}Na sources simultaneously by proton irradiation.

The stopping of protons in Al was simulated using SRIM to estimate the penetration depth and radial distribution of the protons as well as their energy loss in the target. The depth dependent proton energy and the energy dependent cross section for the $^{27}Al(p,x)^{22}Na$ reaction were combined to predict the ^{22}Na production in the target. The target consists of a stack of 66 circular, 0.3 mm thick aluminium discs with a diameter of 20 mm. In this way, we generate several sources at once and can measure the depth distribution of the generated ^{22}Na to compare it to the simulation.

From Al discs to positron emitters

The target was irradiated with a proton beam of 100 nA for 3 hours, which resulted in the production of 140(06) kBq of ^{22}Na spread over 55 discs. Further long-lived nuclides, such as ^{7}Be, ^{48}Sc, ^{54}Mn, ^{51}Cr and ^{56}Co, were produced, but their activity was shown to be negligible 15 days after the irradiation. The production of these radionuclides, apart from ^{7}Be, can easily be prevented by using Al of a higher purity.

The count rate of each disc was measured in order to determine the depth dependent ^{22}Na activity (see Fig. 1). The measurement result was used to calculate a revised cross-section for the $^{27}Al(p,x)^{22}Na$ reaction, which deviates from the literature values in the range of 27–40 MeV.

Our approach inherently avoids wet chemical processes as usually applied in the commercial production of carrier-free ^{22}Na. However, for future application as positron emitters, thinner discs must be used to minimise positron self-absorption. The concept presented here can easily be adapted to produce stronger ^{22}Na sources by increasing the proton current or/and the irradiation time.

[1] L.-M. Krug et al., Proton beam based production of positron emitters by exploiting the $^{27}Al(p,x)^{22}Na$ reaction, Nucl. Instrum. Methods Phys. Res. Sect. B 555, 165488 (2024) DOI: 10.1016/j.nimb.2024.165488

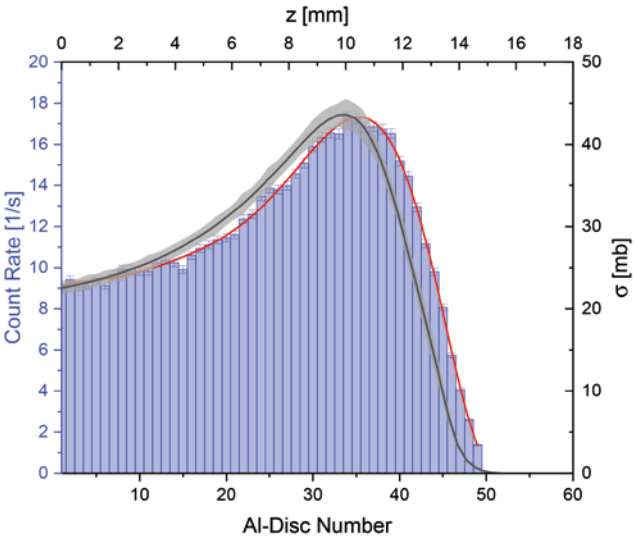

Figure 1: Count rate of the 1275 keV photo peak of ^{22}Na as a function of the disc number, i.e. target depth (blue). The fit to the data (red) and the simulated ^{22}Na distribution (black line; error margin as grey shading) have the same shape and maximum. The offset of about 1.5 mm toward greater depth is attributed to the uncertainty of the cross-section values taken for the simulation.

Design of a pilot-scale microwave freeze dryer for in situ neutron imaging

M. Hilmer[1], S. Gruber[1], Z. Kis[2], M. Schulz[3], P. Foerst[1]

[1] Food Process Engineering, TUM School of Life Sciences, Technical University of Munich, Freising, Germany; [2] HUN-REN Centre for Energy Research, Budapest, Hungary; [3] Heinz Maier-Leibnitz Zentrum (MLZ), Technical University of Munich, Garching, Germany

This article discusses the development of a pilot microwave freeze-dryer for in situ neutron imaging. Combining volumetric microwave energy input with continuous mixing can shorten process times drastically as compared to conventional freeze-drying. In situ neutron imaging was performed to understand the process. Initial tests showed promising results, indicating the potential for significant insights into this specific drying process.

Freeze-drying and possible enhancements

Traditional freeze-drying methods are often inefficient, taking a long time and incurring high costs due to poor heat and mass transfer performance. Therefore, a new approach combines microwave energy, where the heat transfer resistance can be overcome by volumetric heating, with continuous mixing to enhance uniformity and facilitate the removal of water vapor. The article presents the development of a pilot-scale dynamic microwave freeze-dryer designed for in situ neutron imaging. The enhanced procedure aims to improve the drying process of sensitive products in the food and pharmaceutical industries. Neutron imaging is employed to monitor the drying process in detail, as this method is highly sensitive to the hydrogen content in materials and, therefore, can give insights into the drying process.

Monitoring the kinetics of freeze-drying

In situ measurements were performed at the Budapest Neutron Centre, yielding promising results. The 2D images of bulk samples generated with different particle sizes and rotational speeds provided insights into how moisture is removed from the product, highlighting the local drying kinetics within the bulk material (Fig. 1). This information is crucial for understanding and optimising the microwave freeze-drying process, ensuring products are dried uniformly and efficiently.

Overall, the results generated by the pilot-scale in situ microwave freeze-dryer developed, combined with neutron imaging, are a significant step forward in freeze-drying technology.

[1] M. Hilmer et al., Design of a pilot-scale microwave freeze dryer for in situ neutron imaging, Rev. Sci. Instrum. 95, 083704 (2024)
DOI: 10.1063/5.0213685

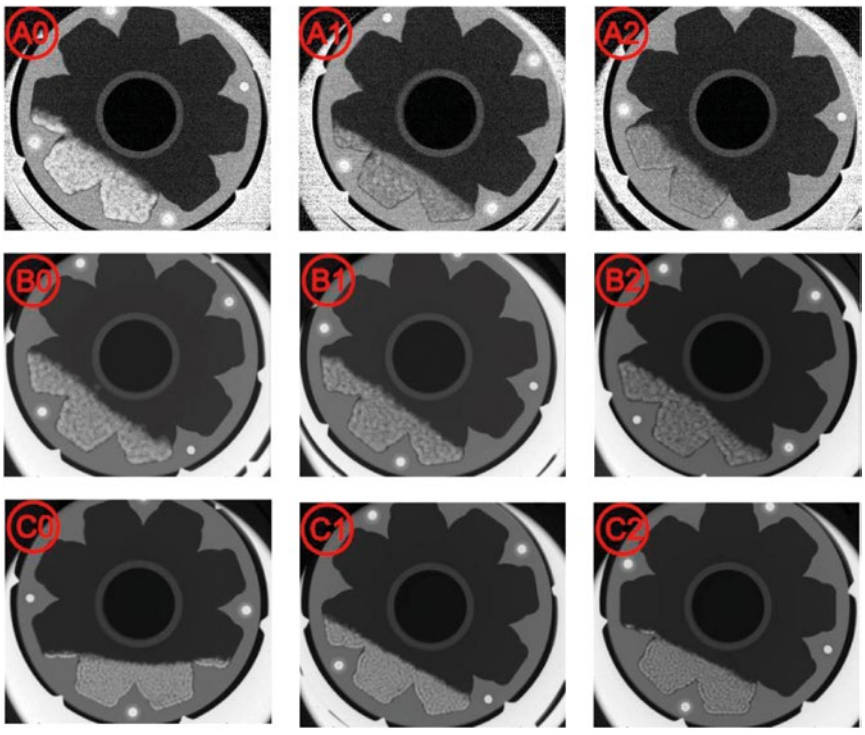

Figure 1: Resulting images (after image correction) of three different experiments: low-resolution continuous imaging (A0–A2), high-resolution interval (B0–B2), and high-resolution small particles (C0–C2). Bright grey equals high absorption and, therefore, high D_2O content.

The aescin-induced decomposition of DMPC vesicles to bicelles is related to the lipid's main phase transition: Direct evidence by using chain-deuterated lipid and SANS

C. Dargel [1,2], L. H. Moleiro [1,3], A. Radulescu [4], T. J. Stank [1], T. Hellweg [1]

[1] Physical and Biophysical Chemistry, Bielefeld University, Bielefeld, Germany; [2] Institute of Physical Chemistry, University of Münster, Münster, Germany; [3] Department of Physical Chemistry, Complutense University, Madrid, Spain; [4] Heinz Maier-Leibnitz Zentrum (MLZ), Technical University of Munich, Garching, Germany

The decomposition of larger sheets or closed vesicles into bicelles upon temperature decrease is investigated for a system containing the phospholipid 1,2-dimyristoyl-*sn*-glycero-3-phosphocholine (DMPC) and the saponin β-aescin using small-angle neutron scattering (SANS). This process is found to be linked to the main phase transition of the lipid, as revealed by comparing DMPC with its chain-deuterated analogue, d54-DMPC.

Due to its unique amphiphilic character, aescin is able to decompose DMPC membranes. This study examines a binary system comprising DMPC, its chain-deuterated analogue d54-DMPC, and the biosurfactant aescin. The deuterated DMPC has a significantly lower main phase transition temperature T_m, making it possible to study the influence of the main phase transition of the used lipid on the interaction with aescin.

Deuterated lipid for studying T_m-dependent processes

To our knowledge, this is the first study to exploit the shifted T_m of a deuterated lipid to reveal a correlation with a T-dependent structural reorganisation in a lipid-based system. At $T < T_m$ and an aescin concentration exceeding the critical micelle concentration, the presence of bicelles rim-stabilised by aescin molecules was confirmed by SANS experiments at KWS-2. Temperature-dependent turbidimetry, as well as SANS measurements, showed that the general sequence of structures formed remains unchanged despite lipid deuteration.

Vesicle-to-bicelle decomposition is T_m-correlated

Upon heating to $T > T_m$, model-dependent fitting reveals a pronounced enlargement of the bicelles in a preferred direction due to the removal of aescin molecules. Whilst high aescin contents (30 mol%) yield relatively modest bicelle growth, intermediate contents (16 mol%) give rise to significantly larger sheets. The sheet asymmetry diminishes for even lower contents and closed vesicles form, as confirmed by SANS measurements on DMPC- and d54-DMPC-based aggregates containing 10 mol% aescin. The results suggest the formation of a trapped state, which appears to be correlated with the lipids T_m. Furthermore, it was shown that the decomposition of vesicles into bicelles requires the membrane to be fully in the rigid phase state. Hence, our findings demonstrate a direct link between the lipid's main phase transition and the vesicle-to-bicelle relaxation, as evidenced by the temperature-shift of the structural transition, which matches the T_m-difference between DMPC and d54-DMPC (see Fig. 1).

[1] C. Dargel et al., Decomposition of mixed DMPC-aescin vesicles to bicelles is linked to the lipid's main phase transition: A direct evidence by using chain-deuterated lipid, J. Colloid Interface Sci. 679B, 209-220 (2025)
DOI: 10.1016/j.jcis.2024.10.074

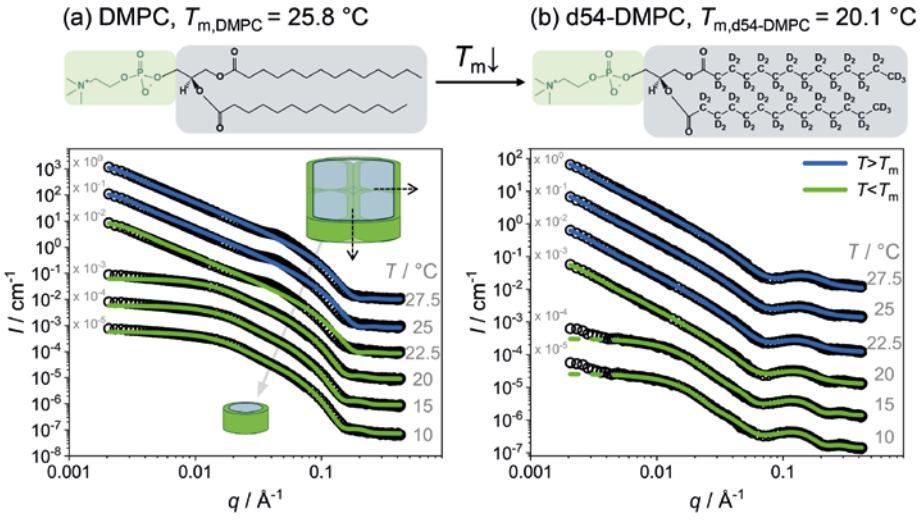

Figure 1: SANS data for (a) DMPC and (b) d54-DMPC with 10 mol% aescin, acquired through stepwise cooling. Model fits reveal a striking transformation: at $T > T_m$, extended sheets emerge from vesicles, whilst at $T < T_m$, small bicelles form. In both cases, the final relaxation step occurs significantly below T_m. Thus, a clear correlation between the vesicle-to-bicelle transition and the lipid's main phase transition is demonstrated.

Protein stabilised emulsions: β-lactoglobulin at the interface of triacylglyceride-oil and water

T. Heiden-Hecht[1], B. Wu[1], Kuno Schwärzer[2], S. Förster[1,2], J. Kohlbrecher[3], O. Holderer[1], H. Frielinghaus[1]

[1] Jülich Centre for Neutron Science (JCNS) at MLZ, Forschungszentrum Jülich GmbH, Garching, Germany; [2] Jülich Centre for Neutron Science (JCNS-1), Forschungszentrum Jülich GmbH, Jülich, Germany; [3] Paul Scherrer Institut, Villingen, Switzerland

Protein shape is predicted to change during interfacial adsorption below the monolayer concentration, known as the critical interfacial concentration (CIC). Contrast variation SANS experiments via deuterated triacylglyceride-oil performed on SANS-I@SINQ, PSI, and complementary β-lactoglobulin (β-LG) concentration dependent SAXS experiments at KWS-X at the MLZ provided insight into oil droplet radius, interfacial coverage and protein structure using scattering models and low-resolution shape reconstruction.

The formulation of protein stabilised emulsions

Emulsions are biphasic and often thermodynamically unstable systems, which are stabilised by amphiphilic components such as proteins. Protein-stabilised emulsions are widely used in food, cosmetic and pharmaceutical applications due to their ability to improve texture, stability and shelf-life. Important characteristics of emulsions are captured by the oil droplet size, and the interfacial properties. For proteins, the interfacial properties include: the migration to the interface, the adsorption at the interface, and the resulting interfacial arrangement and unfolding including the interfacial layer thickness, packing and rheology. These interfacial properties strongly depend – beside other factors – on external parameters such as pH or ionic strength, and protein concentration. The external parameters determine the protein organisation in e. g., dimers or monomers. The protein concentration determines the interfacial packing and interfacial unfolding whereby the CIC displays the protein concentration to cover the entire oil/water interface with an unfolded protein monolayer. It is believed that, above the CIC, proteins form multilayers at the oil/water interface.

The characterisation features of small-angle scattering

SANS and SAXS experiments made it possible to determine the interfacial structure below and above the CIC, as well as oil droplet radius and interfacial coverage [1]. These findings were identified via Q^{-4} Porod scattering and Q^{-2} scattering of the interface at low Q, and the protein scattering at higher Q. The two power laws revealed the otherwise poorly understood interfacial coverage. The higher-Q protein scattering uncovers the low-resolution real space protein structure using the DENFERT algorithm (see Fig. 1). Since SANS with accurate contrast variation highlights the interface in comparison to other techniques such as FTIR, the results presented offer high precision and an impetus to understand interfaces in emulsions.

[1] T. Heiden-Hecht et al., New insights into protein stabilised emulsions captured via neutron and X-ray scattering: An approach with β-lactoglobulin at triacylglyceride-oil/water interfaces, J. Colloid Interface Sci. 655, 319 (2024)
DOI: 10.1016/j.jcis.2023.10.155

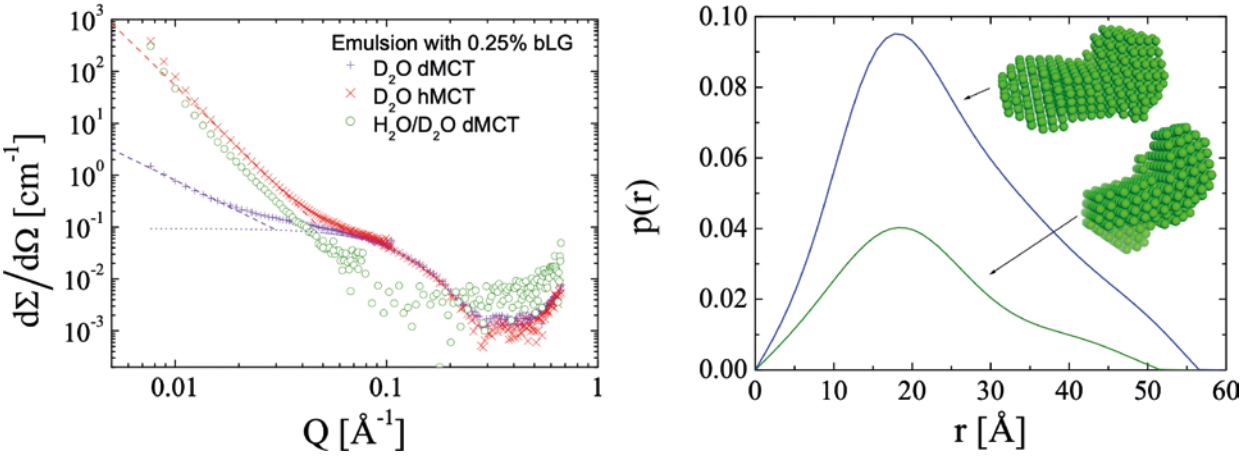

Figure 1: (left) SANS scattering patterns of β-LG stabilised emulsions with 0.25% protein concentration. The different contrasts refer to protein (purple symbols), decorated droplet (red symbols) and full droplet contrast (green symbols). The abbreviation MCT medium-chain-triacylglyceride. The dashed lines indicate the classical Porod scattering (red) and the interface coverage scattering (purple). The horizontal dotted line indicates the protein forward scattering. (right) Pair distance distribution functions and real space reconstruction, using the DENFERT algorithm, from the corrected SANS scattering patterns of β-LG stabilised emulsions with 0.25% (black) and 0.50% (blue) protein concentration.

Testing mixing rules in multi-component crowded protein solutions

A. Gulotta[1], S. Bucciarelli[1], F. Roosen-Runge[1], O. Holderer[2], P. Schurtenberger[1], A. Stradner[1]

[1] Division of Physical Chemistry, Lund University, Lund, Sweden;
[2] Jülich Centre for Neutron Science (JCNS) at MLZ, Forschungszentrum Jülich GmbH, Garching, Germany

Crowding effects significantly influence the phase behaviour and the structural and dynamic properties of concentrated protein mixtures, undermining the ability to predict their solution behaviour. We combine a number of experimental techniques, including neutron spin echo spectroscopy, covering a very large range of length and time scales and test the applicability of simple mixing rules to predict the solution properties of protein mixtures.

The new twist of protein mixtures

Highly concentrated protein mixtures as present in the cytoplasm or in the blood serum pose enormous challenges for our theoretical understanding and our ability to predict the behaviour of these systems. Here, we test the applicability of simple mixing rules to predict the solution properties of binary mixtures of the well-characterised bovine eye lens proteins alpha- and gammaB-crystallin. Combining observations of the phase behaviour via microrheology, static and dynamic light scattering, small-angle X-ray scattering, and neutron spin echo (NSE) spectroscopy using the J-NSE instrument, we obtain a multi-scale characterisation of the mixtures over a very large range of length and time scales.

We focus on macroscopic quantities such as the location of phase boundaries, osmotic compressibility and zero shear viscosity, properties on mesoscopic length scales such as the gradient diffusion coefficient, and finally structural and dynamic quantities on local length scales such as the static structure factor and the local short-time collective diffusion coefficient, D(q). We define different mixing rules for these properties that are based on the same underlying principle: There is no specific interaction between different species other than excluded volume effects, and we estimate the measured quantities from a weighted sum of the properties of the individual proteins at an effective volume fraction that considers the accessible volume due to the presence of other protein species.

High sensitivity of D(q) on protein-protein interaction potentials between like and unlike species

The proposed mixing rules allow for a reasonably accurate description of the measured properties for macroscopic and mesoscopic signatures, while those related to processes on length scales of the individual proteins, such as the local short-time diffusion coefficient D(q) from NSE (see Fig. 1), show qualitative similarities with the predictions but will require more information on cross-component interactions to obtain quantitative agreement.

[1] A. Gulotta et al., Testing mixing rules for structural and dynamical quantities in multi-component crowded protein solutions, APL Bioeng. 8, 026116 (2024)
DOI: 10.1063/5.0204201

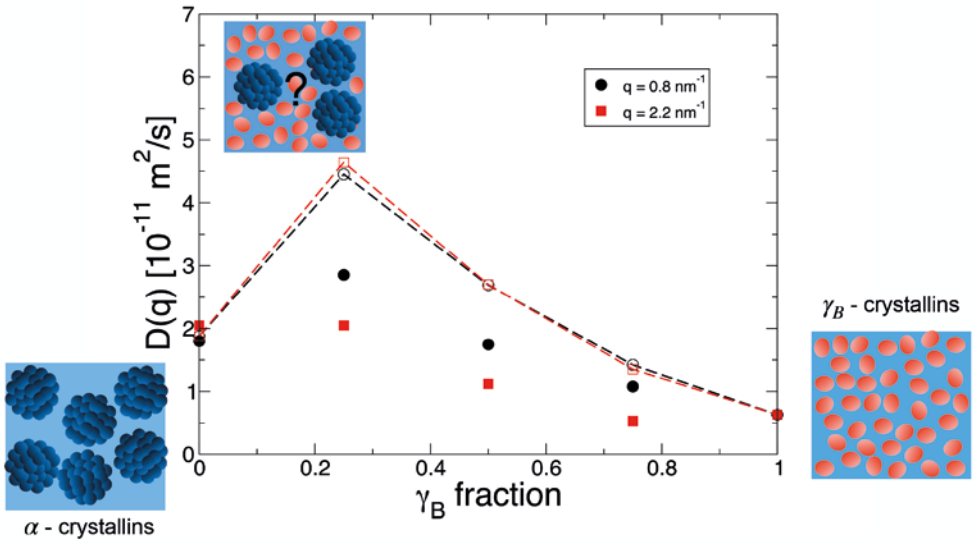

Figure 1: Collective diffusion on the local scale: Diffusion coefficients D(q) from NSE in mixtures of alpha- and gammaB-crystallin as a function of the relative protein composition for two q-values, corresponding to the local protein length scale (black: q=0.8 nm^{-1}; red: q=2.2 nm^{-1}). Solid symbols are measured and open symbols calculated values. Dashed lines are guides to the eye. All data were measured at 35°C and the total protein volume fraction is 0.22.

Dynamical properties of different variants of the orange carotenoid protein

M. Hajizadeh[1], M. Golub[1], M. Moldenhauer[2], W. Lohstroh[3], T. Friedrich[2], J. Pieper[1]

[1] Institute of Physics, University of Tartu, Tartu, Estonia; [2] Institute of Chemistry, Technische Universität Berlin, Berlin, Germany; [3] Heinz Maier-Leibnitz Zentrum (MLZ), Technical University of Munich, Garching, Germany

The orange carotenoid protein (OCP) is of crucial importance in protecting the cyanobacterial photosynthetic apparatus against photodamage. We investigated the dynamics of OCP wild type and two mutants whose structures emulate dark-adapted and active states, respectively. We find that the dynamics of the active state is significantly enhanced due to a larger number of solvent exposed protein residues, which makes important structural adaptations possible.

OCP plays a pivotal role in the protection of the cyanobacterial photosynthetic apparatus against photodamage. Once it senses high light conditions, OCP has to perform a structural change from a compact dark-adapted form characterised by an orange colour to an active form having a red colour. Proteins often require a specific dynamical flexibility to undergo such structural changes in order to carry out their function. The latter dynamics can be directly measured by quasielastic neutron scattering (QENS), as demonstrated here for three variants of OCP.

Structure-dynamics-function relationship in OCPs

Using QENS, we investigated the dynamics of the OCP wild type (OCPwt) in comparison with that of two mutant forms, which mainly differ in their structures. The compact structure of the OCPwt monomer is shown in Fig. 1A. It is composed of two protein domains that jointly encapsulate a carotenoid molecule as a pigment. The orange mutant OCP-MO is assumed to have a compact structure similar to that of the compact dark-adapted state (Fig. 1B), while the pink mutant OCP-MP appears to reflect the more elongated structure of the red active state of OCP (Fig. 1C). Our study reveals that the dynamic flexibility of all OCP variants is suppressed upon temperature decrease (Fig. 1D for OCPwt), but also differs depending on the structure of each of the three OCP variants (Fig. 1E). In particular, the dynamics of the mutant OCP-MP reflecting the structure of the red active state of OCP is significantly enhanced. We attribute this effect to a larger number of solvent exposed protein residues at the enlarged surface of the protein. However, OCPwt and the compact mutant also exhibit a different dynamic attributed to a missing H-bond between pigment and protein resulting in a de-stabilisation of the surrounding protein.

Finally, OCP has to rearrange its active state structure (Fig. 1C) to bind to the photosynthetic apparatus and, eventually, to convert absorbed excess energy into heat. The latter rearrangement is, thus, facilitated by the higher flexibility observed.

[1] M. Hajizadeh et al., The dynamical properties of three different variants of the orange carotenoid protein: A quasielastic neutron scattering study, Crystals 14, 361 (2024)
DOI: 10.3390/cryst14040361

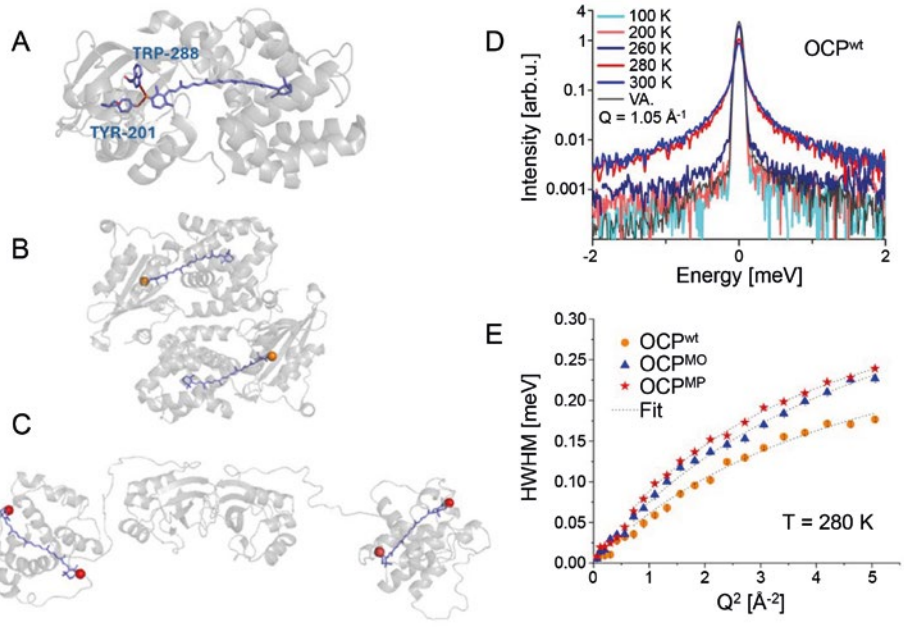

Figure 1: Panel A: X-ray structure of OCPwt (PDB code 7qd0) indicating the two H-bonds formed between the protein and the carotenoid. Panel B: Simulated structure of the mutant OCP-MO. Panel C: Simulated structure of the mutant OCP-MP. Panel D: Quasielastic neutron scattering spectra of OCPwt obtained at a resolution of 80 μeV and Q = 1.05 Å^{-1}. Panel E: Widths of the Lorentzian fit function describing internal protein motions.

Thermal transitions of self-assembled NIPAM-DMA copolymers with varying composition profiles

B. Farias-Mancilla[1], H. Frielinghaus[2], S. Harrison[1], B. Lonetti[1]

[1] Laboratoire Softmat, Université de Toulouse, Toulouse, France;
[2] Jülich Center for Neutron Science (JCNS) at MLZ, Forschungszentrum Jülich GmbH, Garching, Germany

The response of five copolymers with the same molar mass and chemical composition, but with different composition profile, were studied in aqueous solution against temperature. Using complementary analytical techniques, structural properties at different length scales were probed, from the molecular scale with nuclear magnetic resonance (NMR) to the colloidal scale with dynamic light scattering (DLS) and small-angle neutron scattering (SANS) measured at KWS-1.

The new twist of gradient copolymers

The thermoresponsive poly(N-isopropyl acrylamide) (PNIPAM) is soluble in water up to ca. 32°C; above this temperature, known as cloud point temperature, PNIPAM chains undergo dehydration, collapse and precipitate from aqueous solution. This lower critical solution temperature (LCST) behaviour in a biological temperature range makes it an appealing stimuli-responsive system for biomedical applications. Aqueous solutions of diblock copolymers containing a LCST segment and a hydrophilic segment undergo micellization upon heating, while triblock copolymers comprising two LCST blocks connected by a central hydrophilic block form gels if appropriately concentrated, or flowerlike micelles in a dilute regime. Broad transitions are frequently associated with gradient copolymers and are accompanied by modification of the self-assemblies in solution.

Transition from star-like to crew-cut micelles

NMR and SANS investigations strengthen each other and allow a clear picture of the change of copolymer solubility and related copolymer self-assembly as a function of temperature [1]. At the molecular scale, dehydrating NIPAM units drag N,N-dimethyl acrylamide (DMA) moieties with them in a gradual collapse of the copolymer chain; this induces a morphological transition of the self-assemblies from star-like nanostructures to crew-cut micelles (Fig. 1a and 1b). Interestingly, the transition spans a temperature range which depends on the monomer distribution profile in the copolymer chain, with the asymmetric triblock copolymer specimen revealing the broadest one. We have shown that the broad morphological transitions associated with gradient copolymers can be mimicked and even surpassed by the use of stepwise gradient (asymmetric) copolymers, which can be more easily and reproducibly synthesised than linear gradient copolymers.

[1] B. Farias-Mancilla et al., Morphology and thermal transitions of self-assembled NIPAM-DMA copolymers in aqueous media depend on copolymer composition profile, J. Colloid Interface Sci. 662, 99 (2024)
DOI: 10.1016/j.jcis.2024.02.032

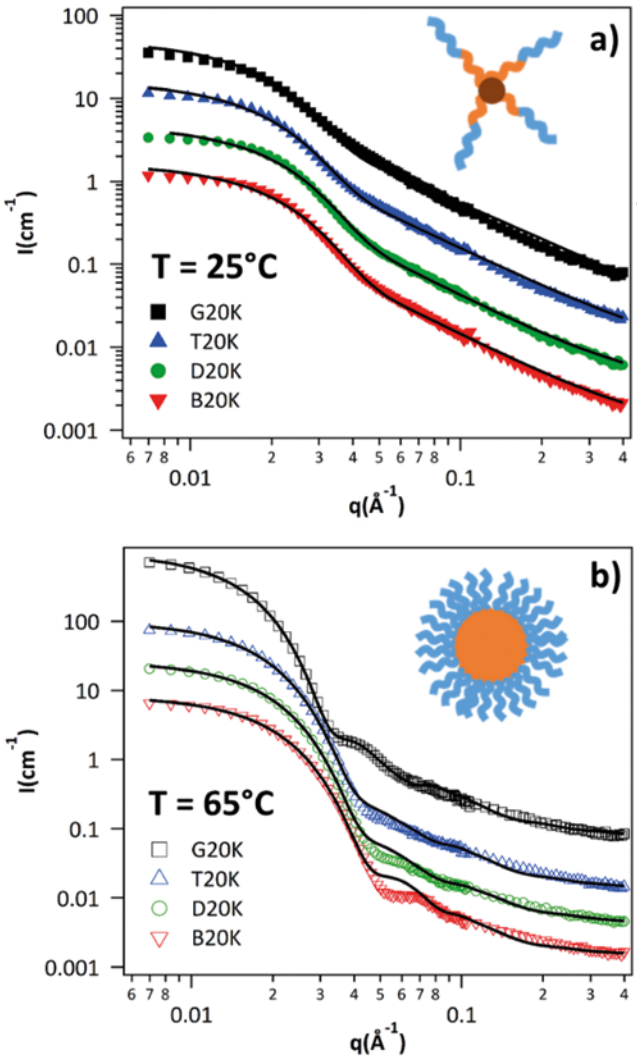

Figure 1: Neutron scattering intensity as a function of the scattering vector for the different copolymers with molar mass of 20 kDa at a) T = 25°C and b) T = 65°C; the curves have been arbitrarily shifted to facilitate comparisons. The black solid lines are the fitted curves using the Dozier model at T = 25°C and core–shell model (homogeneous core and decaying density profile in the shell) at T = 65°C. Copolymers are labelled G20K (linear gradient polymers), T20K (asymmetric triblock), D20K (asymmetric diblock) and B20K (block-block copolymer). For details, see Ref. [1].

PNIPAM mesoglobules' dependence on pressure

C. M. Papadakis [1], B.-J. Niebuur [1], V. Pipich [2], M.-S. Appavou [2]†, D. Mullapudi [3], A. Nieth [3], E. Rende [3], A. Schulte [3]

[1] Department of Physics, TUM School of Natural Sciences, Technical University of Munich, Garching, Germany; [2] Jülich Centre for Neutron Science (JCNS) at MLZ, Forschungszentrum Jülich GmbH, Garching, Germany; [3] Department of Physics and College of Optics and Photonics, University of Central Florida, Orlando, USA

Using very small-angle neutron scattering, the size and water content of mesoglobules formed by PNIPAM in aqueous solution above its cloud point temperature T_{cp} were determined during pressure scans at various temperatures. We observe a distinct transition at pressures of 35 – 55 MPa, the transition pressure being dependent on temperature. At atmospheric pressure, these mesoglobules are small and compact, whereas at high pressure, they are larger and water-rich. The newly identified transition line separates the low-pressure from the high-pressure regime.

Stimuli-responsive polymers, such as thermoresponsive poly(N-isopropylacrylamide) (PNIPAM), are key for applications such as drug delivery and sensors. PNIPAM shows lower critical solution temperature behaviour, transitioning from soluble below its cloud point temperature T_{cp} to forming mesoglobules above. These dense, long-lived mesoglobules with viscoelastic shells exhibit pressure-dependent properties such as water content and size. At atmospheric pressure, they are small, having a radius of about 0.5 µm, while at pressures above 80 MPa, they become larger and water-rich with radii of 1 – 2 µm. T_{cp} increases with pressure up to ~60 MPa and then decreases. Transitions from small mesoglobules to larger aggregates may involve water uptake or coalescence, while reverse transitions involve chain collapse and disintegration.

Mesoglobule transition line determined using optical microscopy and VSANS

Optical microscopy provides initial insights on the micron scale into the temperature- and pressure-dependent structures in a semidilute PNIPAM solution in the two-phase state. To elucidate mesoglobule structures with submicron spatial resolution and greater statistical relevance, we conducted very small-angle neutron scattering measurements during similar isothermal pressure scans at three temperatures: 35.4, 36.2, and 37°C, within a pressure range of 10 to 110 MPa [1]. The transition pressures between compact mesoglobules at low pressures and swollen, large aggregates at high pressures, obtained from the three scans following an increasing pressure protocol, are shown as a tilted line in Fig. 1. Our findings are in qualitative agreement with atomistic simulations on a single PNIPAM chain that revealed a transition between collapsed, dehydrated chains at low pressures and a hydrated globular state at higher pressures.

At high temperatures, far from the coexistence line, mesoglobule transitions are smooth and dominated by swelling. In contrast, at low temperatures near the coexistence line, transitions are abrupt and involve coalescence. Decreasing pressure causes gradual deswelling at high temperatures, while compact mesoglobules and persistent large aggregates form at low temperatures. Cooling to the one-phase state reduces mesoglobule formation upon reheating but does not qualitatively alter the behaviour.

The formation and disintegration of aggregates may prove relevant for applications such as the degradation of microplastics, recycling processes, or polymeric drug-release systems.

[1] B.-J. Niebuur et al., PNIPAM mesoglobules in dependence on pressure, Langmuir 40, 22314-22323 (2024)
DOI: 10.1021/acs.langmuir.4c02952

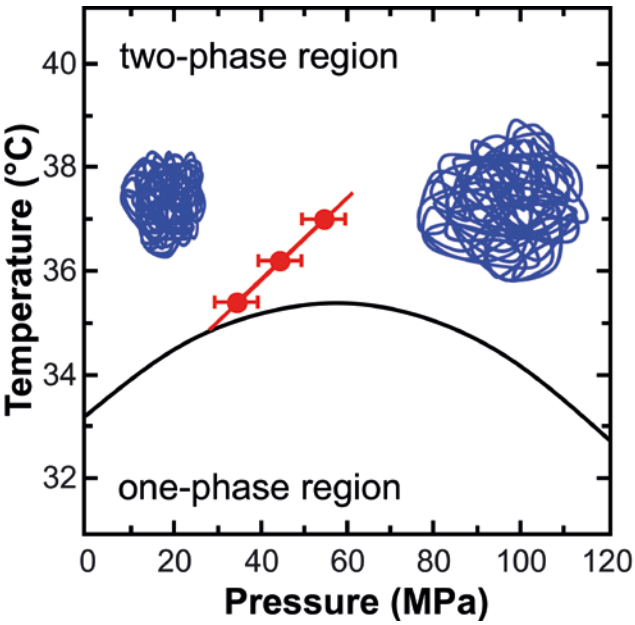

Figure 1: Temperature–pressure phase diagram of the aqueous PNIPAM solution investigated. Solid black line: coexistence line between the one- and two-phase states. Symbols: transition pressures determined from the scans during the increase of pressure. The tilted red line is a guide for the eye. The cartoons depict the compact and small mesoglobules at low pressures and the swollen and large aggregates at high pressures.

Neutron scattering from cellulose solutions in phosphoric acid at different water content

G. Alfassi [1], A. Radulescu [2], S. Lifshiz-Simon [3], S. Rappoport [3], Y. Cohen [3]

[1] Department of Biotechnology Engineering, Braude College of Engineering, Karmiel, Israel; [2] Jülich Centre for Neutron Science (JCNS) at MLZ, Forschungszentrum Jülich GmbH, Garching, Germany; [3] Department of Chemical Engineering, Technion, Haifa, Israel

Cellulose from biomass is a sustainable resource, yet its utilisation requires treatment to release the macromolecules from the tight crystal structure. Phosphoric acid (PA) is an efficient cellulose solvent. However, dissolution requires a certain quantity of water. SANS measurements at KWS-2 indicate that cellulose dissolves molecularly at 81–94% PA. At 97% PA some crystals are undissolved. At 78% PA a mass-surface fractal structure of fibrils is evident.

Cellulose dissolution

Cellulose, the main component of biomass, shows enormous potential as a sustainable resource for chemicals and materials. However, lignocellulosic biomass is recalcitrant towards biological degradation or dissolution in most common solvents, due to its compact crystal structure. Dissolution in aqueous phosphoric acid (PA), studied for almost a century, is used in several technologies. Experience shows that a certain water content is necessary for cellulose dissolution in PA. This study shows the effect of water content on cellulose dissolution, in the range of 78–97 wt% PA.

SANS experiment

SANS measurements are well suited for solutions in D_3PO_4 (dPA), due to its low incoherent scattering and high scattering length density (SLD) contrast to cellulose. Dried microcrystalline cellulose was dissolved at 0ºC in dPA, prepared by mixing 85% dPA solution with either D_2O or P_2O_5. SANS measurements were carried out on the KWS-2 beamline at the FRM II research reactor.

The effect of water

The cellulose solutions at all dPA contents appeared transparent except in 78% dPA which was cloudy, as seen in the vial pictures in Fig. 1a. The SANS patterns from solutions in 81 to 94% dPA were almost identical, exhibiting the marks of molecularly dissolved cellulose chains: q^{-2} power law at low-q expected of semidilute polymer solutions, and q^{-1} power law at high-q due to local chain rigidity. The insert in Fig. 1a shows excess scattering at low-q from solution in 97% dPA, exhibiting a q^{-4} power law indicating some undissolved cellulose crystals. The SANS pattern from the solution in 78% dPA (Fig. 1b) differs significantly from the others. It can be modelled as a "mass-surface fractal", whereby primary nanofibrils with a "rough" surface (partially dissolved chains), form larger fractal aggregates. This model predicts the SANS pattern as: $I(q)=I(0)\{[(1+b^2q^2)]^{D_m/2}[(1+a^2q^2)]^{(6-D_s-D_m)/2}\}^{-1}$, where Ds and Dm are the surface and mass fractal dimensions, and the gyration radii of the primary and aggregated structures are, respectively: $r_g=a[3(6-D_m-D_s/2)]^{1/2}$ and $R_g=b(3D_m/2)^{1/2}$. The fit and the evaluated parameters are presented in Fig. 1b.

[1] G. Alfassi, et al., Small-angle neutron scattering from cellulose solutions in phosphoric acid at different water content, Giant 17, 100246 (2024)
DOI: 10.1016/j.giant.2024.100246

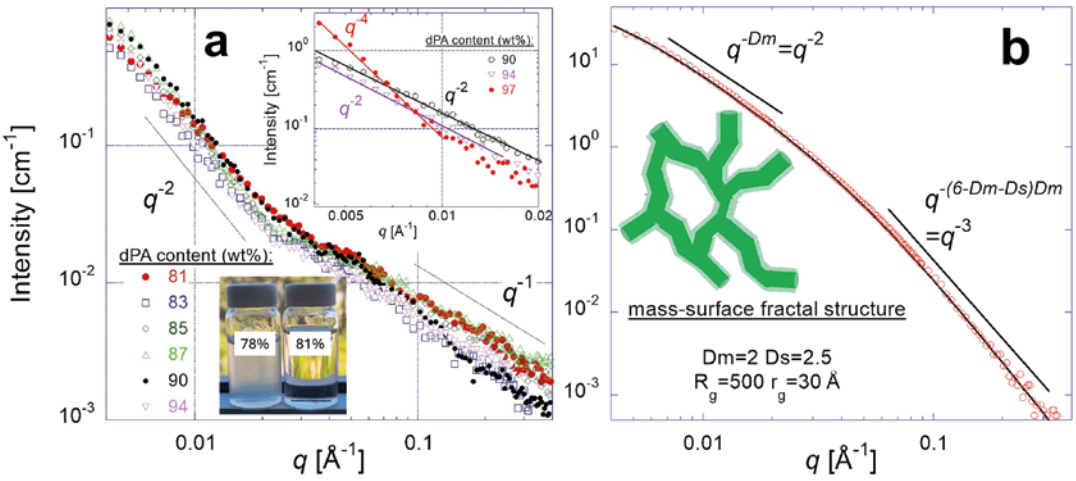

Figure 1: SANS patterns from 2 wt.% cellulose solutions in dPA at different D_2O content. a) 81, 83 85, 87, 90 and 94% dPA. Inset: Comparison of the low-q SANS patterns of solutions in 90, 94 and 97% dPA. b) The SANS pattern from the solution in 78% dPA with the fit of the "mass-surface fractal" model, a sketch of the model structure and the evaluated parameters.

Polymorphic phase transitions of ethane (C_2D_6) in the liquid and supercritical states

V. Pipich[1], J. Kohlbecher[2], D. Schwahn[3]

[1] Jülich Centre for Neutron Science (JCNS) at MLZ, Forschungszentrum Jülich GmbH, Garching, Germany; [2] Laboratory for Neutron Scattering and Imaging, Paul Scherrer Institute, Villingen, Switzerland; [3] Jülich Centre for Neutron Science (JCNS), Forschungszentrum Jülich GmbH, Jülich, Germany

The phase behaviour of ethane (C_2D_6) was investigated in a temperature and pressure range below and above the critical point using small-angle neutron scattering (SANS). Thermal fluctuations of molecular density were explored, from which the vapor-liquid and Widom lines were determined. Scattering of droplets of densely packed C_2D_6 was observed for all temperatures above the vapor-liquid line and at about 10 bar above the Widom line.

Phase diagrams of monomolecular fluids, as treated in classical textbooks, allow a continuous transition from the vaporous to the liquid state on a path above the critical point. This view has changed with the introduction of the Frenkel line, which describes the transition from gaseous to liquid behaviour. However, the position of the Frenkel line remain uncertain. Our introduction to this topic was via supercritical CO_2, where we observed the formation of droplets above the vapor-liquid (v-l) and Frenkel lines, where we have defined the Frenkel line as the formation of a new phase. This study continues our work on CO_2 and should also demonstrate inhomogeneity as a universal property of the liquid phase.

Thermal density fluctuations and droplet formation identified by SANS

The phase behaviour of C_2D_6 below and above the critical point was investigated using SANS-1 instrument at SINQ (PSI) in a temperature and pressure range from 10 to 45°C and 20 to 126 bar, respectively [1]. The scattering of thermal density fluctuations allowed the determination of the v-l and Widom lines, as shown in the phase diagram (Fig. 1). Additional scattering from droplets of densely packed C_2D_6 molecules was observed above the v-l line and in the supercritical regime for all temperatures at ΔP=10 bar above the Widom line, interpreted as a Frenkel line. The droplets have a spherical shape initially and take on a rod-shaped form at higher pressure.

Frenkel line in monomolecular liquids

The observation of the Frenkel line by the formation of larger droplets of spherical and rod-like shape represent a polymorphic phase transition. The consistency with our previous SANS studies on CO_2 indicates a universal phase behaviour for monomolecular liquids below and above the critical point. The correlation lengths (ξ) of the thermal density fluctuations at the critical point and at the Widom line are determined between 20 and 35 Å and thus in the range of the droplet radius between 60 and 80 Å. These long-range fluctuations appear to suppress the formation of droplets, which can only form at about 10 bar above the critical point and the Widom line when ξ becomes smaller than 10 Å.

[1] V. Pipich et al., Thermal density fluctuations and polymorphic phase transitions of ethane (C_2D_6) in the gas/liquid and supercritical states, J. Phys. Chem. B, 128, 5072 (2024) DOI: 10.1021/acs.jpcb.4c01422

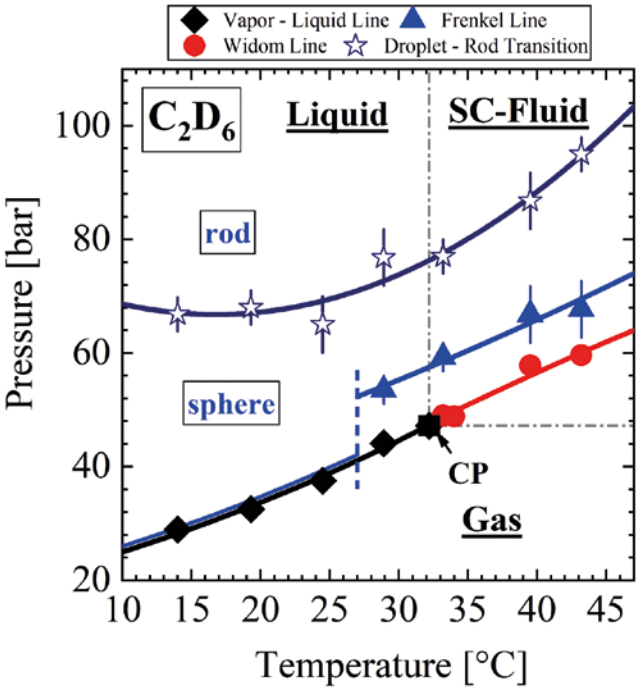

Figure 1: Pressure-temperature phase diagram of ethane (C_2D_6). The Widom line is an extension of the critical point to higher temperatures and is determined from the maximum of the thermal density fluctuations, while the Frenkel line represents the boundary line of droplet formation. Droplets were observed above the vapor-liquid line as well as the Frenkel line. At even higher pressure a transition to rod-like shaped droplets is observed.

Single-crystal growth of rutile-related $V_{0.92}O_2$ at high pressures and temperatures

A. Grzechnik [1,2], B. V. Hakala [1], S. Kurig [3], K. Friese [1,2], N. Walte [4]

[1] Jülich Centre for Neutron Science (JCNS), Forschungszentrum Jülich GmbH, Jülich, Germany; [2] Institute of Crystallography, RWTH Aachen University, Aachen, Germany; [3] Institute of Inorganic Chemistry, RWTH Aachen University, Aachen, Germany; [4] Heinz Maier-Leibnitz Zentrum, Technical University of Munich, Garching, Germany

V_6O_{13} (*C*2/*m*, *Z* = 2), built of alternating V_2O_5- and VO_2(B)-like layers stacked along the *c* axis, transforms to rutile-related $V_{0.92}O_2$ at 4–17.5 GPa above 500 K. The new material is recovered to ambient conditions and its crystal structure (*C*2/*m*, *Z* = 4) is determined via X-ray single-crystal diffraction measured on crystals grown at 10 GPa and 1273 K using the six-anvil press on the beamline SAPHiR.

Multiple pressure and temperature induced phases

Binary vanadium oxides exhibit a wide range of magnetic, electronic and catalytic properties. We studied the high-pressure behaviour of the mixed-valence vanadium oxide V_6O_{13} [1] that occurs in the *Wadsley* homologous series V_nO_{2n+1} between α-V_2O_5 (*Pmmn*, *Z* = 2) and VO_2(B) (*C*2/*m*, *Z* = 8). V_6O_{13} (*C*2/*m*, *Z* = 2) is built of alternating V_2O_5- and VO_2(B)-like layers stacked along the *c* axis. The layers are formed by edge- and corner-sharing distorted VO_6 octahedra.

During compression at ambient temperature, V_6O_{13} becomes amorphous and decomposes above 18.5 GPa. It transforms to rutile-related $V_{0.92}O_2$ above 500 K in the pressure range 4–17.5 GPa. The new material is recoverable to ambient conditions. Its crystal structure (*C*2/*m*, *Z* = 4) was determined from laboratory single-crystal X-ray diffraction data measured on crystals grown at 10 GPa and 1273 K using the large-volume six-anvil press at SAPHiR. The largest crystals have dimensions of about 0.1×0.5×0.4 mm³.

Chains everywhere

The rutile structure ($P4_2/mnm$, *Z* = 2) of VO_2 is built of chains of edge-sharing VO_6 octahedra connected with each other by common corners. In contrast, the vanadium atoms are on two split positions for $V_{0.92}O_2$ (Fig. 1). The characteristic feature is the presence of two *zigzag* V–V chains. One of them has equidistant V1 atoms while in the other there are short and long V2–V2 distances. Our findings demonstrate that the rutile-related phases exist in a wide V_2O_5-VO_2 compositional range and could accommodate at least up to 35 wt.% of V_2O_5. This provides an opportunity to study their crystal structures and physical properties that originate from the charge disproportionation and ordering of vanadium cations for different chemical compositions.

Our work shows that the six-anvil press at SAPHiR is a tool not only for synthesising new materials, but also for growing their single crystals. For some compositions under favourable conditions, which could also be determined in situ with neutron powder diffraction at SAPHiR, the crystal sizes might be suitable for neutron scattering on other beamlines at the MLZ.

[1] A. Grzechnik et al., Structures, phase stability, amorphisation, and decomposition of V_6O_{13} at high pressures and temperatures: Synthesis of rutile-related $V_{0.92}O_2$, Cryst. Growth Des. 24, 5582−5592 (2024)
DOI: 10.1021/acs.cgd.4c00363

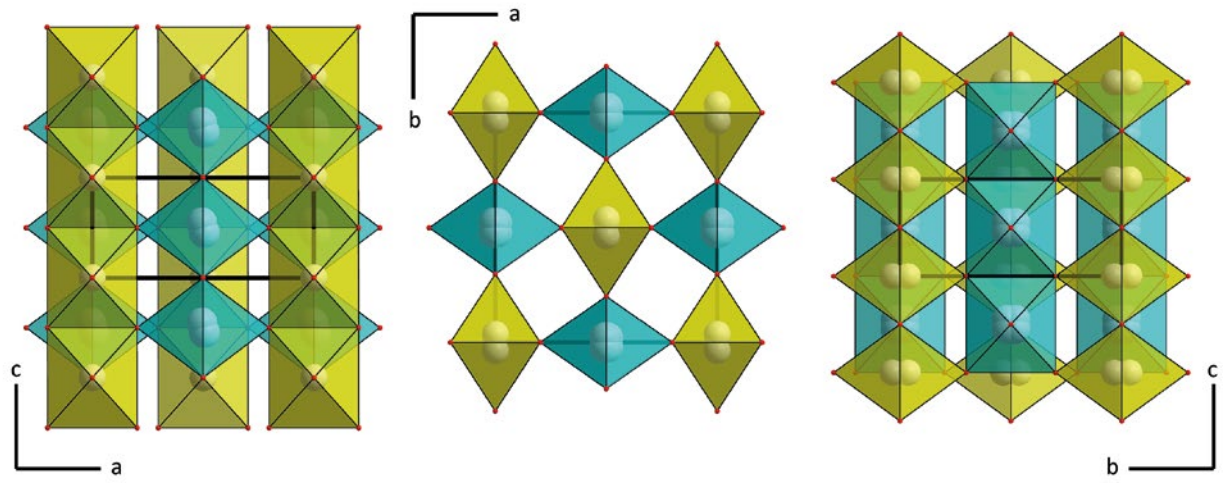

Figure 1: Crystal structure of $V_{0.92}O_2$. The octahedra around the V1 and V2 atoms are drawn in yellow and cyan, respectively.

Single-crystal neutron diffraction for studying high-T behaviour of an intermediate scapolite mineral

P. Lotti[1], G.D. Gatta[1], L. Gigli[2], H. Krüger[3], V. Kahlenberg[3], M. Meven[4,5], D. Comboni[1,6], S. Milani[1], M. Merlini[1], H-P. Liermann[7]

[1]Department of Earth Sciences, University of Milan, Milan, Italy; [2]Elettra Sincrotrone Trieste S.c.P.A., Basovizza, Trieste, Italy; [3]Institute of Mineralogy and Petrography, University of Innsbruck, Innsbruck, Austria; [4]Institute of Crystallography, RWTH Aachen, Aachen, Germany; [5]Jülich Centre for Neutron Science (JCNS) at MLZ, Forschungszentrum Jülich GmbH, Garching, Germany; [6]European Synchrotron Radiation Facility, Grenoble, France; [7]Deutsches Elektronen-Synchrotron DESY, Hamburg, Germany

Single-crystal neutron diffraction experiments performed at the HEiDi diffractometer at the MLZ confirmed an unusual *I*4/*m* symmetry in a scapolite of intermediate composition. Structural refinements revealed a disordered Si/Al distribution with Al enrichment at *T*2 sites. Neutron diffraction data collected at 685°C showed no significant changes in the reflection conditions and structural parameters with temperature.

An unexpected symmetry

Scapolites are microporous aluminosilicate feldspathoid minerals with an open-framework structure known for their complex solid solution and polymorphism. In the scapolite polymorph with *I*4/*m* symmetry, the tetrahedral framework features two distinct *T* sites (Fig. 1), with aluminium preferentially ordered at one of them (*T*2). Intermediate compositions in the solid solution typically exhibit $P4_2/n$ symmetry, but the sample studied, an intermediate scapolite of $(Na_{1.86}Ca_{1.86}K_{0.23}Fe_{0.01})(Al_{4.36}Si_{7.64})O_{24}[Cl_{0.48}(CO_3)_{0.48}(SO_4)_{0.01}]$ composition, displays an unusual *I*4/*m* symmetry.

To investigate this unexpected structural arrangement and its stability, single-crystal neutron diffraction experiments were conducted at the HEiDi diffractometer (MLZ, Germany) at ambient (25°C) and high temperature (685°C). Neutron diffraction provided detailed insights into the distribution of Si and Al within the tetrahedral framework and the structural response to temperature changes.

Confirmation of the unusual *I*4/*m* symmetry

At 25°C, two sets of data were collected using different wavelengths, while high-temperature data were obtained after annealing the crystal at 685°C for 3 hours. Reflection conditions confirmed the preservation of the *I*4/*m* space group at both temperatures. Structure refinements revealed a disordered distribution of Si and Al across the tetrahedral sites, consistent with chemical analysis, with Al slightly enriched at the *T*2 site (Fig. 1). No significant changes in the refined Si/Al ordering or *T*-*O* bond distances were observed as a function of temperature, indicating thermal stability of the unusual *I*4/*m* symmetry of the sample studied.

These findings demonstrate the complementarity of neutron diffraction and X-ray diffraction in studying complex mineral structures at ambient and non-ambient conditions. Further details on the experimental protocol and results are presented in [1].

[1] P. Lotti et al., Thermal and combined high-temperature and high-pressure behaviour of a natural intermediate scapolite, Am. Miner. 109, 243-254 (2024)
DOI: 10.2138/am-2023-8962

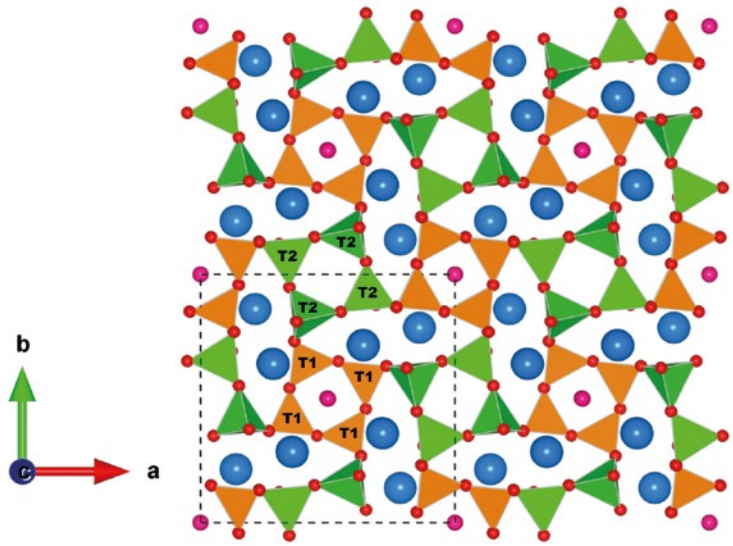

Figure 1: Crystal structure of scapolite viewed down the crystallographic **c**-axis, showing the independent *T*1 and *T*2 tetrahedra of the polymorph with *I*4/*m* space group symmetry, with a disordered distribution of Si and Al. Blue spheres represent the monovalent and divalent cations sites, purple spheres the anion sites.

Lithium distribution in the graphite anode of cylindrical 21700 Li-ion cells during degradation

D. Petz[1], V. Baran[2], J. Park[3,4], A. Schökel[2], A. Kriele[4], J. Rebelo Kornmeier[1], C. Paulmann[2,6], M. Koch[7], T. Nilges[7], P.M. Müller-Buschbaum[1], A. Senyshyn[1]

[1]Heinz Maier-Leibnitz Zentrum (MLZ), Technical University of Munich, Garching, Germany; [2]Deutsches Elektronen Synchrotron (DESY), Hamburg, Germany; [3]National Physics Laboratory, Teddington, UK; [4]Schlumberger Cambridge Research, Cambridge, UK; [5]German Engineering Materials Science Centre (GEMS) at MLZ, Helmholtz-Zentrum hereon GmbH, Garching, Germany; [6]Department of Earth System Science, University of Hamburg, Hamburg, Germany; [7]Department of Chemistry, TUM School of Natural Sciences, Technical University of Munich, Garching, Germany

There is a widely-accepted opinion in the literature that cell aging stabilises the heterogeneous state/distribution of lithium-ions in 18650-type Li-ion batteries. In the current contribution, the heterogeneity of a fresh and aged 21700-type Li-ion battery was investigated using a combination of synchrotron and neutron-based diffraction techniques, focusing on the non-destructive probe of Li distribution caused by cell aging.

Optical signature of lithium content

The structural and spatial degradation of cylindrical 21700 lithium-ion batteries was investigated by combining diffraction and imaging techniques with electrochemical and thermal characterisation. The graphite anode's colour serves as a visual indicator of lithiation: it transitions from dark blue (LiC_{18}) to red (LiC_{12}) to golden (LiC_6) as lithium intercalates. Images of the extracted lithiated graphite anode plates show significant differences between fresh and aged cells. The anodes are predominantly golden in the fresh state, corresponding to a fully lithiated state (LiC_6). Black areas near the electrodes strip's ends and midsection arise from regions lacking counter electrode material. At the same time, a darker band at mid-height may reflect an average lithium content of $Li_{x<0.5}C_6$.

New insights from radiography

The anodes exhibit pronounced changes in aged cells (125 cycles at 2C/1C or 30/60 minute discharge rates, 60% capacity retention), appearing darker with red and dark red shades, reflecting a reduced lithiation level. The central regions of the electrodes display a different colour pattern from the outer areas, suggesting an uneven lithium distribution after cycling. X-ray diffraction radiography (XRDR) performed at beamline P02.1 at PETRA III/DESY was used to generate depth-resolved lithium content maps for fresh and aged electrodes to quantify this. In fresh cells, the lithium distribution is initially uniform with black areas identified during visual inspection correlating with lower lithium content in XRDR false-colour plots (Fig. 1a, b).

In aged cells, XRDR reveals a less uniform lithium distribution, with narrow regions of reduced lithiation linked to the positions of current collectors and areas lacking counter-electrode material (Fig. 1c, d). While the lithium distribution shows significant drops near the top and bottom edges of the cells, no substantial gradient across the electrode height is observed, probably due to the absence of counter-electrode material in these regions. These findings provide insights into lithiation patterns and degradation mechanisms in lithium-ion batteries, emphasising the impact of cell design on performance.

[1] D. Petz et al., Heterogeneity of lithium distribution in the graphite anode of 21700-type cylindrical Li-ion cells during degradation, Batteries 10, 68 (2024)
DOI: 10.3390/batteries10030068

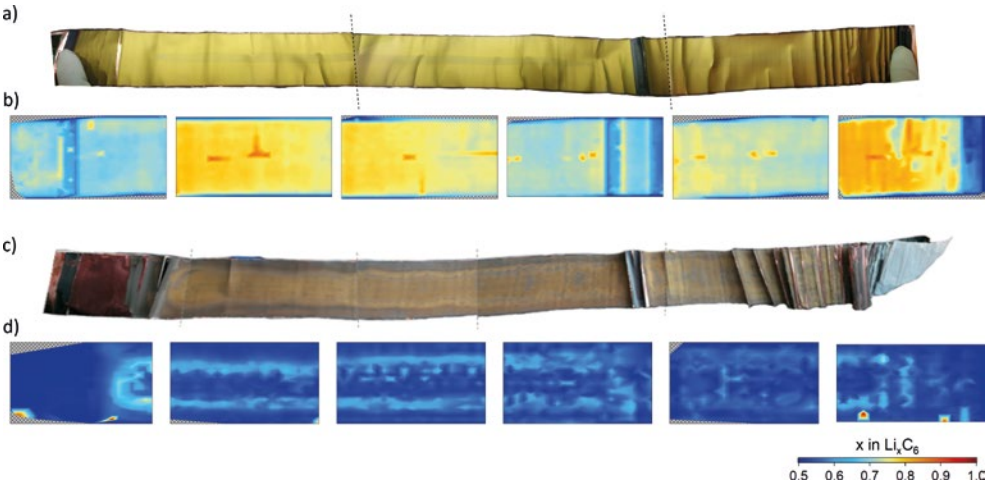

Figure 1: Extracted graphite anode stripes (SOC = 100%) in a) fresh and c) aged state. Thickness averaged lithium concentration in the lithiated graphite anode, calculated from the XRD measurements in b) fresh and d) aged state, shown in false colours.

Pushing the limits of accessible length scales via a modified Porod analysis in small-angle neutron scattering on ordered systems

X. Brems[1,2], S. Mühlbauer[1], R. Cubitt[2]

[1] Heinz Maier-Leibnitz Zentrum (MLZ), Technical University of Munich, Garching, Germany;
[2] Institut Laue-Langevin (ILL), Grenoble, France

Small-angle neutron scattering (SANS) is a technique for studying large-scale structures. We show how a modified Porod law can be used in the special case of highly aligned structures. The method is applied to study the micrometre-sized domain structure found in the intermediate mixed state of superconducting niobium. The analysis approach allows the range of accessible length scales to be extended from 1 µm to up to 40 µm using a conventional SANS setup.

Superconducting vortex matter studied by small-angle neutron scattering

In superconductors such as niobum, with a Ginzburg-Landau parameter close to $\kappa_0 = \frac{1}{\sqrt{2}}$ broadly referred to as intertype (IT) superconductors, a broad range of exotic magnetic vortex matter emerges in the vicinity of the Bogomolnyi point due to the infinite degeneracy of the superconducting condensate, incompatible with the type I/II dichotomy. The intermediate mixed state (IMS), the microscopic coexistence of complete magnetic flux expulsion (Meissner state) and the penetration of an array of superconducting vortices (mixed state), is one of the most prominent examples of IT behaviour and has been studied extensively in recent years.

An extension of the classical Porod law

We were able to showcase a novel approach to stretch the accessible length scales of small-angle neutron scattering on ordered structures far beyond the resolution limit using a novel Porod analysis. The largest accessible length scale in conventional SANS is limited to accessing a few µm. Our novel approach circumvents this limitation and was able to extract much larger length scales from the low-q power-law scattering using a modification of the Porod law connecting the scattered intensity of randomly distributed objects to their specific surface area. We showed that in the special case of a highly aligned domain structure such as the IMS, the specific surface area determined from the modified Porod law can be used to determine the length scale of the domain structure. The standard SANS setup for these experiments, which were performed at the D33 beamline at the ILL, is depicted in Fig. 1. The analysis approach makes it possible to extend the range of accessible length scales from 1 µm to values of up to 40 µm using a conventional small angle neutron scattering setup and should be applicable to any such aligned system.

[1] X. S. Brems et al., Pushing the limits of accessible length scales via a modified Porod analysis in small-angle neutron scattering on ordered systems, J. Appl. Crystallogr. 57, 5, 1358-1372 (2024)
DOI: 10.1107/S1600576724007295

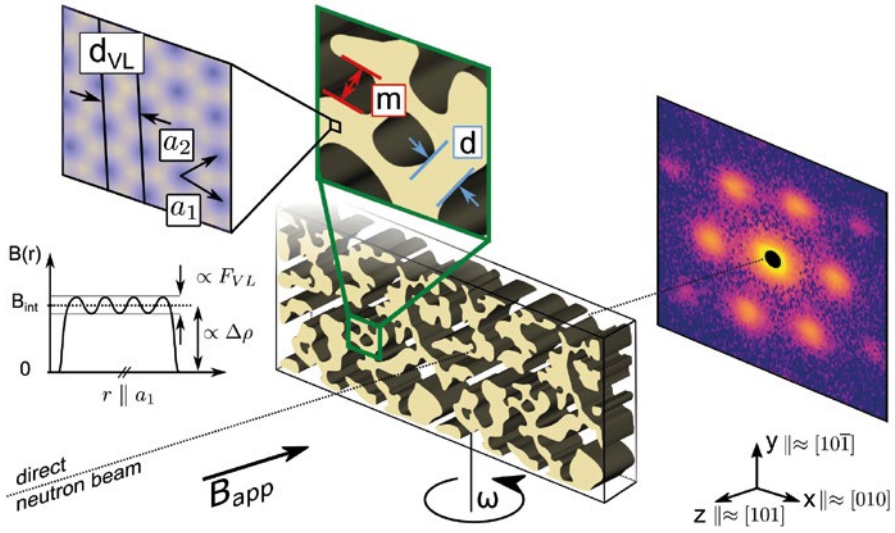

Figure 1: Scattering geometry. The magnetic field is aligned parallel to the neutron beam. The scattered neutrons are recorded using a 2D detector behind the sample. The two VL vectors a_i, the interplanar VL distance d_{VL}, the VL domain size d, and the Meissner state domain size m are marked. A schematic drawing of the magnetic field distribution B(r) along the direction of a_1 is also included. The magnetic scattering length density contrast Δρ is determined by the difference in magnetic field between mixed state domains and Meissner state domains (zero internal field) and connected to the IMS scattering. The VL form factor F_{VL} connected to the Bragg peak scattering results from the field variation inside the mixed state domains.

Evolution of spin dynamics during freezing in the spin-glass Fe_xCr_{1-x} studied by means of MIEZE spectroscopy

S. Säubert[1,2], C. Franz[1,2,3], J.K. Jochum[1,2], G. Benka[1], A. Bauer[1,4], S.M. Shapiro[5], P. Böni[1], C. Pfleiderer[1,2,4,6]

[1] Department of Physics, Technical University of Munich, Garching, Germany; [2] Heinz Maier-Leibnitz Zentrum (MLZ), Technical University of Munich, Garching, Germany; [3] Jülich Centre for Neutron Science (JCNS) at MLZ, Forschungszentrum Jülich GmbH, Garching, Germany; [4] Center for QuantumEngineering (ZQE), Technical University of Munich, Garching, Germany; [5] Physics Department, Brookhaven National Laboratory, Upton, New York, USA; [6] Munich Center for Quantum Science and Technology (MCQST), Technical University of Munich, Garching, Germany

In the iron-chromium system, Fe_xCr_{1-x}, a wide dome of spin-glass behaviour emerges when the ferromagnetism of iron is suppressed and the antiferromagnetism of chromium emerges as a function of increasing iron content x. This study uses MIEZE spectroscopy to investigate spin dynamics across the freezing process into the spin-glass state. The relaxation process is described by a stretched exponential. The spin relaxation exhibits a momentum dependence consistent with a power law, providing evidence of the dispersive character of the spin relaxation.

To explore the spin dynamics in the iron-chromium system, Fe_xCr_{1-x}, we employ modulation of intensity with zero effort (MIEZE) spectroscopy. The MIEZE technique allows us to perform high-resolution neutron spin-echo spectroscopy over a large dynamic range in materials hosting ferromagnetic domains that may depolarise the neutron beam, posing a major limitation in conventional neutron spin-echo spectroscopy. Samples with ferromagnetic, antiferromagnetic, or paramagnetic high-temperature properties may therefore be investigated with the same instrument and sample environment. Conducted at the RESEDA beamline, our research focuses on the spin relaxation in Fe_xCr_{1-x} across various temperatures and iron concentrations x.

Variation of the iron content x

For the reentrant cluster glass (x = 0.145), relaxation is characterised by a broad distribution of relaxation times that may be described well in terms of a stretched exponential over the entire temperature range. In the superparamagnetic regime (x = 0.175, 0.21), a broad distribution of relaxation times at low temperatures that may be described well in terms of a stretched exponential is contrasted by a single relaxation time at elevated temperatures. Fig. 1 shows the normalised intermediate scattering function as measured for different temperatures in Fe_xCr_{1-x}, visualising the exponential vs. stretched behaviour. Further, the spin relaxation in all samples exhibits dispersive behaviour, following a power-law dependence on the momentum q, with the dynamical exponent z decreasing from z ~ 1.5 to z ~ 1.0 as the iron concentration increases. However, for Fe_xCr_{1-x} the origin of the dispersive behaviour may, in principle, comprise a combination of different contributions.

The role of the magnetic correlations

Our study of spin dynamics in Fe_xCr_{1-x} using MIEZE spectroscopy offers valuable insights into spin-glass transitions and magnetic correlations, namely it reveals a broad distribution of relaxation times and dispersive behaviour following a power-law momentum dependence. By providing insights on the interplay between ferromagnetic and antiferromagnetic correlations in spin-glass materials, our study demonstrates the effectiveness of MIEZE spectroscopy for studies of complex magnetic materials in both advancing magnetic technologies and fundamental materials science.

[1] S. Säubert et al., Evolution of spin dynamics during freezing in the spin-glass Fe_xCr_{1-x}, Physical Review B 110, 094422 (2024)

DOI: 10.1103/PhysRevB.110.094422

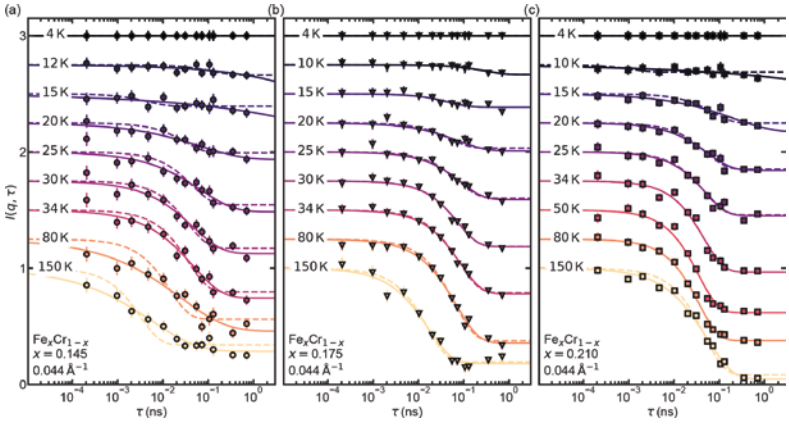

Figure 1: Normalised intermediate scattering function for Fe_xCr_{1-x} at different temperatures and iron concentrations (x = 0.145, 0.175, 0.21). The transition from simple exponential decay at higher temperatures to stretched exponential behaviour at lower temperatures is illustrated, highlighting the evolution of spin dynamics during the freezing process into the spin-glass.

Ferromagnetic interlayer coupling in $FeSe_{1-x}S_x$ superconductors revealed by inelastic neutron scattering

M. Ma[1,2], P. Bourges[3], Y. Sidis[3], J. Sun[2], G. Wang[2], K. Iida[4], K. Kamazawa[4], J. T. Park[5], F. Bourdarot[6], Z. Ren[1], Y. Li[2,7]

[1] Beijing National Laboratory for Condensed Matter Physics, Institute of Physics, Chinese Academy of Sciences, Beijing, China; [2] International Center for Quantum Materials, School of Physics, Peking University, Beijing, China; [3] Université Paris-Saclay, CNRS, CEA, Laboratoire Léon Brillouin, France; [4] Neutron Science and Technology Centre, Comprehensive Research Organization for Science and Society (CROSS), Tokai, Japan; [5] Heinz Maier-Leibnitz Zentrum (MLZ), Technical University of Munich, Garching, Germany; [6] Université Grenoble Alpes, CEA, Grenoble, France; [7] Collaborative Innovation Center of Quantum Matter, Beijing, China

$FeSe_{1-x}S_x$ superconductors are commonly considered layered van der Waals materials with negligible interlayer coupling. Here, using inelastic neutron scattering at PUMA to study spin excitations in single-crystal samples, we reveal that the magnetic coupling between adjacent Fe layers is ferromagnetic, distinguishing the system from most unconventional superconductors. The weak interlayer coupling is estimated at $J_c \sim 0.2$ meV, consistent with the short spin-spin correlation length $\xi_c \sim 0.2c$ along the c axis. The results provide an experimental basis for a microscopic theoretical model to describe the absence of magnetic order in $FeSe_{1-x}S_x$.

Three-dimensional distribution of spin excitations in momentum space

In the superconducting state at $T = 5$ K, the strongly L-modulated spin resonance mode is closely related to the anisotropic distribution of low-energy spin excitations in momentum space observed in the nematic state at $T = 15$ K (Fig. 1a, b). Apart from an intensity enhancement caused by spin resonance, the anisotropic momentum distribution of spin excitations in the nematic state mirrors that in the superconducting state, as seen in the constant energy maps in the (H, L) plane (Fig. 1a, b) and the L scans in Fig. 1c. The spin excitations exhibit an elliptical distribution, elongated transversely and more stretched along the L direction both in the superconducting and the nematic state. Momentum scans along L, shown in Fig. 1c, further clarify this elliptic distribution in three-dimensional momentum space. The intensity of spin excitations in the nematic state at $T = 15$ K, along the longitudinal (H), transverse (K) and L directions is well fitted by Gaussians, revealing the full widths at half maximum (FWHM) values κ_H, κ_K and κ_L as shown in Fig. 1d. Comparing the FWHM along H and K, κ_K is slightly larger than κ_H. With κ_L six times larger than κ_K, the intensity's L-dependence suggests a broadened distribution along L, weakening with increasing energy and persisting up to $E \approx 15$ meV. Using the FWHM, we construct the schematic of the three-dimensional distribution of spin excitations in momentum space at $T = 15$ K and $E = 4$ meV (Fig. 1e). The ellipsoids are periodically located at Q = (±1, 0, L) or (0, ±1, L) in a twinned sample, with L as an integer.

In conclusion, the anisotropic momentum distribution of spin resonance in $FeSe_{1-x}S_x$ mimics the low energy spin excitations in its nematic phase, suggesting a close link between superconductivity and magnetism. The strongly L-modulated spin resonance mode with maximum intensity at integer L, indicates ferromagnetic interlayer coupling unlike other iron-based superconductors, which tend to order antiferromagnetically. The ferromagnetic nature with weak interlayer coupling J_c and short spin-spin correlation length ξ_c might shed light on the absence of magnetic order in $FeSe_{1-x}S_x$.

[1] M. Ma et al., Ferromagnetic interlayer coupling in $FeSe_{1-x}S_x$ superconductors revealed by inelastic neutron scattering, Phys. Rev. B 110, 174503 (2024)
DOI: 10.1103/PhysRevB.110.174503

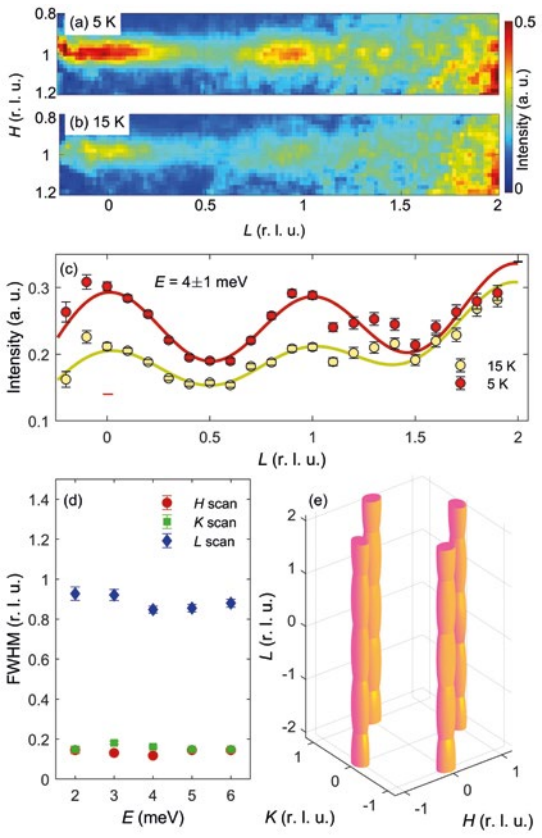

Figure 1: (a–b) Constant-energy maps of $FeSe_{0.93}S_{0.07}$ obtained at $T = 5$ K and 15 K in (H, L) momentum plane with $E = 4\pm1$ meV and $|K| \leq 0.1$. (c) L scans at $T = 5$ K and 15 K with $E = 4\pm1$ meV, $|K| \leq 0.1$ and $|H-1| \leq 0.1$. The horizontal red bar represents the expected momentum resolution. Solid lines are Gaussian obtained by fitting the respective data. (d) Energy dependence of FWHM for H, K and L scans fitted by Gaussians. (e) 3D distribution of spin excitations in momentum space from FWHM data at $E = 4\pm1$ meV.

Topological aspects of multi-*k* antiferromagnetism in cubic rare-earth compounds

W. Simeth [1,2], M. C. Rahn [1,3], A. Bauer [1,4], M. Meven [5,6], C. Pfleiderer [1,4,7,8]

[1] Department of Physics, Technical University of Munich, Garching, Germany; [2] Paul Scherrer Institut, Villigen, Switzerland; [3] Institute for Solid State and Materials Physics, Technical University of Dresden, Dresden, Germany; [4] Center for Quantum Engineering (ZQE), Technical University of Munich, Garching, Germany; [5] Jülich Centre for Neutron Science (JCNS) at MLZ, Forschungszentrum Jülich GmbH, Garching, Germany; [6] Institute of Crystallography, RWTH Aachen, Aachen, Germany; [7] Munich Center for Quantum Science and Technology (MCQST), Technical University of Munich, Garching, Germany; [8] Heinz Maier-Leibnitz Zentrum (MLZ), Technical University of Munich, Garching, Germany

Using neutron diffraction, we studied the series of rare-earth intermetallics *R*Cu (*R* = Ho, Tm, Er). Previous studies of bulk and transport properties established complex magnetic phase diagrams with multiple phase pockets. We identify various multi-***k*** antiferromagnetic ground states that potentially feature topological winding in both real- and reciprocal space, promoting these materials as a new platform for advanced functionalities.

The rare-earth copper compounds

The rare-earth intermetallics *R*Cu (*R* = Ho, Tm, Er) crystallise in the cubic CsCl structure and display antiferromagnetic order at temperatures below 30 K. Complex magnetic order is driven by multiple competing interactions including RKKY, crystal electric fields, magnetic anisotropy, and superexchange. Early neutron diffraction studies on polycrystals reported the possibility of multi-***k*** magnetic ground states, but the states were not discussed in the context of topology. We conducted a comprehensive study of the magnetic properties of single-crystal HoCu, TmCu, and ErCu as a function of temperature and magnetic field (cf. Ref. [1]). Magnetisation and susceptibility measurements established rich magnetic phase diagrams with multiple phase pockets, exceeding ten phases for certain field directions. Electrical transport measurements revealed large anomalous Hall contributions across all ordered phases, potentially due to topological order in spin or reciprocal space.

Single-crystal neutron diffraction

Using single-crystal neutron diffraction, multiple variations of ($\pi\pi$0) antiferromagnetism were identified. As illustrated for HoCu in Fig. 1, diffraction data from HEiDi (MLZ) show three ordered magnetic states at zero magnetic field. At the lowest temperatures, phase I exhibits commensurate wavevectors $\boldsymbol{k}_c$ = (1/2, 1/2, 0). In phases II and III, magnetic satellites at incommensurate wavevectors $\boldsymbol{k}_{ic}$ = (1/2+δ, 1/2, 0) indicate additional superstructures of nanometric extent. Magnetic structure refinements are consistent with multi-***k*** magnetic order in all three phases. Band structure calculations suggest that commensurate ($\pi\pi$0) order of the rare-earth *f*-electrons may result in a topological band structure with finite winding numbers in reciprocal space. A thorough symmetry analysis further reveals that incommensurate modulations, as observed in phases II and III, may be connected to non-trivial winding in real space, suggesting textures as exotic as an antiferromagnetic skyrmion lattice with alternating topological charges as possible magnetic ground states.

*[1] W. Simeth et al., Topological aspects of multi-*k *antiferromagnetism in cubic rare-earth compounds, J. Phys.-Condens. Matter 36, 215602 (2024)*
DOI: 10.1088/1361-648X/ad24bb

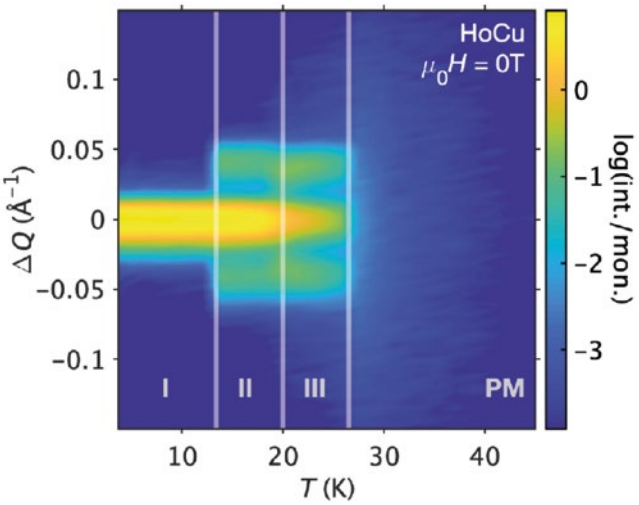

Figure 1: Neutron diffraction intensity as a function of temperature in HoCu at zero magnetic field. Three magnetically ordered phases, denoted I, II, and III, are distinguished. Phase I may be described as commensurate antiferromagnetic order. Phases II and III feature additional incommensurate superstructures on a nanometric scale.

Demonstration of neutron time-of-flight diffraction with an event-mode imaging detector

T. T. Jäger[1,2], A.S. Losko[3], A. Wolfertz[3], S. Schmidt[4], M. Bertelsen[4], A. Khaplanov[5], S. R. Agnew[6], F. Funama[7], M. Morgano[8], M. Roth[2], J. R. Gochanour[9], A. M. Long[1], L. Lutterotti[10], S.C. Vogel[1]

[1] Material Science and Technology Division, Los Alamos National Laboratory, Los Alamos, USA; [2] Institut für Kernphysik, Technical University of Darmstadt, Darmstadt, Germany; [3] Forschungs-Neutronenquelle Heinz Maier-Leibnitz, Technical University of Munich, Garching, Germany; [4] Data Management and Software Centre, European Spallation Source ERIC, Lyngby, Denmark; [5] Second Target Station, Oak Ridge National Laboratory, Oak Ridge, USA; [6] Materials Science & Engineering, University of Virginia, Charlottesville, USA; [7] Neutron Optics and Polarization Group, Oak Ridge National Laboratory, Oak Ridge, USA; [8] European Spallation Source ERIC, Lund, Sweden; [9] Physics Division, Los Alamos National Laboratory, Los Alamos, USA; [10] Department of Industrial Engineering, University of Trento, Trento, Italy

This paper introduces a novel Timepix3-based event-mode imaging neutron diffraction detector system as well as first results of a silicon powder diffraction measurement made at the HIPPO neutron powder diffractometer at the Los Alamos Neutron Science Centre. The results were benchmarked against *McStas* simulations and the standard HIPPO detectors, showing good agreement for peak resolution.

Recently, event-mode camera detectors have started to be used for cold and thermal neutron imaging. We present a demonstration of this technique for neutron scattering too, and in particular time-of-flight diffraction applications.

Measurements at the HIPPO beamline

To compare this novel diffraction detection method utilising imaging detectors with a conventional neutron time-of-flight diffraction detector system, a silicon powder diffraction experiment was conducted on the High Pressure-Preferred Orientation (HIPPO) beamline at the Los Alamos Neutron Science Centre Spallation Neutron Source. The widely used Rietveld code *MAUD* was adapted to calibrate and process the 2D TOF data generated by the camera-based setup. Simulations with the Monte Carlo code *McStas* were carried out and combined with the existing HIPPO detector data to serve as a comparison.

Resolution comparison

We found that the $\Delta d/d$ resolution obtained with the camera-based setup is as expected for the short distance between sample and detector used in this demonstration: at a sample-to-detector distance of 11.3 cm the resolution from the GSAS analysis was 2.1%, in good agreement with simulations carried out with *McStas* yielding $\Delta d/d$ = 2.2% at 90°. The validity of resolutions determined by *McStas* simulations was established by comparing them with the nominal resolution of HIPPO. Simulations indicate that at suitable distances, reducing sample broadening, similar resolutions can be achieved with the novel imaging detector system and with the current HIPPO ^{3}He-based detector system. Furthermore, a larger solid angle can be covered by the camera-based system compared to conventional detector panels, thereby detecting more neutrons and reducing measurement time. The camera-based setup is also able to record energy-resolved radiography data of the sample in the transmitted beam direction (see Fig. 1), thereby facilitating simultaneous neutron diffraction and radiography characterisation, including Bragg-edge and neutron absorption resonance imaging.

[1] T. T. Jäger et al., Demonstration of neutron time-of-flight diffraction with an event-mode imaging detector, J. Appl. Crystallogr. 57, 1107-1114 (2024)
DOI: 10.1107/S1600576724004448

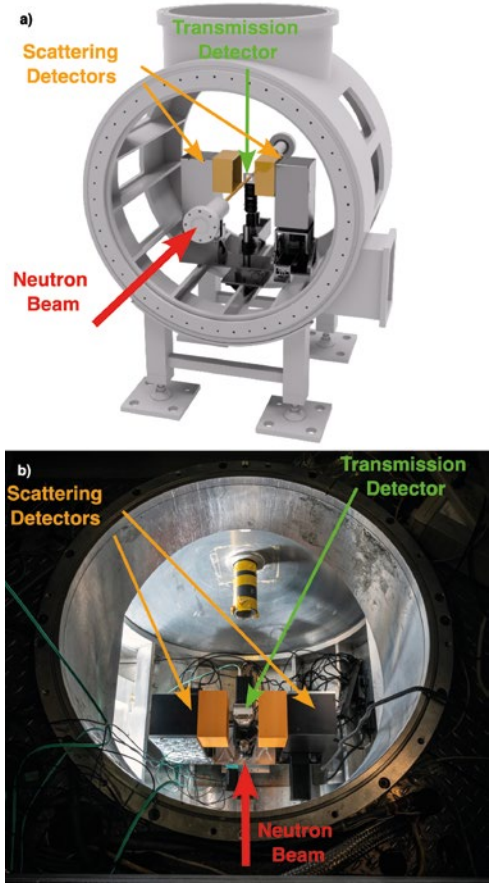

Figure 1: (a) Schematic of the experimental setup inside the HIPPO sample chamber with three event-mode cameras (the transmission detector for radiography is much smaller than the large-field-of-view scattering detectors). (b) Photograph of the actual setup from the top of the HIPPO sample chamber.

Event-based high-resolution neutron image formation analysis using intensified CMOS cameras

A. Gustschin[1], Y. Han[1], A. Losko[1], A. Wolfertz[1], D. S. Hussey[2], L. Szentmiklósi[3], Z. Kis[3], P. Trtik[4], P. Boillat[4], A. Kaestner[4], M. Strobl[4], A. Tengattini[5,6], L. Helfen[5], M. Schulz[1]

[1] Heinz Maier-Leibnitz Zentrum (MLZ), Technical University of Munich, Garching, Germany; [2] National Institute of Standards and Technology (NIST), Gaithersburg, USA; [3] Nuclear Analysis and Radiography Department, Centre for Energy Research, Budapest, Hungary; [4] Laboratory for Neutron Scattering and Imaging, Paul Scherrer Institut (PSI), Villigen, Switzerland; [5] Institut Laue-Langevin (ILL), Grenoble, France; [6] Université Grenoble Alpes, Grenoble INP, CNRS, Grenoble, France

We present a high-resolution neutron imaging setup using an image intensifier and a CMOS camera. Its performance is evaluated via neutron radiography of a Siemens star pattern and resolution analysis, comparing gadolinium gallium garnet (GGG) and gadolinium oxysulfide (GOS) scintillators. Both achieve a similar resolution of 4 – 5 µm in event-mode acquisition. This evaluation approach makes it possible to optimise scintillator design beyond conventional methods.

Compact neutron imaging setup

The imaging setup developed is a compact, modular system using mostly off-the-shelf components (see Fig. 1), offering flexibility for customisation with different optics and cameras. The scintillator is mounted on a custom C-mount holder attached to an optical system allowing for zooming (3 – 8×) and focusing. Possible effective pixel sizes are in the range of 0.8 – 2.2 µm and a field of view up to 4.2 mm in diameter can be reached. The crucial component is an image intensifier allowing amplified weak light signals from the scintillator to be detected. A high-speed Hamamatsu ORCA-Fusion BT CMOS camera captures images on a 2304 × 2304 pixel array. The system was tested at the NIPS-NORMA station at the Budapest Neutron Centre for high-resolution neutron radiography. Neutron radiographs were taken using 5 µm thick GOS:Tb and 20 µm thick GGG:Eu scintillators at 5.9 × magnification (1.1 µm eff. pixel size).

Interesting finding of image formation process

While the optical resolution of the system is at about 2 µm (limited by the hexagonal multi-channel plate of the intensifier), in event-based neutron radiography it was in the range of 4 – 5 µm. The resolution loss is related to the scintillation process, where captured neutrons trigger secondary particles leading to light emission. Although the image formation process of both tested scintillators (GOS and GGG) differs in terms of light generation, the resolution achieved is similar. The data acquired suggests that for GGG the challenge in event-based imaging is the low light conversion efficiency and low quantum efficiency of the light intensifiers, while for GOS the light scattering in the grainy scintillator limits the resolution. The study quantifies how much the light spread is reduced by halving the GOS scintillator thickness and discusses resulting aspects for future system development. By quantifying these different aspects of image formation, one can effectively determine the technical improvements needed for both the scintillator and the optical system to improve the imaging system.

This work was funded by the BMBF within the ErUM-Pro project NeutroSense (05K19WO2).

[1] A. Gustschin et al., Event-based high-resolution neutron image formation analysis using intensified CMOS cameras, Sci Rep 14, 26941 (2024)
DOI: 10.1038/s41598-024-78104-z

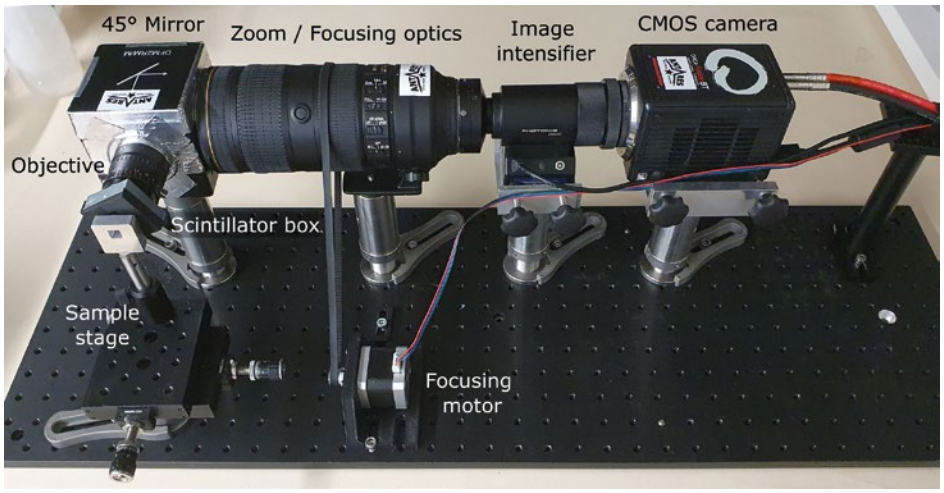

Figure 1: Setup of the high-resolution neutron imaging system with sample stage, scintillator box on objective, beam turning cage, zoom and focusing optics, image intensifier and CMOS camera.

Pencil beam kernel-based dose calculations on CT data for a mixed neutron-gamma fission field

L. B. Sommer[1,2,3], S. Kampfer[2,3], T. Chemnitz[2], H. Breitkreutz[2], S. E. Combs[3,4], J. J. Wilkens[1,3]

[1] Department of Physics, TUM School of Natural Sciences, Technical University of Munich, Garching, Germany; [2] Heinz Maier-Leibnitz Zentrum (MLZ), Technical University of Munich, Garching, Germany; [3] Department of Radiation Oncology, TUM School of Medicine and Health and Klinikum rechts der Isar, Technical University of Munich, Munich, Germany; [4] Institute of Radiation Medicine (IRM), Helmholtz Zentrum München, Deutsches Forschungszentrum für Gesundheit und Umwelt (GmbH), Neuherberg, Germany

A dose calculation method on patient CT data for fast neutron therapy at MEDAPP at FRM II is presented. It is based on pencil beam kernels (PBK) for neutron and gamma radiation generated from a combination of measured and simulated data. For the calculation of neutron dose deposition, tissue-specific correction factors were generated for soft tissue, bone, and lung tissue.

Accurate dose calculation, including tissue-specific interactions, is of paramount importance for fast neutron therapy. To date, no software for dose calculation on patient CT data has been available for MEDAPP. The similarities in the characteristics of depth dose curves and the exponential attenuation in water motivate the application of dose calculation algorithms originally developed for photons also for neutrons. Two sets of PBKs were generated, one for neutron radiation and one for gamma radiation. They were validated through depth dose curves and beam profiles. Monte Carlo simulations were performed to include the build-up region close to the phantom surface in the depth dose curves and to distinguish between the direct and the scattered components of the neutron and the gamma dose. For the purpose of dose calculation using PBKs, the open-source research treatment planning software matRad was used. A correction method for tissue heterogeneities previously suggested was applied.

Dose calculation in water

For both beam components, the applied dose calculation approach gives good results with reference to dose calculations using simulated and measured data. For the neutron dose deposition in water, an agreement within ± 10% for the first 100 mm was found. Depending on the field size, this depth comprises the 70 – 85% dose fall-off region. A comparison for one field size is shown in Fig. 1 a.

Dose calculation on patient CT

As presented in this work, dose calculations for heterogeneous media could be vastly improved by the application of tissue-dependent corrections that account for the tissue composition. For bone tissue, the effect of the correction factors is clearly visible in Fig. 1 b.

In conclusion, the generated pencil beam kernels for the mixed neutron-gamma field facilitate the time-efficient reproduction of depth dose curves from Monte Carlo simulations within tens of seconds for the neutron and gamma components separately.

[1] L. B. Sommer et al., Pencil beam kernel-based dose calculations on CT data for a mixed neutron-gamma fission field applying tissue correction factors, Phys. Med. Biol. 69, 045022 (2024)

DOI: 10.1088/1361-6560/ad209b

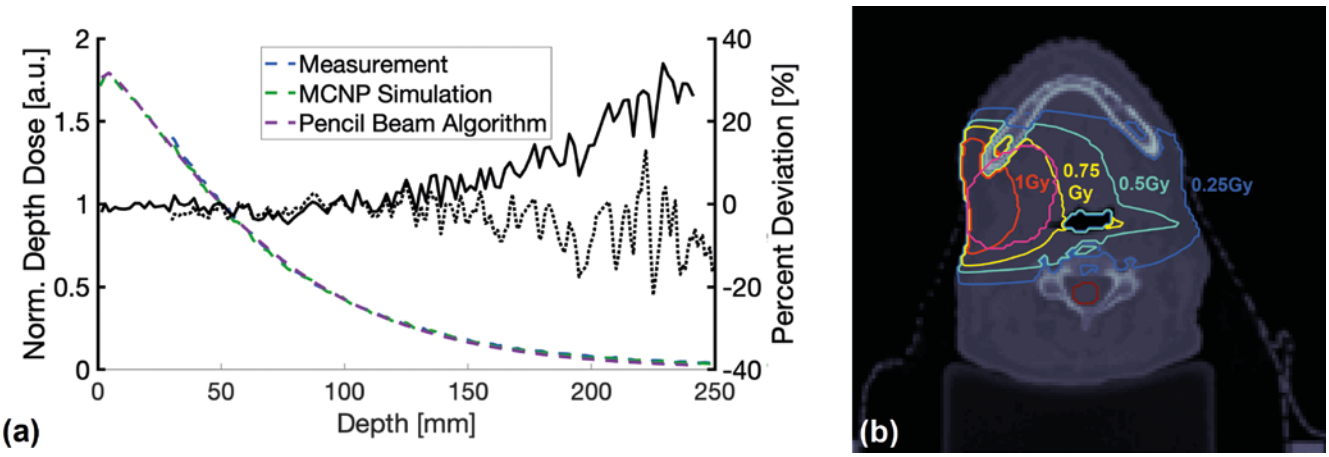

Figure 1: (a) Comparison of the measured depth dose curve (blue) and the calculated ones using Monte Carlo (green) and the PBK algorithm (purple) for the neutron component for field size of 82 mm. Relative errors of the PBK calculations with respect to MC simulations are shown as a black solid line and relative deviations between MC data and measurements are depicted as a black dotted line. (b) Dose distribution of neutron radiation field overlaid on CT data calculated using PBK based dose calculation and tissue-specific correction factors.

High-precision visual servoing for the neutron diffractometer STRESS-SPEC

M. Landesberger[1,2], O. Kediioglou[3], L. J. Wang[1], W. M. Gan[4], J. Rebelo Kornmeier[1], M. Hofmann[1]

[1] Heinz Maier-Leibnitz Zentrum (MLZ), Technical University of Munich, Garching, Germany; [2] Faculty of Engineering and Management, Technische Hochschule Ingolstadt, Ingolstadt, Germany; [3] Institute for Factory Automation and Production Systems (FAPS), Friedrich-Alexander-Universität Erlangen-Nürnberg (FAU), Erlangen, Germany; [4] German Engineering Materials Science Centre (GEMS) at MLZ, Helmholtz-Zentrum hereon GmbH, Garching, Germany

A visual servoing system consisting of an industrial six-axis robot enhanced by a multi-camera tracking system is introduced. The goal is to use it as a highly flexible and precise sample manipulator at the instrument STRESS-SPEC. So far, an absolute positioning accuracy of better than 50 µm was achieved with this system, which is sufficient for strain and local texture measurements even with small sample gauge volumes.

With neutron diffraction, the stress tensor as well as the local texture within engineering components can be analysed non-destructively. In both cases, highly accurate positioning of the sample is essential, requiring the measurement at the same sample location from different directions. Current sample-positioning systems in neutron diffraction instruments combine XYZ tables and Eulerian cradles to facilitate the accurate six-degree-of-freedom (6DoF) handling of samples. However, these systems are not flexible enough with respect to the high complexity of today's components that stem from modern production processes such as additive manufacturing. In particular, the choice of the rotation centre and their range of motion are limited.

Robotic sample manipulator

A means of overcoming these limitations is to use industrial six-axis robots instead of conventional sample manipulators as they offer the necessary flexibility and large movement ranges. However, until now these robots have lacked the absolute accuracy required for strain measurements with small gauge volumes. Therefore, the large industrial robot with high load-capacity, available at STRESS-SPEC since 2012, has been upgraded with a multi-camera setup (Fig. 1). The cameras are used to track the sample motion during a neutron diffraction experiment. A complete process chain was developed to first identify the position of the sample with the help of concentric contrasting circular (CCC) markers attached to it and correct the robot movement in a feedback loop to detect deviations of the actual position from the target position.

Position accuracy

In a proof-of-concept experiment using a laser tracker as an external reference measurement system, a positioning accuracy of better than 50 µm was achieved. In most cases just one compensation movement step was necessary to reach the required target position. After the feasibility of high position accuracy was shown, further enhancements in automation, user-friendly system handling, and portability of other instruments have to be addressed. For this purpose, a digital twin is in development to integrate various data sources from the instrument and the sample in order to pave the way for a fully automatic measurement procedure.

[1] M. Landesberger et al., High-precision visual servoing for the neutron diffractometer STRESS-SPEC at MLZ, Sensors 24, 2703 (2024)
DOI: 10.3390/s24092703

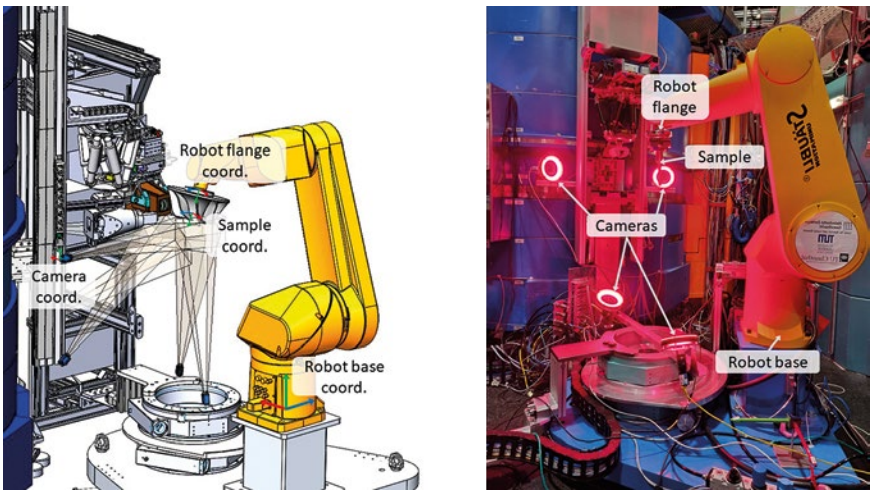

Figure 1: Final multi-camera setup at STRESS-SPEC consisting of six cameras, whereby a camera pair looks from each of three mutually perpendicular directions in order to increase the robustness of the position estimation (from [1]).

Model selection assistance for small-angle neutron scattering users

J. I. Robledo[1], H. Frielinghaus[2], P. Willendrup[3], K. Lieutenant[1]

[1] Jülich Centre for Neutron Science 2 (JCNS-2), Forschungszentrum Jülich GmbH, Jülich, Germany; [2] Jülich Centre for Neutron Science (JCNS) at MLZ, Forschungszentrum Jülich GmbH, Garching, Germany; [3] Data Management and Software Centre, European Spallation Source, Lyngby, Denmark

The advantages of virtual small-angle neutron scattering (SANS) experiments carried out by Monte Carlo simulations were combined with recent advances in computer vision to generate an assistance tool for model selection. A dataset of 260.000 virtual SANS experiments at KWS-1 was generated for machine learning purposes (Fig. 1). A recommendation system of convolutional neural networks was trained to predict SANS models from the two-dimensional scattering pattern.

The challenge of model selection assistance

Small-angle neutron scattering (SANS) experiments provide valuable insights into the structural and morphological properties of materials at the nanoscale, making SANS an important method to investigate nanometre-sized biological systems, polymers, magnetic particles, etc. While an averaged particle size is easily available from SANS data, detailed information about size distribution and geometry is difficult to obtain, making any support by machine learning (ML) algorithms desirable. Some efforts to use ML algorithms for SANS data have already been made in one-dimensional curves and in two-dimensional images and show great potential on small datasets. Nevertheless, algorithms such as deep neural networks require large datasets and this becomes a problem in neutron science because conducting experiments in real-world settings is time-consuming (due to complex sample preparation, experimental setups, and data collection processes). Moreover, most of the available data lack metadata and have format compatibility issues that do not allow for easy usability. As a consequence, there is only a limited amount of experimental data, which hinders the construction of a comprehensive and large-scale dataset required for machine learning applications. The use of Monte Carlo simulations provides researchers with a cost-effective and efficient virtual testing ground for exploring various instrument setups, optimising parameters, and identifying the most promising configurations for specific experiments.

Progress made using the new algorithm

The results show that the convolutional neural networks can learn the model prediction task, and that this recommendation system has a high degree of accuracy in the classification task on 46 different SANS models [1]. The network was also tested with real scattering data. Finally, a recommendation system in the SANS user data analysis procedure is successfully obtained.

[1] J. I. Robledo et al., Learning from virtual experiments to assist users of small-angle neutron scattering in model selection, Sci. Rep. 14, 14996 (2024)
DOI: 10.1038/s41598-024-65712-y

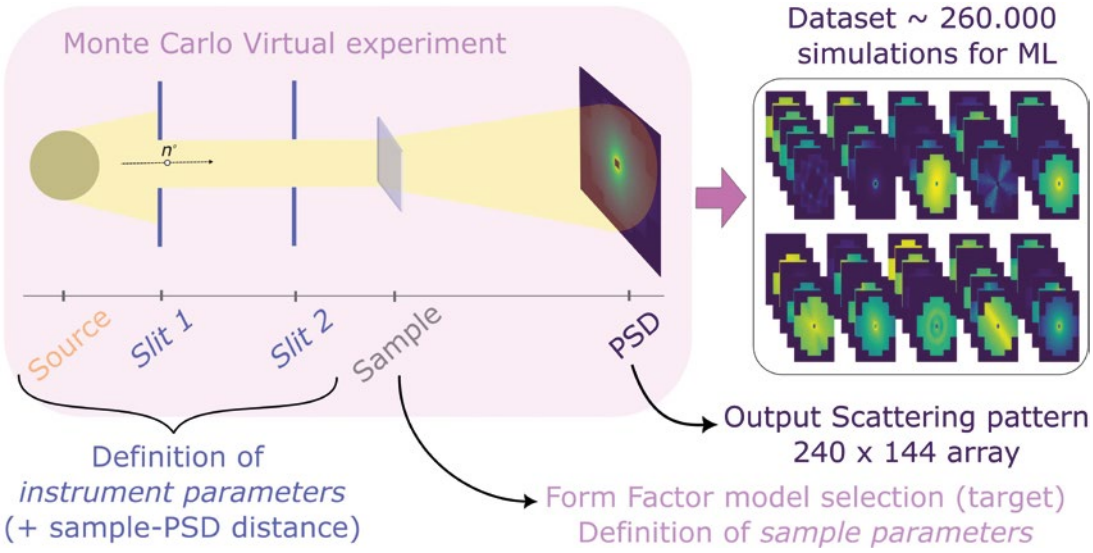

Figure 1: Schematic of how the database was generated. The virtual experiment arrangement is shown on the upper left. A set of 330.000 simulations of our virtual experiment setup was simulated under different instrument and sample parameter configurations. After clearing the database of null and low intensity images, the resulting 259.328 data arrays are separated in train, test, and validation partitions, which are stored in HDF files.

Benchmarking atomistic simulations against X-ray and neutron scattering data

A. Majumdar[1], M. Müller[1,2,3], S. Busch[1]

[1] German Engineering Materials Science Center (GEMS) at MLZ, Hemlholtz-Zentrum hereon GmbH, Garching, Germany; [2] Institute of Materials Physics, Helmholtz-Zentrum hereon GmbH, Geesthacht, Germany; [3] Institut für Experimentelle und Angewandte Physik (IEAP), Christian-Albrechts-Universität zu Kiel, Germany

Different materials at the atomic level can be studied using computer simulations. However, the simulations must be benchmarked against experiments such as X-ray and neutron scattering experiments to ensure that the simulations represent reality. In this work, we benchmark atomistic simulations of different materials against scattering data using the program Sassena in a fast and error-free manner.

Simulations: Attempt at modelling the real world

With modern-day fast computers, it is possible to simulate billions of atoms based on mathematically modelled atomic interactions. These simulations can be used to understand the fundamental reasons behind an observed material behaviour, or to predict an unobserved material behaviour. However, a correct representation of reality through simulations must be ensured before using simulations for the analysis or prediction of material behaviour.

At the atomic level, Molecular Dynamics (MD) and Monte Carlo (MC) simulations are two simulation methods that perform well. These simulation methods capture dynamics on the timescale of picoseconds to nanoseconds and structures ranging from a few angstroms to hundreds of nanometres.

Neutrons: Verifying the model matches the real world

X-ray and neutron scattering techniques probe the same time and length scale, making them ideal for benchmarking the atomistic simulations. The simulations provide a description of time-dependent atomic positions, and the scattering data include the intensity of scattered X-rays and neutrons. To benchmark the simulations against scattering data, a program is required to calculate the scattering intensity from simulations in a fast and error-free manner. In this work, we used the program Sassena to calculate scattering data from simulations of some reference systems and the calculated data were benchmarked with published measured scattering data (Fig. 1). A good match between calculation and scattering data was achieved with computation times lower than other similar programs.

This work confirms Sassena to be a fast and error-free solution for benchmarking atomistic simulations against scattering data. A benchmarked simulation can be used for the analysis and prediction of complex material behaviours in the future.

[1] A. Majumdar et al., Computation of X-ray and neutron scattering patterns to benchmark atomistic simulations against experiments, Int. J. Mol. Sci. 25, 1547 (2024) DOI: 10.3390/ijms25031547

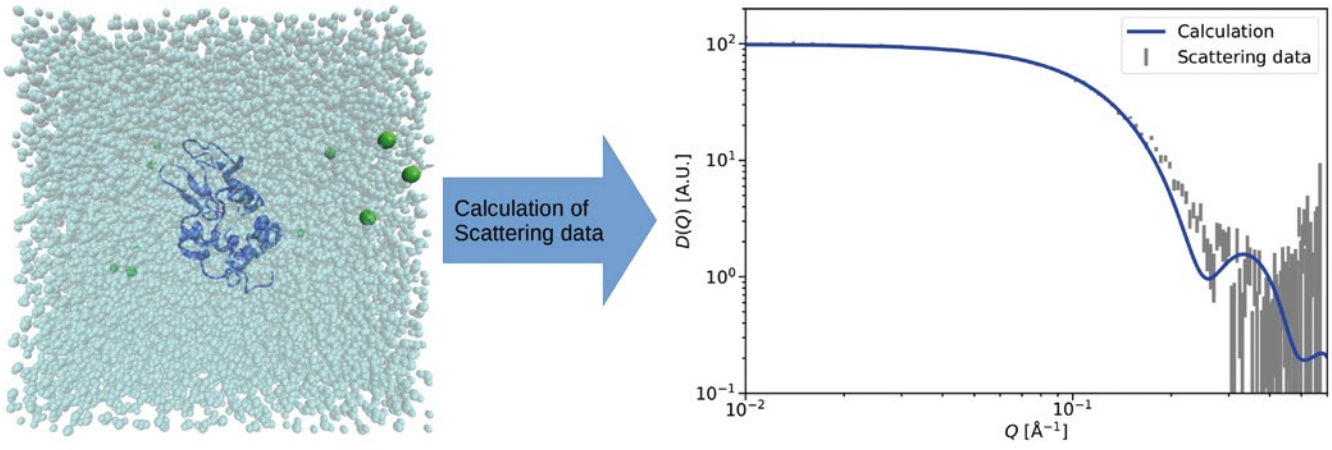

Figure 1: [Left] MD simulation of a lysozyme protein molecule immersed in water, [Right] Benchmarking MD simulation against scattering data by comparing the calculation from Sassena with scattering data.

A buffer-gas trap for the NEPOMUC positron beam: Optimisation studies with electrons

A. Deller[1,3], C.W. Rogge[1,2], S. Desopo[3], E.V. Stenson[1], J.R. Danielson[3], M.R. Stoneking[1,4], C. Hugenschmidt[2], T. Sunn Pedersen[1,5], C.M. Surko[3]†

[1]Max Planck Institute for Plasma Physics, Garching, Germany; [2]Technical University of Munich, Garching, Germany; [3]Physics Department, University of California San Diego, La Jolla, USA, [4]Lawrence University, Appleton, USA; [5]University of Greifswald, Greifswald, Germany

Buffer-gas traps (BGTs) are invaluable in studies of matter-antimatter interactions, antihydrogen research, and positronium laser spectroscopy. We report on the optimisation using electrons of a BGT system designed to accumulate positrons from the NEPOMUC (NEutron-induced POsitron source MUniCh). Efficient positron accumulation is vital for APEX (A Positron Electron eXperiment), which aims to trap an electron-positron pair plasma.

Buffer gas trap

BGTs utilise inelastic interactions with nitrogen molecules to capture positrons from a continuous source. The scattered positrons collect in an electrostatic potential minimum superimposed with a uniform magnetic field.

The cylindrical electrodes of the BGT are grouped into three stages of increasing internal diameter (Fig. 1). The pressure gradient and shape of the electric potential maximise inelastic scattering in stage 1 and minimise losses in stage 3 (e.g., collision-driven diffusion and annihilation). The energy-dependent cross-sections are intrinsically linked to the electronic and ro-vibrational energy levels of the target molecules. Although cross-sections for electron and positron scattering are not identical, they are similar enough for the BGT to be tested using electrons.

An electron beam from an yttria-coated iridium disc cathode was tailored to mimic the NEPOMUC positron beam. The large operational parameter space of the BGT was then systematically explored to optimise the electron trapping efficiency ($\varepsilon \approx 50\%$). We anticipate the trapping efficiency will be $\varepsilon = 10-20\%$ for positrons, due to losses via positronium formation.

Accumulator

Bunches of trapped electrons were ejected from the BGT by lowering the voltage applied to the gate electrode. The ramp rate can be tuned to prioritise narrow energy spreads (< 0.1 eV) or very short pulses (< 100 ns). Ejected electrons were dynamically recaptured in a separate Penning trap. The inlet potential of the accumulator was lowered to allow each bunch to enter, and then raised to prevent its escape. The vacuum pressure ($\lesssim 10^{-5}$ Pa) is much lower than in the BGT, allowing for longer confinement times (≈ 600 s). Over 100 bunches were accumulated to create a non-neutral plasma of $> 10^8$ low-energy electrons.

[1] A. Deller et al., A buffer-gas trap for the NEPOMUC positron beam: Optimisation studies with electrons, J. Plasma Phys. 89, 935890602 (2023)
DOI: 10.1017/S0022377823001241

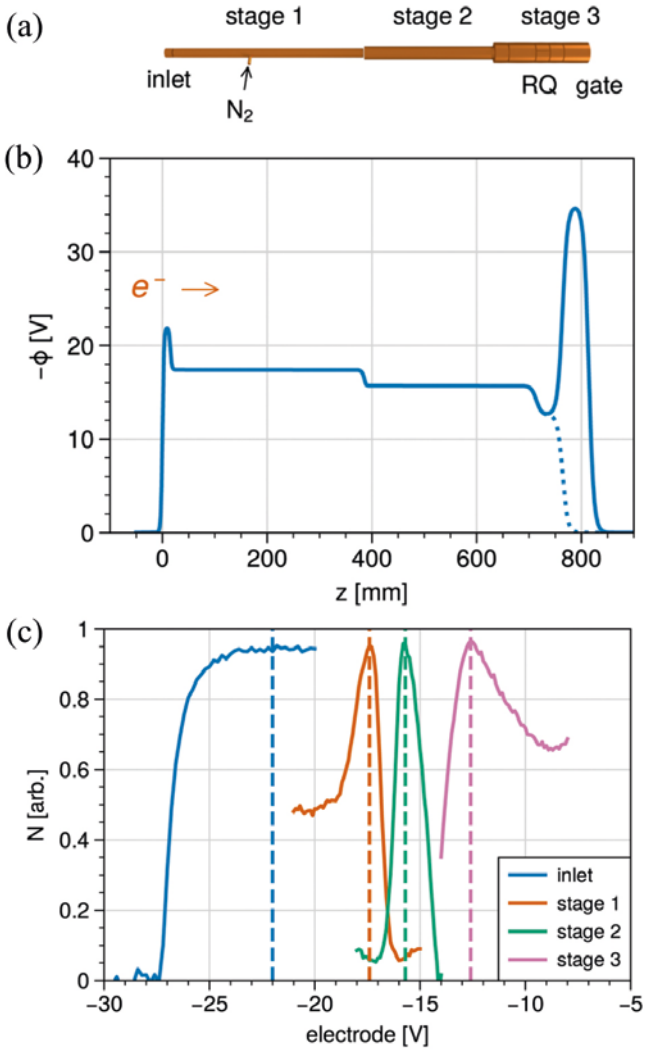

Figure 1: (a) Schematic of the BGT electrodes (approx. to scale). (b) On-axis electric potential configured for trapping 27 eV electrons in the BGT. (c) Relative number of electrons captured in the BGT for different electrode biases following a 200 ms filling cycle with 0.1 Pa of N_2 in stage 1. The dashed lines represent the optimised electrode voltages.

FPGA-stabilised magnetic levitation of the APEX-LD high-temperature superconducting coil

A. Card[1,2], A. Deller[1,3], M.R. Stoneking[4], J. von der Linden[1], E.V. Stenson[1]

[1] Max Planck Institute for Plasma Physics, Garching, Germany; [2] Technical University of Munich, Garching, Germany; [3] University of California San Diego, La Jolla, USA; [4] Lawrence University, Appleton, USA

We demonstrate magnetic levitation in vacuum of a compact high-temperature superconductor (HTS) coil designed for the magnetic confinement of an electron-positron pair plasma. Stable levitation was achieved by continuous adjustment of the lifting coil current using a proportional-integral-derivative (PID) feedback loop implemented by a field-programmable gate array (FPGA). A levitation time in excess of 3 hours was achieved with a mean vertical displacement from the setpoint position of −3 µm and a standard deviation of σ_z = 18 µm.

APEX-LD (A Positron Electron eXperiment Levitating Dipole) is designed for the magnetic confinement of a low-energy electron-positron pair plasma. This is a compelling goal for fundamental plasma physics investigations, because the perfect mass symmetry of the positive and negative charges is predicted to suppress many of the instabilities associated with magnetically confined electron-ion plasmas. To achieve plasma conditions, low energy positrons, supplied by the NEPOMUC positron beam, will fill the compact dipole trapping volume provided by a novel HTS floating coil (F-coil). In this work, we demonstrate PID feedback-stabilised magnetic levitation of the F-coil using an FPGA.

Actively stabilising a levitating coil

The closed, no-insulation (NI) rare-earth barium copper oxide (ReBCO) F-coil is energised with a persistent current to generate a dipole magnetic field, then magnetically levitated by a water-cooled copper lifting coil (L-coil) located above. The FPGA-based PID feedback algorithm continuously adjusts (1 kHz) the L-coil current in response to the vertical position of the F-coil (measured by an array of laser-ranging sensors). The PID feedback parameters were optimised with a 1D simulation of the levitation system.

Successfully launching an HTS coil

Initiating levitation is challenging because induced eddy currents in the cryogenic copper launch pad persist for several seconds and magnetically resist the motion of the F-coil. By running the L-coil at maximum current, we free the F-coil from the launch pad, then catch it in free space using feedback control (Fig. 1). Stable levitation (σ_z = 18 µm) is a crucial milestone for the APEX project, and the 3-hour-long levitation time is more than sufficient for initial plasma confinement studies.

[1] A. Card et al., FPGA-stabilised magnetic levitation of the APEX-LD high-temperature superconducting coil, IEEE Trans. Appl. Supercond. 34, 4606709 (2024)
DOI: 10.1109/TASC.2024.3462796

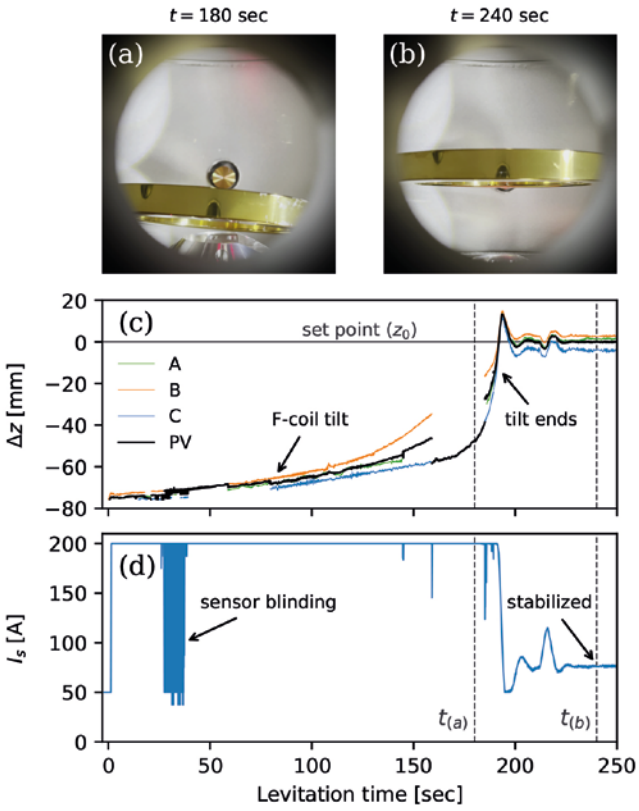

Figure 1: Photographs of the F-coil launch at (a) t = 180 s & (b) t = 240 s. (c) Laser displacement sensor measurements (A, B, C) of the F-coil vertical position and the filtered average (PV) over the first ~4 min of a levitation cycle. (d) L-coil supply current (I_s) over the same time period. The F-coil requires ~200 s to break free from induced eddy currents in the launch pad at which point the feedback control can react normally, achieving stable levitation.

Injection, confinement, and diagnosis of electrons and positrons in a permanent magnet trap

J. von der Linden[1], S. Nißl[1,2], A. Deller[1,3], M. Singer[1,4], N. Belmore[1,5], C.P. Hugenschmidt[2], T. Sunn Pedersen[1,6], H. Saitoh[1,7], E.V. Stenson[1]

[1]Max Planck Institute for Plasma Physics, Garching, Germany; [2]Technical University of Munich, Garching, Germany; [3]University of California San Diego, La Jolla, USA; [4]Applied Materials, Heimstetten, Germany; [5]TicketSwap, Amsterdam, The Netherlands; [6]Type One Energy Group, Madison, USA; [7]Graduate School of Frontier Sciences, The University of Tokyo, Kashiwa, Chiba, Japan

The APEX collaboration reports progress on three prerequisites for a magnetically confined antimatter-matter plasma: 1) electron injection into a permanent magnet trap, 2) strategies for extending positron confinement time, and 3) diagnosis of confined positrons via their annihilation gamma rays. These studies provide the basis for further experiments to demonstrate positron injection into a confined electron plasma.

Electron injection techniques

Electron injection into a permanent magnet trap has been demonstrated using two methods. The first employs $E \times B$ drift injection, where electric fields perpendicular to the confining magnetic field cause electrons to drift across field lines into the trap. This technique is suitable for injecting low-density beams with small spatial and velocity spreads. The second method, edge injection, uses a heated filament placed inside the confinement region. Electrons emitted from the filament can enter the trap, aided by fluctuations arising from collective behaviour. The resulting space charge and electrostatic modes were detected using wall probes, indicating the successful buildup of electron density.

Extending positron confinement

The confinement of positrons from NEPOMUC at FRM II in the dipole trap was studied experimentally by measuring their lifetime. Single-particle simulations using a model of elastic collisions with background neutrals were able to qualitatively reproduce the observed time scales. The simulations also identified strategies for extending the confinement time, such as optimising the trap geometry and radial injection profile of positrons. These findings provide valuable guidance for future experiments aiming to achieve longer positron confinement times.

Localising annihilation with a detector array

To improve the diagnosis of confined positrons, a new array of 25 gamma detectors was commissioned. The detectors facilitate the localisation of positron losses. Two analysis techniques are employed: single-photon counting, which uses the detector distribution of counts to reconstruct the source position, and coincident detection, which counts back-to-back gamma pairs on lines of response. Preliminary measurements using a test source confirmed the array's ability to accurately locate annihilation events (Fig. 1). This new diagnostic capability will be crucial when it comes to understanding the spatial and temporal evolution of confined positrons and distinguishing between different loss processes.

[1] J. von der Linden et al., Injection, confinement, and diagnosis of electrons and positrons in a permanent magnet dipole trap, Eur. Phys. J. D 78, 146 (2024)
DOI: 10.1140/epjd/s10053-024-00821-x

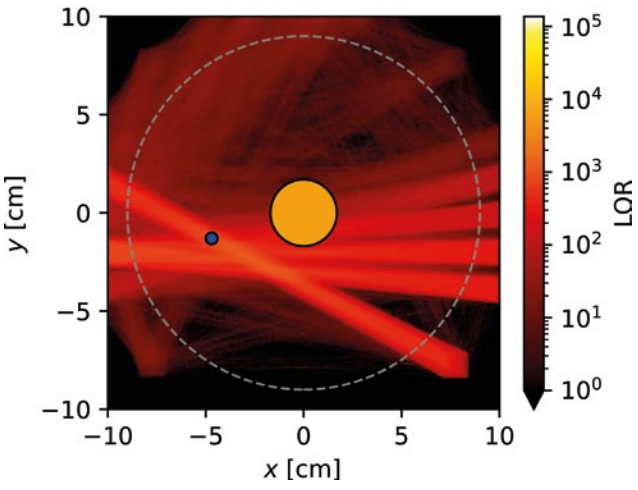

Figure 1: Detector array locates a positron emitting sodium radioisotope source (blue dot) at the intersection of the dominant lines of response (red) between the permanent magnet (orange) and the trap wall (dashed grey). Each coincident detection on two detectors of back-to-back gammas from positron annihilation adds a count to the lines of response connecting the detectors with the brightness corresponding to the counts.

4D Neutron depth profiling at MLZ

R. Neagu[1], R. Gilles[1], Z. Révay[1], R. Gernhäuser[2], S. Golenev[2], B. Märkisch[1,2]

[1] Heinz Maier-Leibnitz Zentrum (MLZ), Technical University of Munich, Garching, Germany;
[2] Department of Physics, TUM School of Natural Sciences, Technical University of Munich, Garching, Germany

NDP is a high-resolution nuclear analytical technique used to study the concentration profiles of light elements, such as Li. Operating batteries containing lithium require monitoring investigations to explain interface effects with a view to increasing their reliability. However, there is a lack of detectors with high detection efficiency and temporal resolution. We have developed such a system based on double-sided silicon strip detectors to permit laterally resolved NDP measurement types for the N4DP instrument.

The neutron depth profiling (NDP) technique is based on neutron capture with the subsequent emission of two back-to-back charged particles with well-defined energies. From the energy loss of these ions, concentration profiles in the upper 50 microns of a sample can be determined with a precision of tens of nanometres.

N4DP instrument upgrade

Until now, the N4DP instrument used unsegmented surface barrier silicon detectors which determine the average profile over the irradiated surface. For many studies, however, it is crucial to measure volume profiles, i.e. 2D mapping combined with the depth profile and also to follow the time dynamics. For example, when operating thin-film Li-ion batteries, tracking the movement of the lithium clouds during (dis-)charging with high precision is of great interest. To upgrade the instrument to four-dimensional profiling, a position-sensitive detector system based on double-sided silicon strip detectors (DSSSD) with extremely thin (~100 nm) and homogeneous entrance windows was developed in combination with customised ASIC-based electronics from the SKIROC family.

First two-dimensional mapping experiment

The highly segmented DSSSD featuring 32 × 266 strips, and the integrated, self-triggering electronics, was characterised in an NDP experiment at the Reactor Institute Delft (RID). For this experiment, different patterns (i.e. a TUM logo) were created by vapor deposition of lithium on 5-µm-thin mylar films. In a dual-detector setup, two methods were probed to reconstruct the lithium-containing image: (i) using a pinhole in a camera-obscura geometry and (ii) detecting coincidence events from the two particles emitted in opposite directions. Fig. 1 shows the TUM pattern based on the coincident particles with a lateral resolution of nearly 100 µm. In the case of the camera obscura, this was found to be in the order of 1 mm. The achievable resolution is highly dependent on the strip granularity, and for the camera obscura also on the pinhole diameter. The time resolution was calculated to be around two frames per second, a rate that can be further improved using the focused cold neutron beam at the FRM II. The new detector system will be used for NDP experiments at FRM II, such as operando measurements in 3 + 1D to explore batteries.

This project was supported by the BMBF, contract No. 05K16WO1, 05K19WO8.

[1] R. Neagu et al., 4D Tomography for neutron depth profiling applications, Nucl. Instrum. Methods Phys. Res. Sect. A 1065, 169543 (2024)
DOI: 10.1016/j.nima.2024.169543

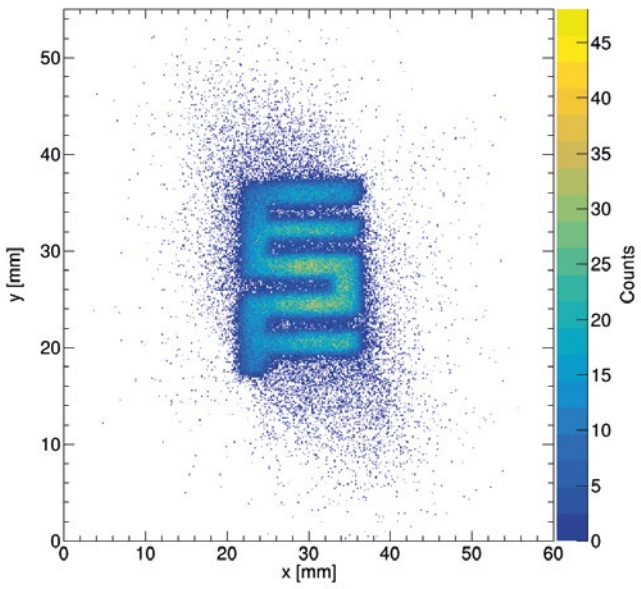

Figure 1: Reconstructed TUM logo from coincident events of the diametrically emitted particles from NDP reactions. The lateral resolution is in the order of 100 µm.

BNPLA – borated plastic for 3D-printing of thermal and cold neutron shielding

S. R. Sebold [1], T. Neuwirth [1], A. Tengattini [2,4], R. Cubitt [4], I. Gilch [3], S. Mühlbauer [1], M. Schulz [1]

[1] Heinz Maier-Leibnitz Zentrum (MLZ), Technical University of Munich, Garching, Germany; [2] Université Grenoble Alpes, Grenoble INP, Grenoble, France; [3] Chair of metal forming and casting (utg), Technical University of Munich, Garching, Germany; [4] Institut Laue-Langevin (ILL), Grenoble, France

We have developed a novel material to facilitate 3D printing of neutron shielding using common enthusiast-grade fused filament fabrication printers. The focus on a cost-effective and easy-to-print material makes rapid manufacturing of custom shielding components viable. We have been able to show good shielding properties using neutron methods.

New material allows for rapid manufacturing of custom neutron shielding

The ability to 3D print neutron shielding using the common fused filament fabrication (FFF) process offers great opportunities to permit the rapid fabrication of complex geometries without access to a workshop or knowledge of machining. By adding neutron absorbing hexagonal boron nitride (h-BN) particles to polylactic acid (PLA), filaments can be created that make 3D printing of neutron shielding possible. We manufactured BNPLA25 with 25%wt h-BN and BNPLA35 with 35%wt h-BN and compared their properties to the commercially available Addbor N25 material. To qualify the applicability of BNPLA25 and BNPLA35 as shielding material for neutron instrumentation, such as neutron imaging, we investigated the overall neutron attenuation and the influence of non-optimised print settings, as well as characterised the incoherent neutron scattering and the microstructure using instruments for neutron imaging and time-of-flight (ToF) small-angle-neutron-scattering (SANS) at ILL.

Neutron measurements verify applicability and performance

The neutron attenuation measured shows excellent agreement with analytical calculations using NCrystal. Approximately 6 mm (8 mm) BNPLA35 are needed for 10^{-3} transmission of a cold (thermal) neutron beam. We were able to show that clearly visible defects due to lack of extrusion arising from suboptimal print settings can be compensated by an 11% to 18% increase in thickness. Incoherent scattering is shown to be strongly reduced compared to pure PLA. The good agreement between the measured attenuation and calculation, combined with the adoption of safety factors, makes for quick and easy development and performance estimation of shielding components.

BNPLA is uniquely suited for 3D printing of neutron shielding (see Fig. 1) because of the combination of non-abrasive h-BN particles in standard PLA, which results in a filament that can be printed with almost any off-the-shelf printer and virtually no prior experience of 3D printing. This mitigates the slightly lower attenuation observed as compared to filaments containing B_4C, which is highly abrasive.

[1] S. R. Sebold et al., BNPLA: Borated plastic for 3D-printing of thermal and cold neutron shielding, Sci Rep 14, 19348 (2024)
DOI: 10.1038/s41598-024-70030-4

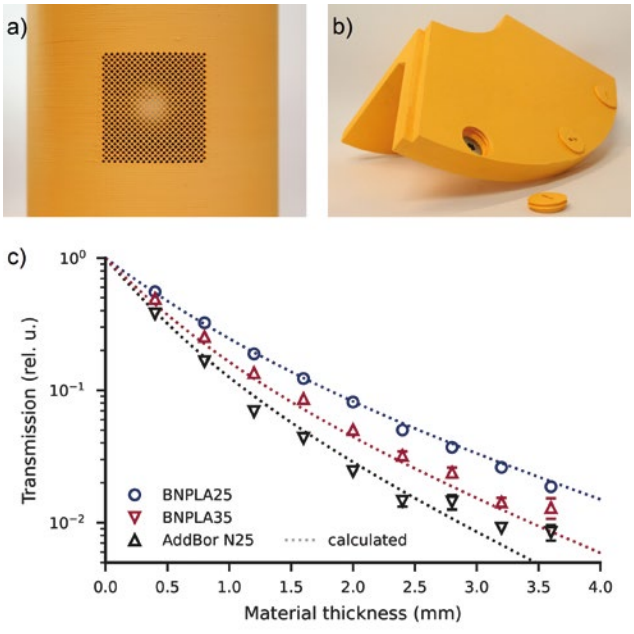

Figure 1: Printed parts using BNPLA35, a) channel array of 684 1 × 1 mm² channels in the cylindrical absorber of a chopper system for the NECTAR instrument. b) Shielding part for a goniometer with printed caps to cover stainless steel bolts. c) Neutron transmission of BNPLA35, BNPLA25 and Addbor N25 depending on material thickness. The measurements were performed at the NeXT instrument of ILL with a polychromatic cold neutron beam.

News from the instruments

News from the instruments

During the reactor outage, significant progress was made in performing advanced and time-consuming installations and upgrades on various instruments. Numerous extensive projects initiated in previous years continued into 2024. Below are selected updates on the tasks accomplished in 2024.

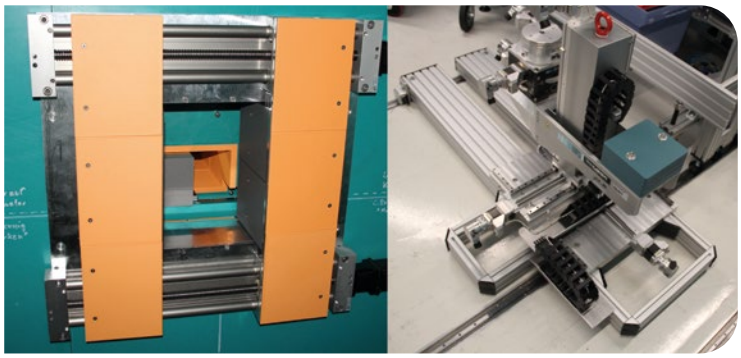

ANTARES

The new high-energy beam limiter of ANTARES (left image) reduces the background produced by epithermal neutrons and gamma radiation. A new cryocooled MgF_2 filter further reduces the epithermal neutrons in the beam, enhancing the Cd-ratio of the instrument. The refurbishment of the second measurement chamber with a new sample manipulator (right image) and detector table is in the process of being completed, allowing for quick and flexible switching between experimental environments.

APEX@NEPOMUC

APEX-LD is the APEX Collaboration's compact levitated dipole trap, designed for positron-electron pair (e^+e^-) plasmas. In 2024, we reported on the levitation stability – see p. 56 – and first pure e^- plasma experiments. When FRM II has resumed operation for users, APEX-LD will be installed in the East Hall, where we will trap positrons (from NEPOMUC) and electrons together. In this photo, an e^- beam trajectory is made visible with background He gas; it follows the dipole magnetic field, plus a small toroidal drift.

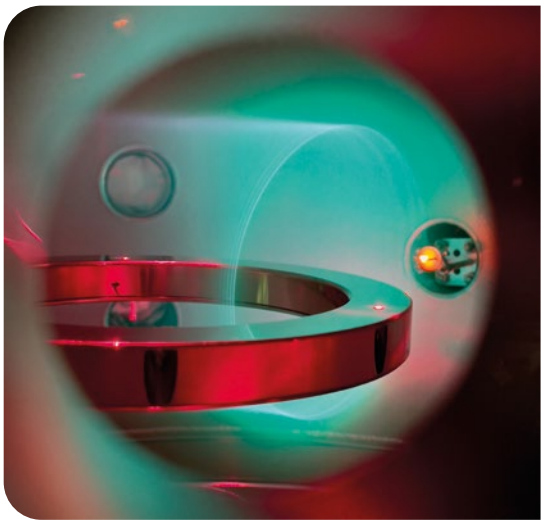

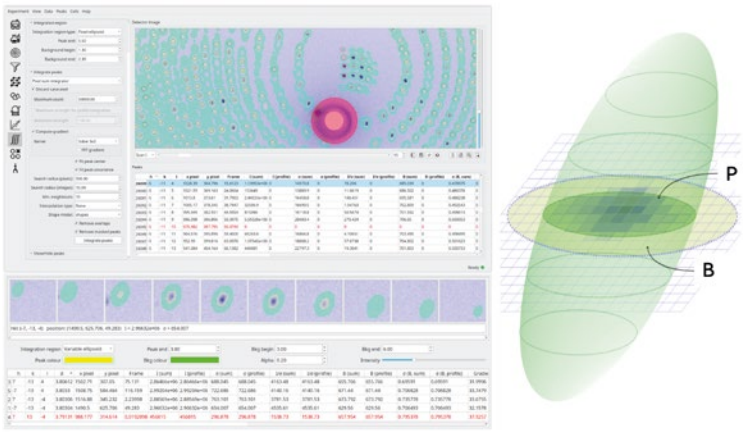

BIODIFF

The JCNS SimLab together with the BIODIFF instrument team is developing a standalone program, called OpenHKL, with a modern graphical user interface that facilitates the data reduction workflow. It is written in C++ for excellent speed, is open-source, natively handles neutron diffraction experiments with different detector geometries, and has a convenient Python scripting interface. This project was initiated in cooperation with Institut Laue-Langevin (ILL).

ERWIN

In 2024, major progress was made in the construction of the ERWIN diffractometer. The optical bench, sample stage and detector bench components were completed and optically adjusted. The CHARM detector was installed on the instrument, including the radial oscillating collimator, the gas handling system and the readout electronics. The main axes of the instrument have been integrated into the instrument control system. Work on the monochromator unit and primary optics is scheduled for 2025.

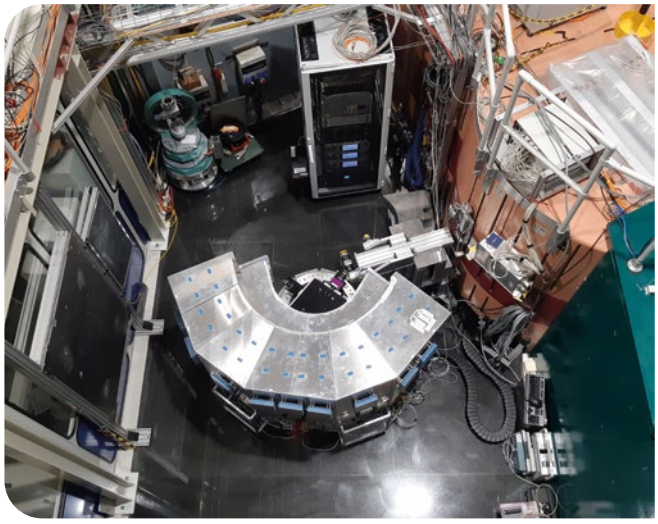

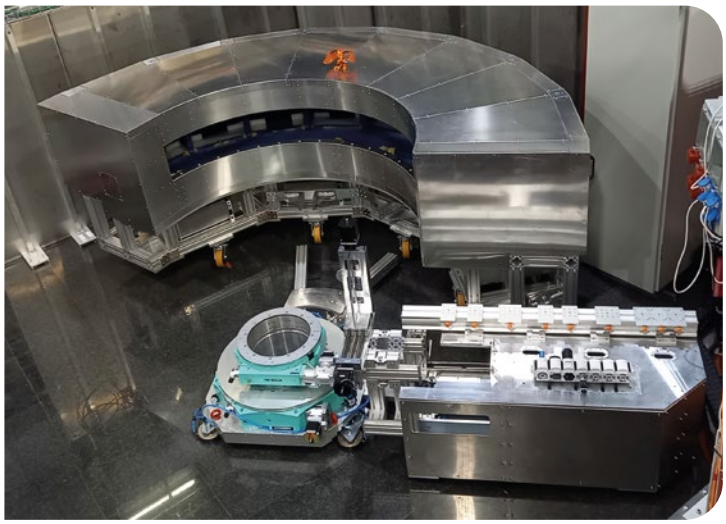

FIREPOD

The new instrument FIREPOD (**F**Ine **RE**solution **PO**wder **D**iffractometer) was successfully transferred from Berlin to Garching as part of a BMBF-funded project. At the MLZ, it will have a “second life” as a dedicated high-throughput diffractometer. In 2024, we integrated the transferred instrument parts as well as additionally acquired optimised components in its dedicated position next to the instrument SPODI on the thermal beam tube SR8a.

HEiDi

The hot single crystal diffractometer HEiDi has been equipped with a small (250 × 150 mm^2 sensitive area) detector (PSD) based on ^{6}Li scintillator glass (in yellow) (a) and 5 × 3 high resolution photomultipliers (b) in cooperation with the JCNS detector group and the central mechanical workshop ZEA-1 at the Forschungszentrum Jülich. The work was funded by BMBF 05K19PA2. The complex detector shielding (c) has active cooling of the readout-electronics inside.

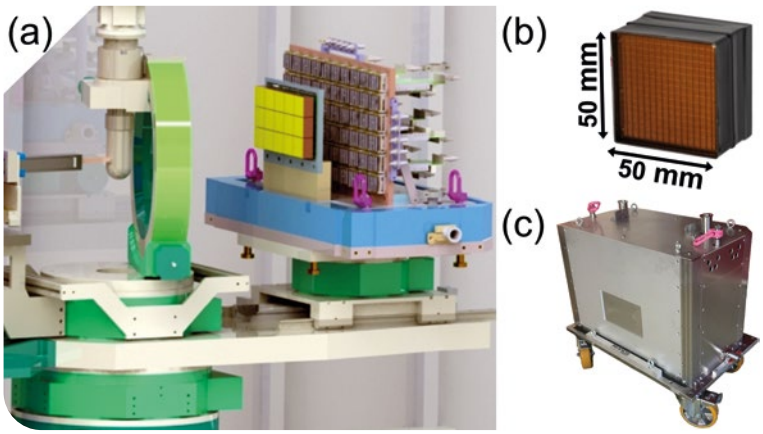

J-NSE

A new friend and assistant at the neutron spin echo spectrometer J-NSE “PHOENIX” is the sample changing robot. It allows for automated sample changing with different sample environments. In addition, the sample aperture can be changed by the robot. The enormous flexibility of the system makes new, and so far unforeseen, applications possible in the future.

KWS-2

Upgrades have been carried out at KWS-2 to provide the instrument with suitable environmental conditions for the samples in order to make significant advances in the field of proton and anion exchange membranes for energy applications and biomembranes for biophysical and health applications. A new versatile dew point generator specifically customised for neutron scattering was recently acquired, calibrated and added to the suite of specialised ancillary equipment at KWS-2. The setup, which includes a new multi-position sample chamber equipped with temperature control and a dew point sensor based relative humidity monitoring system on the sample, will improve the performance of the instrument due to the great versatility that allows for in situ variation of the neutron contrast with H_2O, D_2O or mixed vapours in the beam on the hydrated samples.

KWS-3

Several components of the KWS-3 very small-angle neutron scattering instrument, located between the selector and the main sample position, were covered or “decorated” in the same style as other JCNS instruments. This is the final step in the instrument upgrades carried out over the last decade, also enhancing the “visibility” between neighbouring instruments.

LaDiff

The installation of the new triple-axis spectrometer, LaDiff, based on the former FLEXX instrument is progressing. Our project ensures a triple-axis spectrometer, primarily for magnetic neutron scattering experiments, at the position of the former MIRA instrument at the NL6-guide, in the Neutron Guide Hall West. Emphasis is placed on an option to measure Larmor diffraction and neutron resonant spin-echo in the cold neutron regime. The picture shows the multi-analyser bank equipped with 155 detector channels in (Q,E) space after reassembly in Munich.

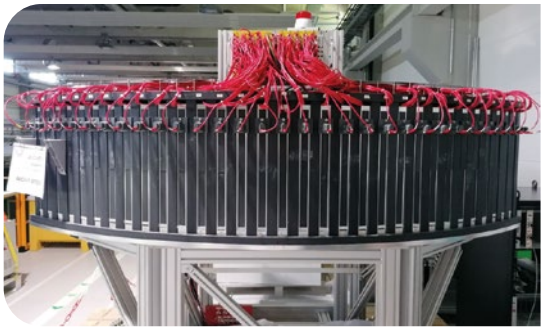

MARIA

Anticipating the operation of the reactor without a cold source and in order to boost the neutron flux at the sample position, a series of upgrades have been undertaken over the past year. These include a) procurement of a second velocity selector with high transmission and relaxed resolution ($\Delta\lambda/\lambda = 20\%$) b) the installation of removable highly curved neutron guides (picture) after the collimation section that increase the vertical neutron focusing and may boost the flux at the sample position even further (~20 – 30%).

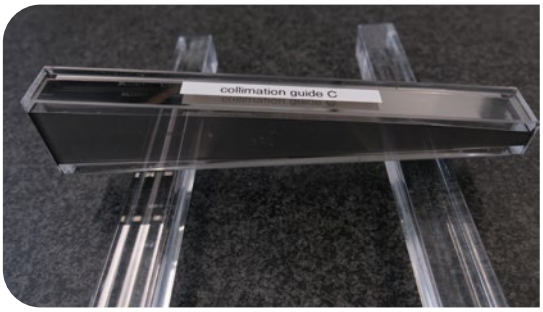

NECTAR

In 2024, NECTAR has been rebuilt from the ground up. This includes a new rail system that was built into the NECTAR floor. Additionally, a newly designed translation stage with a width of 2.5 m can now position and rotate samples of up to 500 kg. The additional width of the new translation system allows larger samples to be placed out of the direct beam when needed. Together with the lowering of the NECTAR floor, a total of ~25 cm in additional sample height can now be imaged at the NECTAR instrument.

NEPOMUC

We have leveraged the expertise developed at NEPOMUC with the use of commercial CMOS technology to detect antimatter and applied it to the construction of the highest spatially resolved antiproton detector ever constructed. OPHANIM (Optical PHoton and ANtimatter IMager) with its active area of 55 × 56 mm, efficiency of 45% and sub-micron resolution will be crucial for the success of the CERN-based experiment AEgIS in which the TUM positron group became a collaborative partner in 2024.

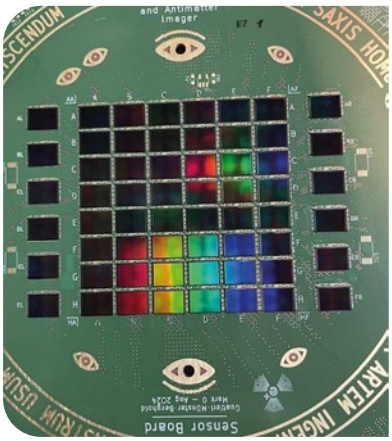

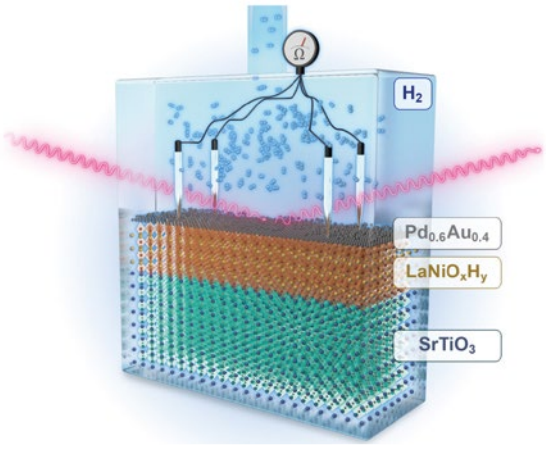

NREX

The sample environment of NREX was upgraded to permit in situ hydrogenation of thin films with simultaneous measurement of the neutron and X-ray reflectivity, and the measurement of electrical transport in 4-point van der Pauw contact geometry with an automated switch matrix. The spring-loaded copper-beryllium contacts eliminate the need for bonding. This simultaneous measurement is essential for the interpretation of kinetic processes, such as the reduction of $LaNiO_3$ shown in the figure.

PANDA

Developments at the cold three-axis spectrometer PANDA focused on: (a) Flexibility in the use of sample environments. (b) Sustaining instrument reliability. (c) Preparation for thermal neutrons.

(a) The new compact sample table combines translational degrees of freedom in x, y (±50 mm), and z (±25 mm) with two goniometer axes (±15°/4°) up to a load of 350 kg/900 kg, enabling the heaviest cryomagnets to be used without mechanical modifications. (c) The new double focusing Cu monochromator is prepared for the optimal usage of thermal neutrons.

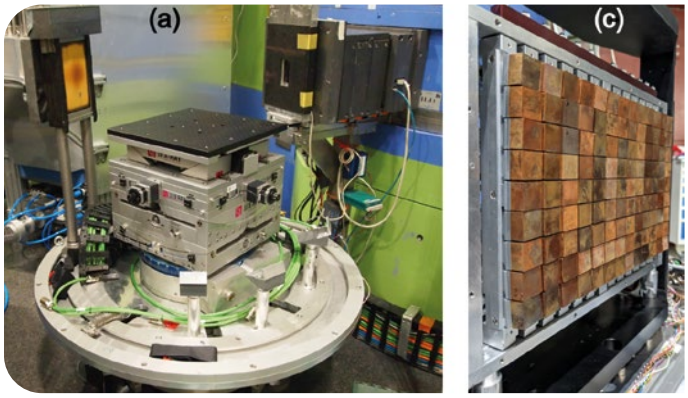

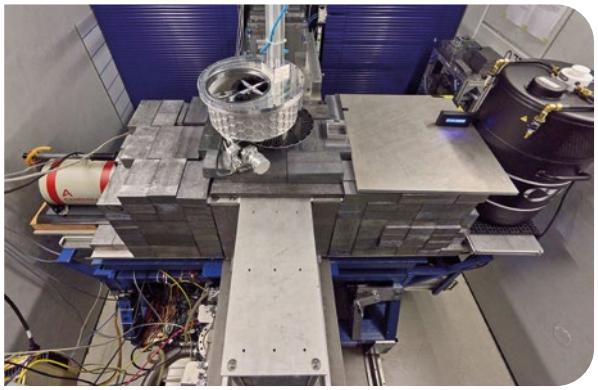

PGAA

The Prompt Gamma Activation Analysis instrument has been upgraded with a recycling cooler and vibration-free electromechanical coolers for all PopTop detectors. The spectrometers now offer 64k high-resolution spectra. The elliptical neutron guide has also been replaced by a shorter low-background borosilicate one that keeps the focal point in the centre of the target chambers, making conditions optimal for small sample irradiations and Neutron Depth Profiling with high-resolution time dynamics.

POLI

In November 2024, the new polariser of POLI (black box on the incoming neutron beam side) was first installed on the instrument. It will produce in situ spin-polarised neutrons via spin-exchange optical pumping (SEOP) for half-polarised diffraction experiments as well as zero-field spherical neutron polarimetry.

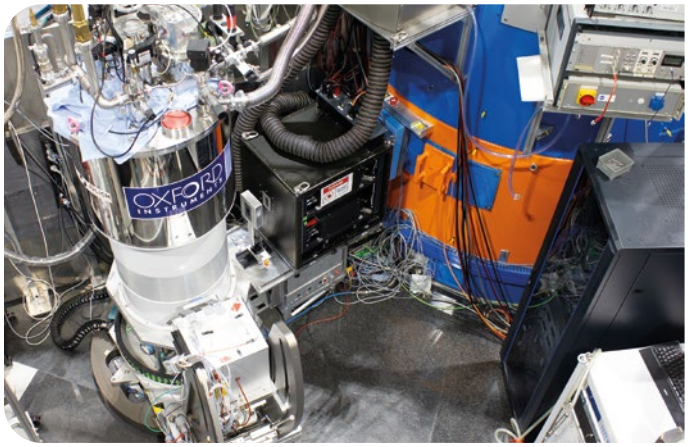

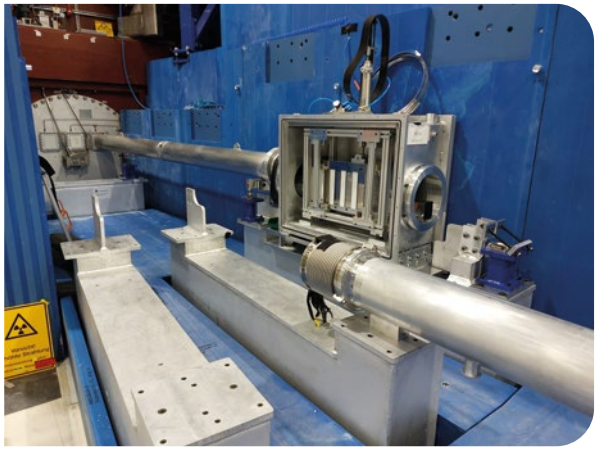

POWTEX

In 2024, significant progress was made not only in the Guide Hall East, particularly on the secondary instrument of POWTEX, where all cylinder surface detectors were recently installed. The picture shows the installation work on POWTEX's primary instrument, including the common SR5 shielding, the POWTEX neutron guide (SR5a), and the POWTEX instrument shutter. This work was carried out by the Infrastructure Instrumentation service group of FRM II and our neutron guide manufacturer, SwissNeutronics.

PUMA

The Nested Mirror Optics (NMO) from SwissNeutronics was delivered to Garching last October and is currently waiting for neutrons to be tested (top). Using the McStasScript Python API, we have developed a user-friendly GUI for the PUMA instrument (bottom), capable of running virtual experiments. This allows the instrument to be tested without neutrons, for new components or to see the effect of different configurations on flux and resolution; any experimentally accessible configuration can be set, and new or potential components can be simulated.

RESEDA

RESEDA has completed the implementation of the MIASANS upgrade, now featuring a large SANS-like detector tank that minimises air scattering, along with new superconducting coils designed to enhance field homogeneity. These advancements are expected to improve RESEDA's resolution in both the momentum transfer and Fourier time ranges.

SANS-1

SANS-1 is jointly operated by FRM II and the Helmholtz-Zentrum Hereon. As well as being a general-purpose instrument, it is optimised for strongly correlated electron systems and cutting-edge materials science research. For in situ and in operando experiments under extreme conditions and access to the highest magnetic fields, SANS-1 has now been upgraded with a new six-axes heavy-duty goniometer capable of precisely positioning a load of 1000 kg. The goniometer is compatible with the full suite of ovens and magnets at MLZ, and is in line with the MORIS magnet roadmap and the planned European collaboration.

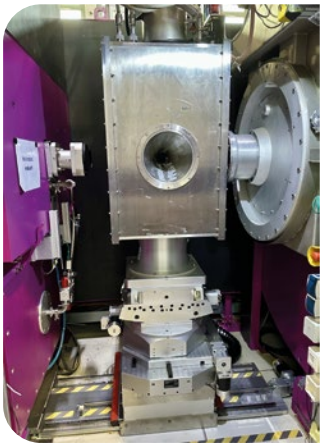

SAPHiR

In 2024 the helium-3 detector system of the SAPHiR instrument was installed by the FRM II detector group. This will be used for time-of-flight neutron diffraction under extreme pressure and temperature conditions (left, the project leader Alan Howard attaches the last cables). The system combines 648 position-sensitive detector tubes with a position resolution of 3 mm that are concentrically arranged on three detector banks situated 90° from the primary beam and in the forward scattering direction (right, note the beam tube for the primary beam). Subsequent to installation, the system was successfully tested with a portable californium-252 neutron source and awaits further commissioning upon restart of the reactor.

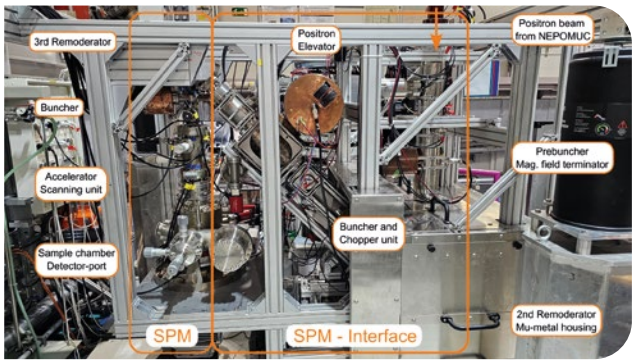

SPM@NEPOMUC

The installation of the Scanning Positron Microscope (SPM) at NEPOMUC was completed in 2024. The SPM is a worldwide unique instrument for spatially resolved non-destructive investigations of inhomogeneously distributed atomistic defects with positron annihilation lifetime spectroscopy. The continuous monochromatic NEPOMUC positron beam is pulsed, accelerated to the desired implantation energy, focused to a spot size of < 1 micrometre, and scanned over the sample. For the first time, the 2D- and 3D-mapping of atomistic defects becomes possible for the user at the MLZ.

SPODI

The high-resolution powder diffractometer SPODI is actively being prepared and adapted for the extension of the powder diffraction suite at SR8 by the dedicated high throughput instruments ERWIN and FIREPOD. In line with the preparations for the reactor start, the function-relevant instrumental components (communication, instrument control, pneumatics, detector system) as well as “working horse” sample environments (closed cycle refrigerators and vacuum furnace) have been explicitly tested.

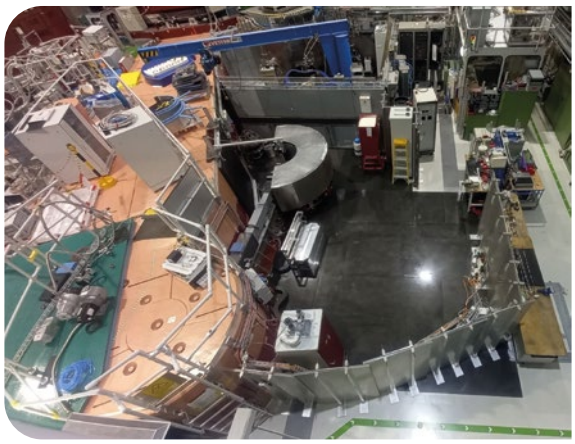

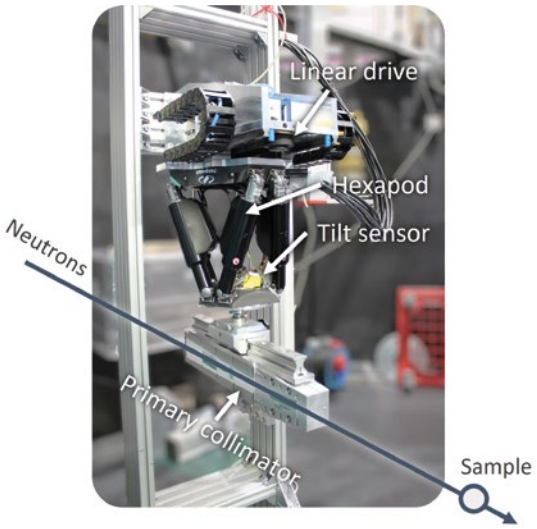

STRESS-SPEC

New double-converging radial collimators for defining the incoming beam dimensions at STRESS-SPEC mounted on a heavy-duty hexapod positioner are now available. The hexapod is used to align the collimators with respect to the neutron beam axis and the sample centre. A range of collimators for defining measurement gauge volume between 1×3 mm^2 and 5×5 mm^2 is available for spatial resolved strain and texture measurements. They can easily be exchanged contingent on the measurement task.

TOFTOF

A design study for a new chopper system to replace the current system which is at the end of its life-time was initiated, as a first step towards the TOFTOF renewal. In parallel, a new elliptically focusing guide is being designed which will enhance the neutron flux at the sample over all available wavelengths. Additionally, a new sample environment for applying humidity and temperature while the sample is characterised by in situ Raman and neutron spectroscopy, was successfully tested for the first time at the TOF-spectrometer FOCUS, PSI.

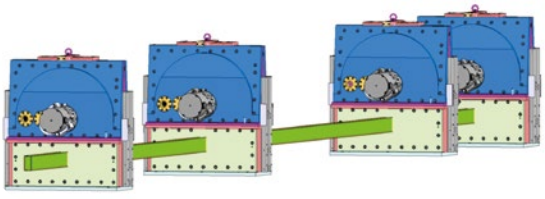

TOPAS

The construction of the thermal neutron time-of-flight spectrometer TOPAS is progressing toward commissioning, driven by the combined efforts of engineers and instrument scientists. Several milestones were achieved last year, including the installation of ^{3}He detectors, the placement of neutron choppers, and testing of the vacuum system. Neutron guides have been installed and await alignment. With these advancements, we remain on track for completion and eagerly await neutrons.

TRISP

The transfer of TRISP from the Experimental Hall to the Neutron Guide Hall East is making good progress. The image shows the final polishing of the new Tanzboden, made of very robust Gabbro granite. Other new components include the 30 meter long focusing neutron guide with integrated transmission polariser, and improved coils for the spin-echo units. The installation of TRISP will begin in early 2025 and will be completed within nine months.

UCN

The cooling system of the new ultracold neutron source has recently been extended via a helium recovery system. It collects approximately eight kilograms of the currently rare and costly helium gas, when the cooling system has to be warmed up for maintenance or repair in its current non-nuclear test phase, which otherwise would have to be blown off. Later, under nuclear conditions, the helium reservoir, which is recovered, will be isotopically pure ^{4}He, which is far more expensive and difficult to produce.

Reactor & Development

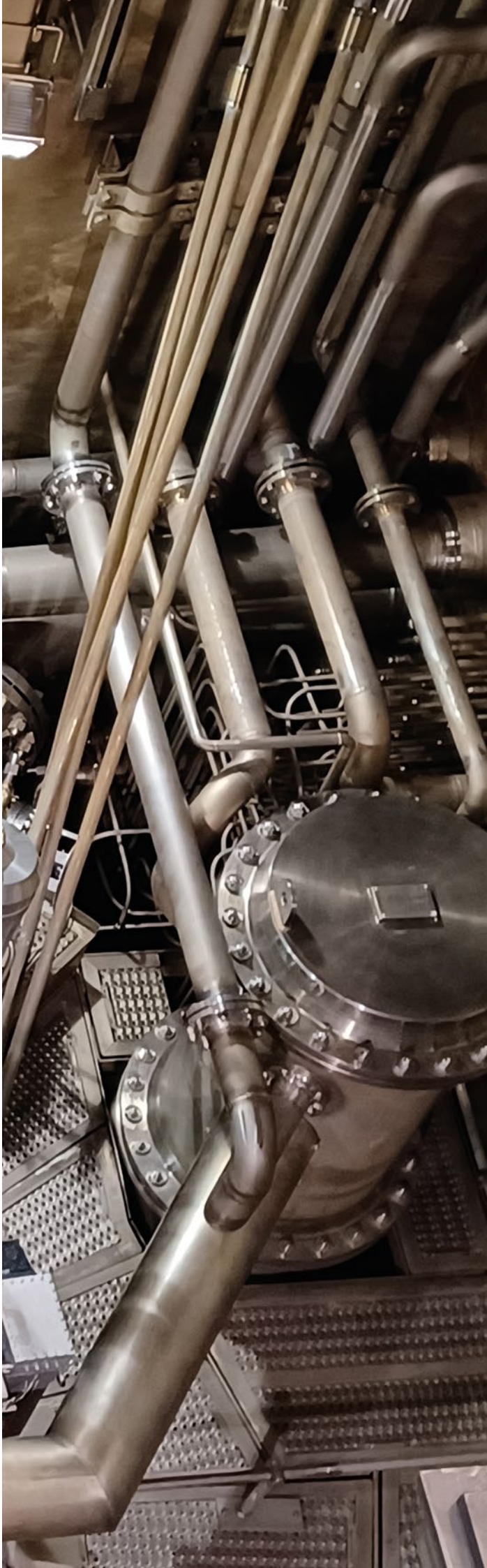

Despite strong head winds – still moving forward

A. Pichlmaier, Technical Director

Forschungs-Neutronenquelle Heinz Maier-Leibnitz (FRM II), Technical University of Munich, Garching

In 2024, the FRM II is still in the state “shut-down operations, fuel unloaded”. This term, strictly speaking, is somewhat misleading and applies only to nuclear operations limited to the fission of uranium. In every other aspect, the FRM II operational groups were busy keeping the reactor systems operational or improving them, thereby making the best of this highly undesirable shutdown.

The year 2024 has been quite a ride for the FRM II team, with many ups and downs that have given us opportunities to excel and new challenges to meet just about every time we turned around. On the plus side, we met all the legal requirements despite a challenging environment. There were no incidents to report. The generally impeccable condition of the FRM II twenty years after its first criticality (March 02, 2004) was attested to by the large number of periodic tests and site inspections carried out internally, by the state regulator (StMUV) and its TSO (technical safety organisations, here: TÜV Süd IS GmbH) and even the international authorities (EURATOM, IAEA) with very few and only minor deviations from the specified condition. In most cases, it proved possible to fix these even while the inspection was still on-going. We made progress towards the restart of the reactor in every field. While this is certainly good news, it is only the minimal result expected by the operator and success sometimes feels painstakingly slow. We have no reason to allow ourselves to drift into complacency, nor to accept that the old ways of doing things are always the best answer. All the time, though, we have worked tirelessly and with ingenuity, adaptability and patience to bring the reactor back online and to learn from events and experience, both internally and from others. I am happy to say that I have great faith and feel proud because of the talents and skills of our teams, but also about the support we tirelessly see from our friends worldwide.[1]

The central channel, a vital component still not ready

Technically, it is still the lack of a new central channel, this crucial and most central component, with the old one having been out of service since the reportable incident in 2022, that prevents the FRM II from functioning. The year 2024 was packed with activities dedicated to its construction, but our efforts have not yet been rewarded with tangible success. Before production of the central channel may start, a number of conditions have to be met. A particular requirement is proof that all the manufacturing steps have been well understood and meet the specified conditions. It is a prerequisite that

Figure 1: Welding test for the plugs of the central channel. What might look to some like the apprentice’s joke in reality represents the high art of TIG welding with all possible tricks played to achieve weld seams according to the specified parameters.

qualified processes be applied. This means that qualified material (FRM II AlMg3 chemically only slightly, but for manufacturing purposes significantly different from the material specified in EN 573-3), qualified machinery and qualified personnel are to be used. Here are some examples.

- Friction stir welding (FSW) of bellows: after a long time of unsuccessful trial using tungsten inert gas (TIG) welding (as specified), finally the triad of casting fresh raw material, rolling it into sheet metal and assembling it using FSW, turned out to be a success for the most part, albeit not completely. The material was left with too small a fracture toughness after transformation, and it has as yet not been possible to identify a truly reproducible heat treatment to overcome this issue.
- Electron beam welding (EB) of bigger pieces: once defined, EB takes not much more than a minute per weld seam. However, manufacturers willing to take on “prototyping” of this kind are not easy to find (the world market is ex-

[1] Inspiration to this report I especially owe to S. O’Kelly, Associate Lab Director – Advanced Test Reactor, Idaho National Laboratory, Idaho, USA.

tremely small). The one manufacturer eventually identified spent months on research and tests before the qualification was finally to be carried out. Spirits ran high when all the non-destructive tests (NDT) had successfully been carried out, only to be crushed when the very last test, a destructive microscopy, revealed an unacceptable crack invisible to the NDT. That meant: analyse the situation and fix it, so, in essence, back to the drawing board.
- Tungsten inert gas (TIG) welding of small plugs. It sounds like a job for an apprentice. However, it kept failing with fractures appearing, seemingly unstoppable, independent of the welding parameter set chosen. Finally, a solution was found, but so far it covers only plugs of small size.

So, there remains serious development work to be undertaken in 2025. The manufacturing of the component, which comprises more than 50 individual steps to be carried out serially and coordinated among roughly a dozen of contractors, will start once the qualification has been completed successfully. No immediate progress can be guaranteed.

Some of the other tasks accomplished in 2024

In arbitrary order and without much further explanation, here is a list of the most important tasks accomplished in 2024 that exceed the regular inspection programme or the daily routine management of minor mishaps:

- Renovation of the primary and tertiary cooling loop, including water treatment facilities and instrument cooling system,
- Upgrade of the cranes in the Reactor Hall (ongoing) and Experimental Hall (completed),
- Overhaul of parts of the ventilation systems,
- Upgrades of irradiation facilities,
- Renovation of the reactor protection system,
- Progress towards new emergency electric systems,
- Periodic safety review (PSÜ) 2024,
- Preparation for installation of the new central channel.

Transport of fresh and spent fuel

Fresh fuel was shipped to the FRM II in 2024. Together with the 2023 shipment, the maximum licensed number of fresh fuel assemblies is now available at the FRM II. The transportation license was used to its full extent, and thanks are due in particular to our reliable partners for transport and manufacturing, Orano and Framatome. However, the federal authorities made it clear that these two transports were no blue print for further transports and that an in-depth risk-assessment will again be necessary for the next transportation license.

Despite progress on the part of all the parties involved and advancement on every sub-task, the overall situation remains essentially the same. No real break-through on the question of spent fuel transportation has been achieved to date. FRM II has done its part to meet operational and regulatory requirements. The next steps, concerning the transportation of spent fuel, now rest with the licensing authority. We remain committed to supporting the process and working collaboratively to achieve a resolution as soon as possible.

Manufacturing of the in-pile part of the cold neutron source

Second only to the central channel, the in-pile section of the cold neutron source might be the spare part most needed at FRM II. Qualification work similar to that for the central channel is required, but it is even more complex. Overall, around 170 weld seams that can be grouped into roughly 90 different kinds must be qualified. The qualification towards its manufacturing was able to proceed mainly according to schedule in 2024. A particular question that remains unresolved is the custom qualification of welding wire at Helium-temperature (4 K). On the positive side, the dedication of the contractor to moving forward should be mentioned as well as the production of the first (dummy) components required to verify the correct programming of the manufacturing equipment.

Conversion of FRM II to fuel of low enrichment (from HEU to LEU)

The conversion-project is arguably the most important for the long-term provision of neutrons for science, medicine and industry. Significant progress has been made. In March, a four-year contract for the pre-industrialisation of the whole process was signed with Framatome, the European research reactor fuel manufacturer. The initial round of the design specification was accomplished, with two more iterations foreseen in the coming years. The first completely European-made full-size fuel plates were manufactured in close cooperation between the FRM II and Framatome. These plates are scheduled for irradiation tests in 2025 in the BR2-reactor in Belgium.

The FRM II is also in close exchange with the StMUV and its TSO in order to prepare the submission of the application for the conversion license in 2025.

Outlook

Our scientists and customers depend on us, and our waiting list continues to grow. The difficulty of the challenges we face cannot be overstated as we work towards the restart of the reactor. All our achievements could be considered useless as long as the one and main task is not realised: getting the FRM II reactor back into scheduled power operation. In fact, it is vital to constantly fulfill the conditions of our operating license and thus maintain it. We will not tire in our efforts to bring the reactor back into operation in 2025, but the path remains long and winding, and there will be surprises ahead. Still, it remains a challenge I am confident our teams will meet.

Extending capabilities: Full core calculations to support the conversion of FRM II

C. Reiter, D. Bonete Wiese, K. Shehu

Forschungs-Neutronenquelle Heinz Maier-Leibnitz (FRM II), Technical University of Munich, Garching, Germany

The Forschungs-Neutronenquelle Heinz Maier-Leibnitz (FRM II) is a world-leading high-flux research reactor, optimised for beam tube applications. As part of its conversion from highly enriched uranium (HEU) to low-enriched uranium (LEU) fuel, a comprehensive reassessment of the core performance is required. A full-core model of the FRM II has been developed to assess the impact of secondary neutron sources on power and temperature distributions. Serpent 2 calculates the power density for each individual fuel plate, which is then used in Ansys CFX to determine the velocity, pressure, and temperature fields. The coupling is sequential, without thermal feedback from CFX to Serpent 2, ensuring efficient and validated modelling.

Two key effects influence the fission rate: (1) neutron spectrum shifts due to temperature differences in the secondary sources, leading to spectral modifications in neutrons diffusing back into the fuel, and (2) absorption and scattering variations caused by structural materials, reducing neutron back-diffusion into the core. These effects were quantified through neutron flux detectors placed at different locations.

Results show that asymmetric power distributions lead to localised temperature increases in the fuel, cladding, and coolant, while total core power and overall thermal-hydraulic behaviour remain stable. This study confirms the feasibility of full-core modelling and provides insights into secondary source effects on reactor performance.

Full-core calculations for FRM II with Serpent 2 and Ansys CFX

The FRM II has a thermal power of 20 MW and an undisturbed thermal flux of ~$8 \cdot 10^{14}$ n/(cm^2·s), achieving the highest flux-to-power ratio globally. Designed for beam tube applications, it currently operates with a single fuel element using U_3Si_2 with 93% highly enriched uranium (HEU).

To enhance global nuclear security, FRM II is advancing its conversion to low-enriched uranium (LEU) by qualifying a high-density monolithic U10Mo fuel. This conversion requires the fuel element and core geometry to be redesigned, along with a comprehensive reassessment of neutronic, thermal-hydraulic, and thermal-mechanical aspects.

The TUM Centre for Nuclear Safety and Innovation (TUM.CNSI), in collaboration with the Argonne National Laboratory, Oak Ridge National Laboratory (ORNL), and the Institut Laue-Langevin (ILL), contributes to the verification and validation of commercial Computational Fluid Dynamics (CFD) and Computational Structural Mechanics (CSM) codes for high-performance research reactors. Within the

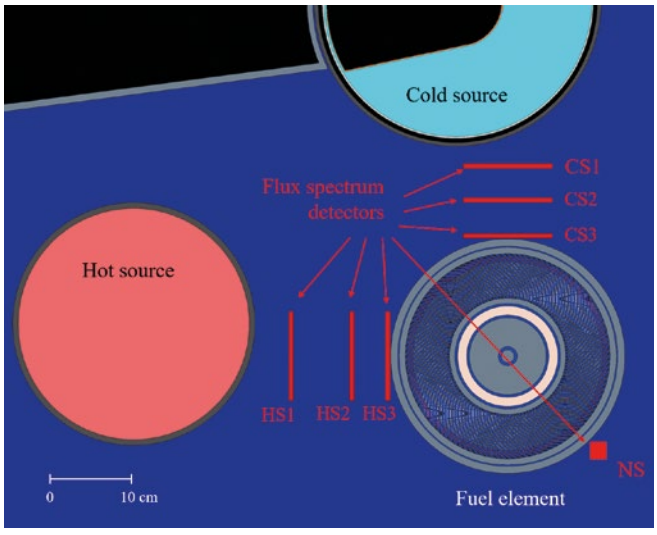

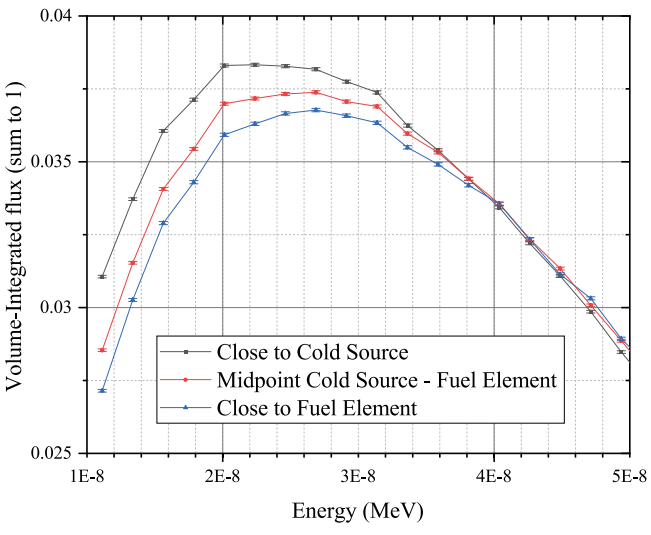

Figure 1 (left): Close-up plot of the Serpent model of FRM II, cut horizontally at the mid-height plane of the fuel element, which is depicted on the bottom right. The hot source (red circle to the left) and the cold source (circle in turquoise and black at the top) are also shown, including some beam tubes pointing to the latter (in black around the cold source). Finally, the plot includes the location of detectors that were used to assess the phenomena influencing the power deposition in the fuel. The term NS in the figure stands for No Source. Figure 1 (right): Energy-resolved neutron flux in the vicinity of the cold source. The closer the detector is placed to the cold source, the colder the neutron spectrum becomes.

Involute Working Group (IWG), TUM.CNSI has also developed advanced coupling schemes integrating Serpent 2 for neutronics, Ansys CFX for hydraulics, and Ansys Mechanical for structural analysis. These high-fidelity simulations provide essential insights into FRM II's current and future performance post-conversion. This report is based on a scientific paper and examines the effects of secondary neutron sources on the performance of FRM II.

Methodology

Due to the rotational symmetry of the FRM II core, the Serpent 2 - Ansys CFX coupling has so far been applied to a single fuel plate out of the 113 in the fuel element. While this approach provides validated and efficient modelling, it does not fully capture the power and temperature distributions in the fuel element as these are influenced by the secondary sources in the heavy water moderator tank.

The cold and hot neutron sources, essential for FRM II's scientific performance, affect the fission rate and lead to asymmetric power density distributions. To assess this impact, a full-core model, which has been extensively validated was used. For this model, Serpent 2 calculates the power distribution for each plate, and Ansys CFX uses this data to determine the velocity, pressure, and temperature fields.

The sequential coupling does not include thermal feedback from CFX to Serpent 2 but allows for realistic core modelling, incorporating the effects of secondary sources. To elucidate whether the secondary sources cause a local shift of the neutron spectrum at the outer edge of the fuel element, several additional neutron flux detectors have been defined (see Fig. 1, left).

Two physical effects related to the secondary sources may influence the fission rate in individual fuel plates:

1. Neutron spectrum shift due to temperature

Neutrons in the secondary sources follow a Maxwell-Boltzmann spectrum at the respective source temperature. As they diffuse back into the fuel element, they may not fully thermalise, causing a spectral shift. For the cold source, this could increase the fission rate in nearby plates, as lower neutron energies enhance the fuel's fission cross-section. Conversely, the hot source may reduce the fission rate. Serpent 2 correctly captures this spectral shift, as seen in Fig. 1, right, where the neutron spectrum peaks at colder energies near the cold source and shifts to higher energies closer to the fuel.

2. Absorption and scattering effects

The secondary sources contain materials with higher absorption and lower scattering cross sections than heavy water (e. g., Al, AlMg3, Zr alloys). This reduces neutron back-diffusion into the fuel element, leading to a lower fission rate in adjacent fuel plates. Additionally, the cold source has a lower atomic density than heavy water, further decreasing the number of back-scattered neutrons.

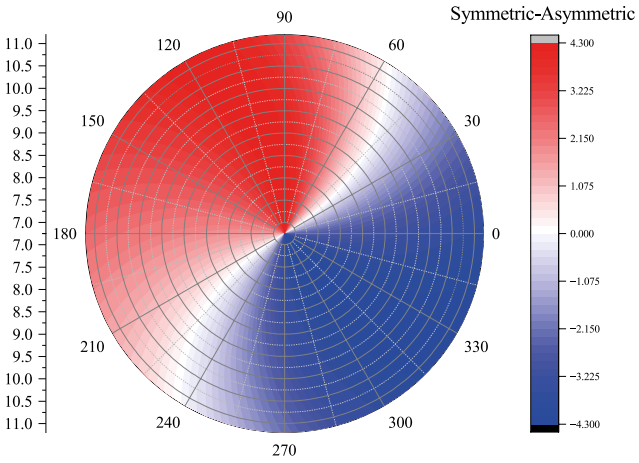

Figure 2: Relative difference in terms of power between each plate and the median power value for the asymmetric case. The vertical axis on the left shows the radial coordinate.

The calculations presented here are not designed to characterise these two individual effects, but to rather quantify the integral effect of both phenomena.

Results

The relative difference between the power deposited in each plate and the median power for the asymmetric case is shown in Fig. 2. The asymmetric power density profiles caused by the secondary sources result in higher maximum temperatures in the fuel, cladding, and water domains, while the total core power remains unchanged. Additionally, average values remain consistent with the nominal symmetric power density case. This work demonstrates the feasibility of modelling the full FRM II core using the CFD code Ansys CFX. Furthermore, the findings confirm that the asymmetry introduced by the cold and hot sources has no significant impact on the thermal-hydraulic behaviour of FRM II's current core.

Original publication

K. Shehu, D. Bonete Wiese, C. Reiter: Assessment of the influence of the secondary sources on the thermal-hydraulic behavior of FRM II using Serpent 2 and Ansys CFX, Nucl. Sci. Eng. 1-12 (2025),
DOI: 10.1080/00295639.2025.2455348

Acknowledgement

This work was supported by a combined grant (FRM2023) from the Bundesministerium für Bildung und Forschung (BMBF) and the Bayerisches Staatsministerium für Wissenschaft und Kunst (StMWK).


00
SIEMENS

Facts & Figures

The year in pictures

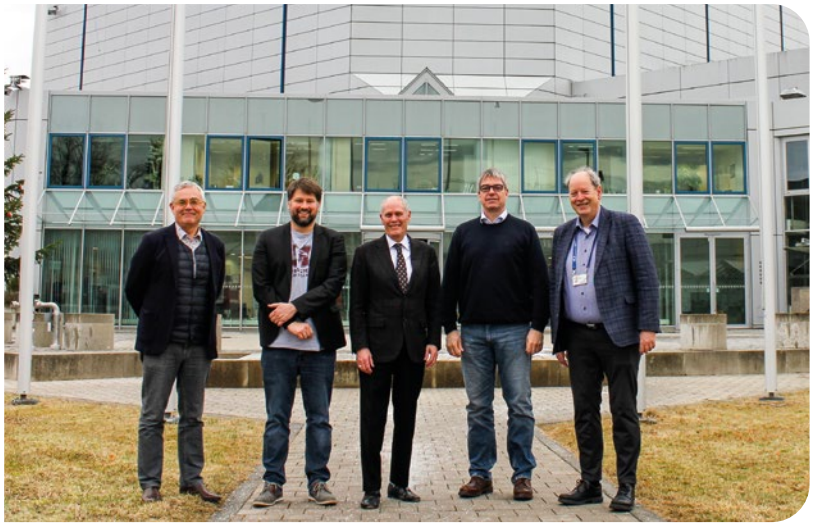

JANUARY 22nd

International collaboration: A delegation from McMaster University, including President David Farrar (centre), visited the FRM II to strengthen ties and discuss advancements in nuclear safety and research. With him (from left): Soren Harbel, Advisor to McMaster University, Dr. Christian Reiter, FRM II Reactor Physicist and Head of the Center for Nuclear Safety at TUM, Prof. Dr. Christian Pfleiderer, Scientific Director of the FRM II, and Dr. Jürgen Neuhaus, formerly Deputy Scientific Director, now Administrative Director of the FRM II.

FEBRUARY 5th, JUNE 19th, and OCTOBER 17th

Happy Welcome: Throughout 2024, new employees at the FRM II were warmly welcomed during three special “Welcome Days”. These events included a joint introduction, presentations about the FRM II and exclusive tours of the facility.

FEBRUARY 28th

Science for everyone: At the Deutsches Museum, Dr. Michael Schulz captivated over 200 attendees with insights into neutron imaging. From dinosaur eggs to prefilled syringes and batteries, his lecture showcased the versatile applications of neutron research at MLZ.

FEBRUARY 26th

Constructive dialogue: Members of the Garching City Council, including Mayor Dr. Dietmar Gruchmann (right), visited the FRM II for discussions on reactor safety, research highlights, and future plans. A guided tour and open exchange provided insights and strengthened local collaboration.

MARCH 2nd

A milestone celebrated: The FRM II marked 20 years of operation, contributing to research in fields such as medicine, energy and materials science. To celebrate this achievement, a special cake was prepared and ceremonially cut by Mariko Hermanns (right) and Florian Jeschke (left).

MARCH 14th

Pioneering innovation: Representatives from FRM II and Framatome signed a new agreement to advance the production of low-enriched uranium fuel for the reactor's conversion (front row, left to right): Cyrille Rontard, François Gauché (both Framatome), Prof. Dr. Christian Pfleiderer, and Robert Rieck (both FRM II), (back row from left): Dominique Geslin, Ralf Gathmann (both Framatome), and Dr. Bruno Baumeister (FRM II).

APRIL 20th

Empowering young scientists: The inaugural MLZ Young Researchers Assembly united PhD students, master's students and young postdoctoral researchers from diverse institutions. This cross-institutional, self-organised group aims to enhance collaboration and skills development through workshops and events.

APRIL 25th

Inspiring curiosity: At this year's Girls' Day, 23 young participants explored the world of neutron science at MLZ. They learned about famous scientists, discovered neutron imaging, and conducted hands-on experiments in the lab.

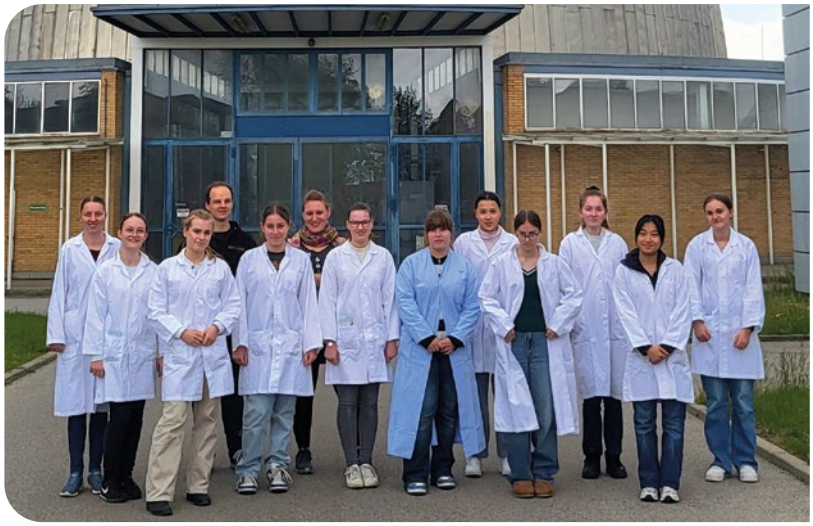

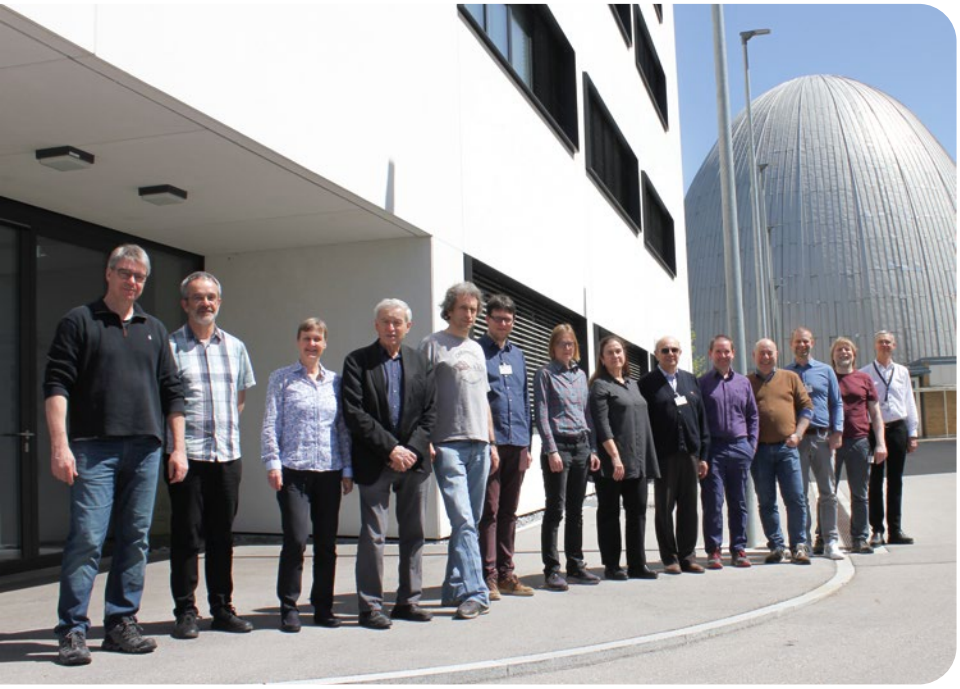

APRIL 29th – 30th

Shaping the future: The in-person meeting of the European Neutron Scattering Association (ENSA) at MLZ with chair Dr. Astrid Schneidewind (3rd from left) brought together neutron science experts to discuss strategy development, collaboration opportunities, and upcoming initiatives.

JUNE 10th – 14th

Promoting sustainability: As part of the TUM Sustainability Week, the FRM II hosted insightful lectures and guided tours on June 12 and 13, highlighting the facility's contributions to sustainable research and innovation.

JUNE 18th

Legal clarity: The Bavarian Administrative Court upheld the lawful operation of the FRM II, dismissing a complaint by the Bund Naturschutz. This decision reinforces the reactor's vital role in global scientific research and medical progress.

JULY 16th

Science at zero gravity: At the public lecture Café & Kosmos, Dr. Lucas Kreuzer captivated the audience with insights into experiments conducted in microgravity. From unusual candle flames to precise measurements on the ISS, he shared his personal experiences and the discoveries facilitated by weightlessness.

JULY 29th – 30th

Politics at the pool: Representatives from the Federal Ministry of Education and Research (BMBF), including Dr. Karsten Hess (4th from the left) and Dr. Jochen Leyendecker (3rd from the right) , visited the FRM II. The tour given by the FRM II and MLZ directors focused on ongoing projects and future collaborations.

JULY 31st

Summer fun with science: As part of the Nachbarschaftshilfe Garching e.V holiday programme, children explored the FRM II and discovered the wonders of neutron science. From hands-on experiments with liquid nitrogen to peeking into the reactor pool, the young participants enjoyed an inspiring day.

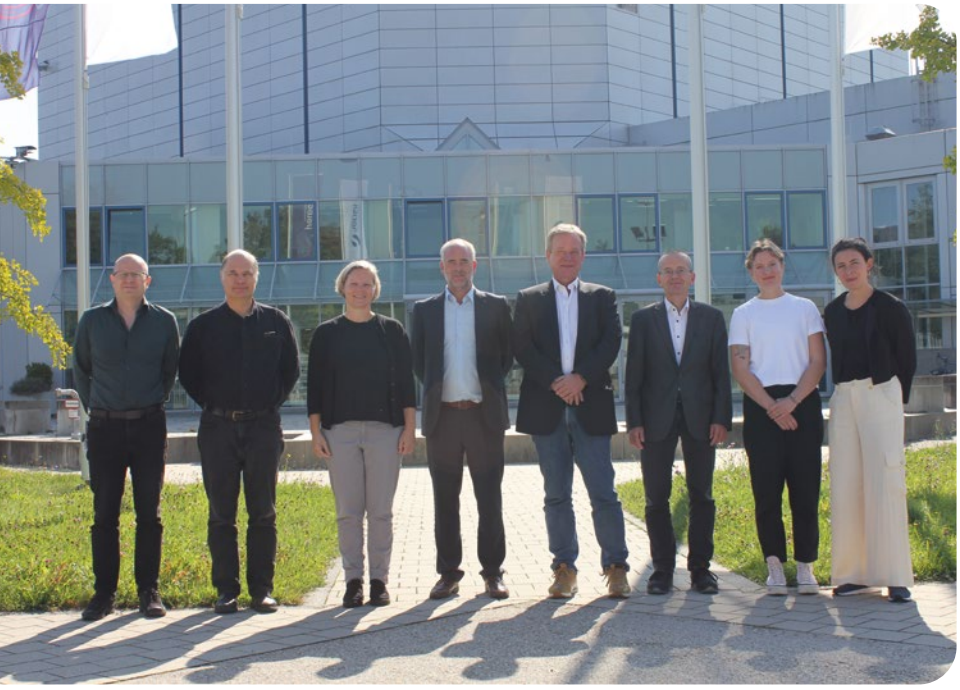

SEPTEMBER 20th

Strengthening international collaboration: A delegation from the Dutch Ministry of Health, Welfare, and Sport visited the Forschungs-Neutronenquelle Heinz Maier-Leibnitz (FRM II) to discuss advancements in nuclear medicine and medical isotope production.

OCTOBER 17th

Liberal visit: Members of the Ismaning-Unterföhring local branch of the FDP visited the FRM II. During the visit, engaging discussions provided an opportunity to answer insightful questions and offer a detailed overview of the FRM II's contributions to scientific advancements.

OCTOBER 3rd

Biggest open door on the campus: More than 15,000 visitors flocked to Garching on German Unity Day, with 444 guests including 80 children exploring the Forschungs-Neutronenquelle Heinz Maier-Leibnitz. In addition to engaging tours, interactive stations for children, talks by Dr. Michael Schulz and Dr. Sebastian Busch offered a fascinating glimpse into neutron research and its applications.

NOVEMBER 6th

Representing FRM II at HOKO 2024: At their booth, employees of the FRM II shared opportunities for Bachelor and Master theses, internships, student jobs and permanent positions with prospective applicants during the Hochschulkontaktmesse (HOKO) in Munich.

NOVEMBER 14th

Focus on fuel elements: Christian Kühn (3rd from left) and Christoph Bunzmann (2nd from left) visit the FRM II. The president of the Federal Office for the Safety of Nuclear Waste Management (BASE) and his head of the approval procedure department discussed challenges in the supply and disposal of the fuel elements with the FRM II board of directors and representatives of the regulatory authority.

NOVEMBER 19th – 21st

MLZ Evaluation: Every five years, the cooperation between TUM, Hereon, and FZ Jülich undergoes a comprehensive review. The international MLZ review panel toured all the experimental halls and was informed through presentations, posters and discussions.

Awards

MAY 6th

Recognising excellence: Dr. Iaroslav Meleshenkovskii (2nd from right) received the 2024 Young Scientist Award at the 16th International Conference on Modern Trends in Activation Analysis (MTAA-16) for his groundbreaking research on recycling rare-earth magnets. The award was presented by Prof. Amares Chatt (Dalhousie University, Canada), Prof. Elisabete A. De Nadai Fernandes (CENA, Brazil) (2nd from left), and Dr. Zsolt Révay (FRM II, TUM) (right).

SEPTEMBER 6th

Outstanding poster: Dr. Danny Russell from the TUM research group "Physics with Positrons" received the 1st prize for his poster presentation at the International Workshop on Positron Studies of Defects (PSD-24) in Como, Italy. His work was on "Modeling backscattered positron capture at the coincidence Doppler broadening spectrometer".

SEPTEMBER 18th

Prize for conversion: Recognised for excellence in leading the FRM II's conversion project, Dr. Bruno Baumeister received the KFN Instrumentation Award at the Deutsche Neutronenstreutagung in Aachen. His significant contribution to European programmes on high-density uranium fuel development underscore his pivotal role in advancing sustainable neutron research.

SEPTEMBER 18th

Award for simulation: Celebrated as the "king of simulation", Dr. Christian Reiter earned the KFN Instrumentation Award for his groundbreaking 3D modelling work on reactor core simulations. His expertise has been instrumental in charting the path for the FRM II's conversion to low-enriched uranium, a development with global impact.

DECEMBER 5th

Heinz Maier-Leibnitz Medal: Prof. Dr. Christian Pfleiderer, Scientific Director of the FRM II and MLZ, was awarded the Heinz Maier-Leibnitz Medal during the Dies Academicus at TUM. The medal recognises his exceptional contribution to experimental solid-state physics, his dedication to establishing the TUM Centre for Quantum Engineering and his leadership at the Heinz Maier-Leibnitz Research Neutron Source.

DECEMBER 6th

MLZ Award for positron research: Prof. Dr. Günther Dollinger (middle) from the University of the Bundeswehr Munich was honoured with the 2024 MLZ Prize for Instrumentation and Scientific Use for his instrumental contributions to the development of the Positron Source at FRM II. The award ceremony with the two MLZ directors Prof. Dr. Martin Müller (right) and Prof. Dr. Christian Pfleiderer took place during the MLZ User Meeting.

Workshops, Conferences and Schools

January 15 – 19: **FoPra 61 internship hands-on learning**

January 17 – 18: **DAPHNE TA2 Meeting**

March 14 – 15: **Automation in Diffraction Workshop**

April 8 – 10 **Machine Learning Conference**

May 27–28: **LLB MLZ Workshop 2024**

June 4–7: **MLZ Conference 2024**

July 8–12: **TUM FoPra at the MLZ**

July 8–12: **Internship for high school students**

September 4 – 5: **Matrac School hereon**

September 9 – 13: **JCNS Laboratory Course**

September 12: **9th TUM Expert Forum: Non-destructive testing for the sustainable energy technology of the future**

September 30 – October 2: **FullProf Workshop**

October 2 – 10: **Czech-Bavarian Mini School on Large Scale Facilities and Open Data**

October 8 – 11: **JCNS Workshop Tutzing**

December 5 – 6: **MLZ User Meeting**

Changing media presence

A. Voit, A. Görg, K. Kleinstück, S. Habold

Heinz Maier-Leibnitz Zentrum (MLZ), Technical University of Munich, Garching, Germany

Despite long downtimes and declining research results, the Research Neutron Source (FRM II) and the Heinz Maier-Leibnitz Zentrum (MLZ) continued to demonstrate transparent and impactful communication in 2024. In a year marked by ongoing operational challenges, particularly due to the extended downtime of the neutron source, the media presence of MLZ and FRM II remained remarkably strong. More than 500 media articles in 2024, increased engagement on social media platforms and a diverse range of events were recorded. Over the year, the FRM II visitors' service welcomed in total 4069 visitors, further strengthening our public relations work.

Media coverage: Adapting to changing media landscapes

With a total of 547 media articles in 2024, ranging from various scientific topics to conversion projects, in print and online media as well as on TV and radio, the FRM II and MLZ remain in the spotlight. This year, we recorded 24 press inquiries.

The number of 314 (57%) scientific media articles covering research with neutrons at the MLZ and FRM II is mainly due to the media resonance generated by a press release issued jointly by the Technical University of Munich and Isotope Technologies Munich ITM SE. Highlighting the FRM II as a source of vital radioisotopes, this press release alone resulted in 294 media contributions. A big reactor-related topic in 2024 was the 20th anniversary of FRM II's commissioning, celebrated on March 2nd with a comprehensive social media campaign and media coverage. While 40 articles recognised the facility's contributions to science, industry and society, the prolonged reactor downtime overshadowed

Media contributions in 2024 by topic area

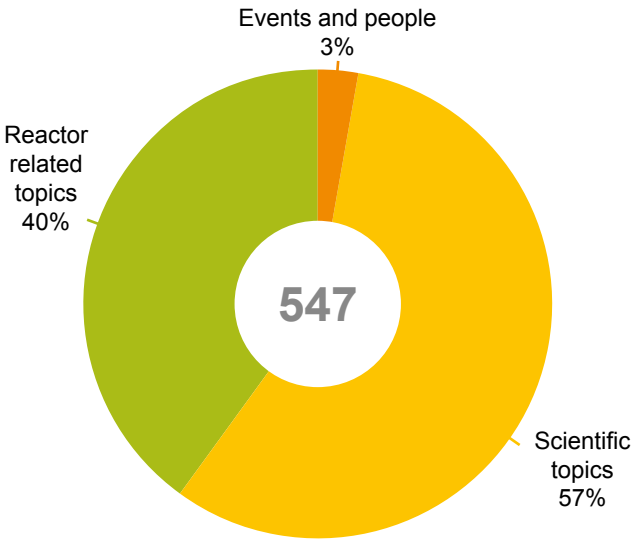

Figure 1: 57 percent of all media reports on the MLZ and FRM II in 2024 were on scientific topics. Reactor related topics include the nuclear phase-out, conversion and the future medical supply of important radioisotopes.

Number of media articles from 2016 to 2024

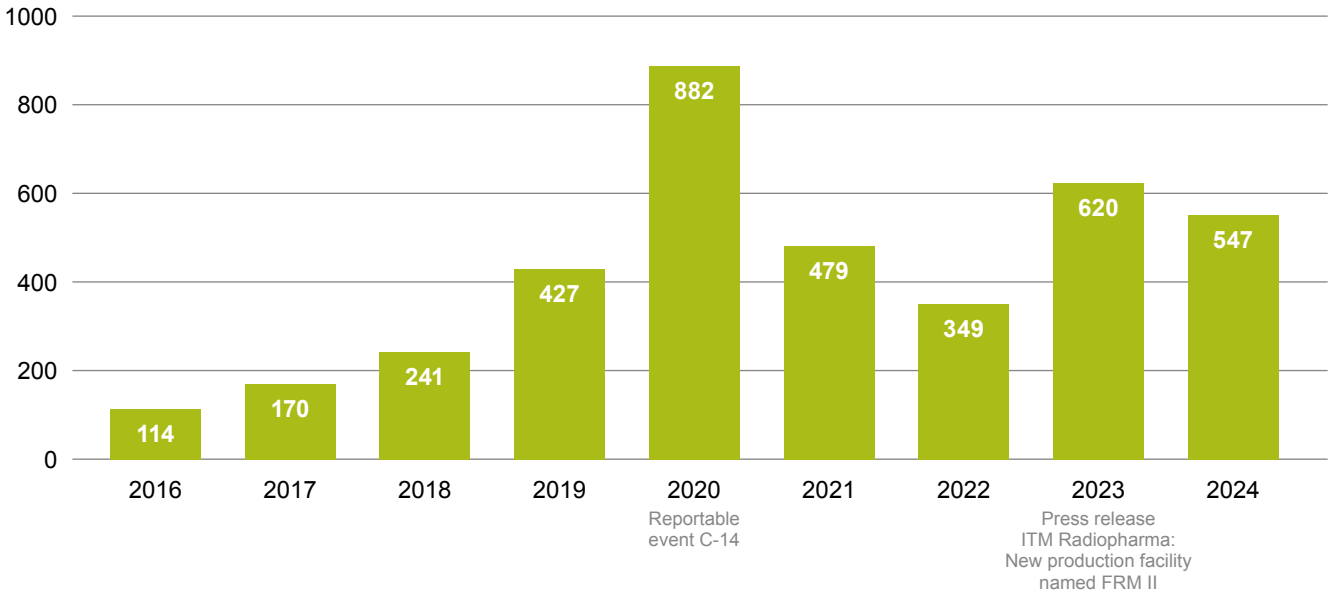

Figure 2: 547 media articles appeared in 2024 about the Research Neutron Source (FRM II) and the Heinz Maier-Leibnitz Zentrum (MLZ). This confirms the unbroken media interest that we have experienced for years despite the long shutdown of the neutron source and the lack of research results.

Figure 3: Examples of the “PhD Students Campaign” of the FRM II and MLZ

the positive narrative. Another big news item for a large media coverage was the judgement of the Bavarian Administrative Court, which confirmed the legality of the operation of the FRM II with highly enriched uranium (121 articles).

As always, FRM II and MLZ’s own 37 news items of the year can be found on our two websites frm2.tum.de and mlz-garching.de. In addition, we published two articles in the section “From Behind the Sciences”.

Social media: The new stage for engagement

In 2024, the shift from traditional print media to digital platforms became even more pronounced. Therefore, we placed significant emphasis on platforms such as LinkedIn, Instagram and YouTube to connect with both scientific and non-scientific audiences. LinkedIn, in particular, emerged as the most effective channel, with 302 posts published throughout the year. These posts ranged from updates on scientific advancements to employer branding initiatives, such as the highly successful “PhD Students Campaign“, which showcased the diverse research and career opportunities at MLZ and FRM II. In total we gained 658 Followers across our social media channels in 2024.

Additionally, Instagram continued to grow as a platform for engaging younger audiences through visually appealing and interactive content. By the end of 2024, the MLZ Instagram account had gained 71 new followers, reaching a total of 317 followers. Highlighted campaigns, such as the 20th-anniversary celebrations of FRM II, effectively combined testimonials from prominent political figures, industry partners, and researchers. At the end of 2024, we also decided to leave Twitter/X due to its declining relevance for engaging scientific audiences and low interaction rates, as well as the political issues. Instead, we will focus on more effective platforms like LinkedIn and Instagram, ensuring our resources are used where they have the greatest impact.

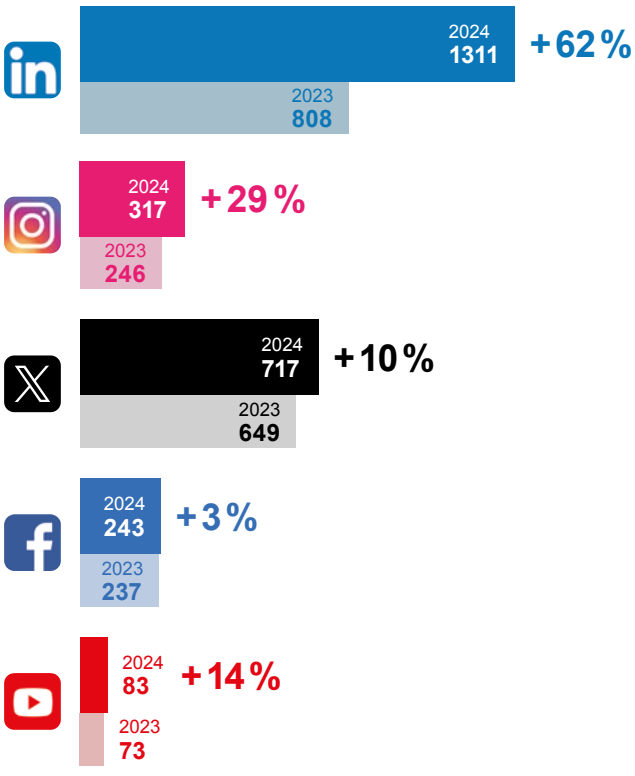

Figure 4: 2024’s followers on MLZ and FRM II social media channels in comparison to the previous year

The direct line to the target groups

Events play a crucial role in engaging directly with the public to make scientific topics accessible to a wide audience. Whether through public lectures, virtual conferences or face-to-face meetings with policy makers, these are great opportunities to promote dialogue with the public and raise awareness of the great research being done. We reach out to our different target groups:

Public engagement

The Open Day has almost become a tradition for us. In 2024, it was organised centrally by the Technical University of Munich for the Garching research campus. More than 15,000 visitors were recorded in total. On our Open Day and Mouse Day, we were able to show 444 visitors around our site (364 adults / 80 children). In addition, we had the opportunity to present the science of neutrons and the operation of the FRM II to the public at numerous stands in the physics department. The feedback from 239 respondents to an online survey was overwhelmingly positive.

Another highlight was the FRM II's renewed participation in the "Science for Everyone" series organised by the Deutsches Museum. In February 2024 Dr. Michael Schulz gave the lecture "Eiskalt durchleuchtet". He explained how neutrons non-destructively analyse objects such as archaeological finds, batteries or dinosaur eggs. The lecture took place in the auditorium of the Deutsches Museum and was also broadcasted via livestream on YouTube to reach as wide an audience as possible. In total, over 200 spectators watched the presentation on site and the corresponding video on YouTube has now been clicked more than 7,300 times.

Policy makers and other stakeholders

In 2024, the FRM II strengthened relationships with policymakers and stakeholders through various visits and discussions.

The organisation and participation of the PAERI Conference (Public Awareness and Engagement with Research Infrastructures) continued, providing an international platform to track trends in science communication and exchange best practices. Despite the long shutdown of our reactor, this exchange enables us to network internationally and to remain on the "radar" of other research institutions. We also aim to revive the neutronsources.org website with communicators from European and international neutron sources under our organisation. The website offers users the ideal opportunity to track the operation of neutron sources, their

Figure 5: Dr. Michael Schulz gives the lecture "Eiskalt durchleuchtet" as part of the Deutsches Museum's "Science for Everyone" event series.

Figure 6: Our crew at the Open Day and Mouse Day 2024. Thanks to all the hard-working helpers!

beamtime and much more information on the individual neutron sources worldwide. An initial meeting for this initiative was held in January.

Employees and potential employees

Targeted outreach to potential candidates remains a key focus of the FRM II's public relations efforts. In 2024, we once again participated in the HoKo career fair at the Munich University of Applied Sciences, a platform we have utilised for over 15 years to showcase job opportunities, internships, and thesis projects. As part of the "HoKo Weeks", we organised a pre-event guided tour of the research neutron source for the second consecutive year. This gave participants a unique opportunity to explore our work environment and connect directly with potential colleagues.

Conclusion

Despite the challenging circumstances caused by the continued shutdown of the FRM II and reduced research output, the FRM II and MLZ successfully maintained a strong media presence in 2024. An increased focus on social media engagement – we were able to generate 33% more followers within a year by regularly publishing high-quality posts (2,013 Followers in 2023 versus 2,671 in 2024) – helped to showcase the importance of neutron science and to keep the MLZ at the forefront of public and scientific attention. Through continuous presence in the media, adaptation to changing trends in social media and direct interaction with the audience through events, we have been able to successfully communicate our research results and explain the importance of our neutron source to the different target groups.

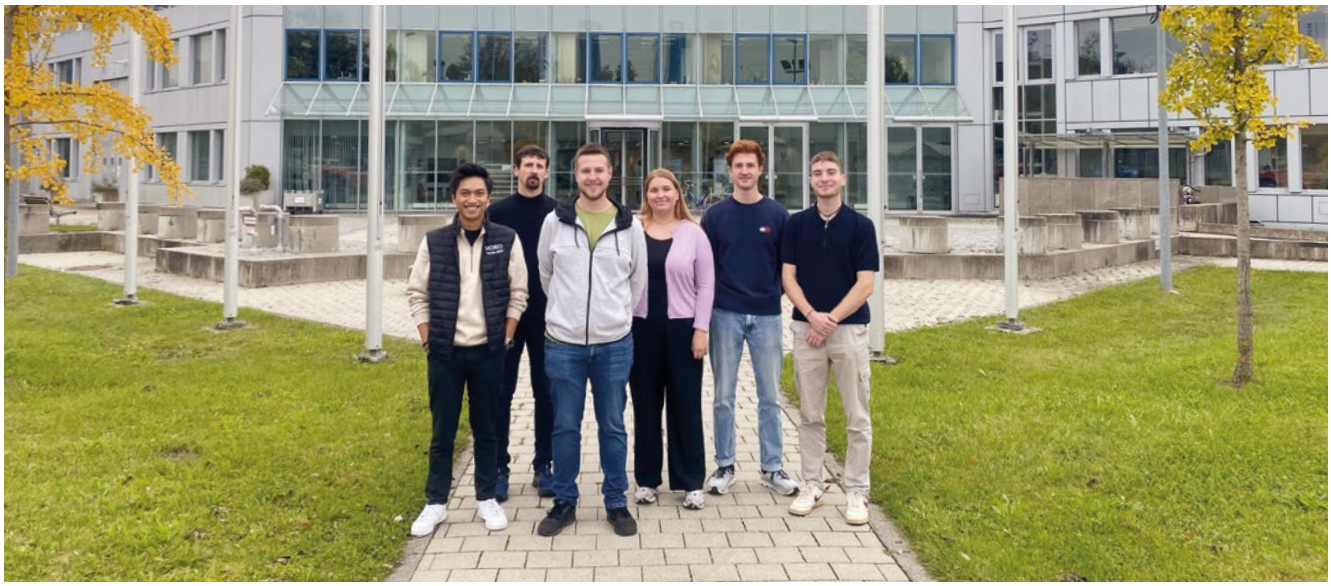

Figure 7: Students from Munich University of Applied Sciences took advantage of the HoKo Weeks before the actual job fair to visit the FRM II and find out about work opportunities at the neutron source.

Various activities at the MLZ User Office

T. Burmann[1], I. Köhler[2], I. Lommatzsch[2], R. Schurek[2]

[1] Heinz Maier-Leibnitz Zentrum (MLZ), Technical University of Munich, Garching, Germany;
[2] Jülich Centre for Neutron Science (JCNS) at MLZ, Forschungszentrum Jülich GmbH, Garching, Germany

Users were once again thin on the ground this year, but the two neutron schools (the JCNS Laboratory Course and GEMS' MATRAC School) went some way towards creating the feeling of welcoming users. Besides, we represented the MLZ at conferences, met other user offices, circulated newsletters, organised the annual User Meeting – and finally, celebrated an anniversary!

The third week in March saw many, many physicists strolling through Berlin: The DPG Spring Meeting of the Condensed Matter Section took place on the campus of the TU Berlin. As usual, the MLZ User Office was available to answer any question about neutron scattering at a dedicated booth. But this time, it was different: Due to new fire protection regulations at TU Berlin, all booths had to be moved from the usual university building to three tents at various locations on the campus.

Figure 1: Crowded MLZ booth at the DPG Spring Meeting.

As parts of the poster sessions were also housed in the tents, there was always quite a crowd visiting the booths. Many interested scientists at all stages in their careers used the opportunity to learn about MLZ and what role neutrons could play in their research.

In September, about 190 neutron scatterers, mainly from Germany and neighbouring countries such as France, gathered at the RWTH Aachen for the German Neutron Scattering Conference 2024 (DN2024), organised this time by RWTH Aachen and Forschungszentrum Jülich GmbH. Parallel and plenary sessions showcased the breadth of the field and furnished many topics for discussion during the coffee breaks. However, fire protection strikes again – this time not only with regard to booths, but also all posters. Thus, the poster session had to be outsourced to an event location in downtown Aachen – beautifully located opposite the famous dome. But the MLZ User Office contrived ways to advertise the upcoming User Meeting: All MLZ colleagues who had the pleasure of giving a talk showed a prepared slide, postcards materialised on the standing tables during the breaks, and finally, a big poster welcomed the participants at the poster session.

Figure 2: The multitasking User Office promoted and documented at the DN.

Networking in Bucharest

Romania's beautiful capital, Bucharest, was the place to be for European user officers in April. This time, the user office of the Extreme Light Infrastructure – Nuclear Physics facility (ELI-NP) at Magurele/Bucharest invited the hitherto unknown networkers behind the scenes. Even if we are from different facilities such as neutron sources, synchrotrons, spallation sources, laser labs, etc., – in the end, we all work in the same field and thus face the same problems. Roughly every two years, we all meet for an exchange, discuss current challenges, and how to improve the user experience.

Figure 3: (Most of) the ladies and gentlemen who keep the European user facilities up and running!

Figure 4: 250 happy users and MLZ colleagues at the MLZ Users 2024. As evidenced in the pictures below, discussions were very lively!

6th MLZ User Meeting in a row

For the 6th time, the MLZ User Meeting provided a platform for neutron scatterers. The format has remained unchanged since 2019 (with two online events due to the COVID-19 pandemic): On the first day, the seven parallel workshops organised by the MLZ Science Groups offered an overview of the various fields of neutron research. But other topics are also currently in the mix: What is the status of the planned electronic logbooks, or the open data catalogue at MLZ?

The lively discussions that began during the coffee breaks continued over dinner in a typical Bavarian restaurant. And unlike last year, when everyone was in a hurry because of the freezing rain that halted public transport, this time everything went smoothly.

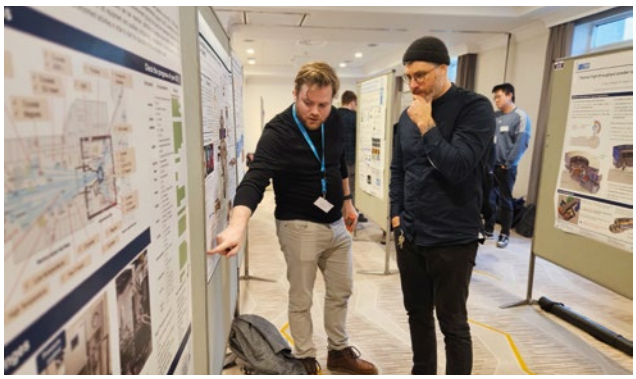

Judith Houston (ESS and former JCNS@MLZ colleague!) opened the second day with her plenary talk on “Squishy stuff probed by small-angle scattering and rheology”. Afterwards, the “MLZ Prize for Instrumentation and Scientific Use 2024” was presented for the first time at a User Meeting. The prizewinner, Günther Dollinger (University of the Bundeswehr Munich), received the award for his services to positron instrumentation at the MLZ. His presentation then showed various ways in which pulsed positrons can help in materials science.

As always, the annual review and updates from the MLZ directors were eagerly anticipated. Tommy Nylander, Chair of the MLZ User Committee, emphasised in his contribution that it will be essential that new and old users alike return to the MLZ as part of the restart, besides all upgrades at the instruments and additional labs. This part was rounded off with short presentations from KFN, ENSA, and LENS before the poster session began, providing plenty of material for discussion.

GhOST
Garching Online System Tool

Celebrating a 5th birthday!

The User Office software GhOST was launched during the MLZ USERS 2019 – five years ago! Even without user operation, we developed this system further, and with the restart, it will be the entry point for all user-related tasks – not only proposals, reviews, scheduling, visits, reports and publications but also data management and remote access. GhOST will be happy to welcome users again and looks forward to receiving their feedback!

Organisation

FRM II and MLZ

The Forschungs-Neutronenquelle Heinz Maier-Leibnitz (FRM II) provides neutrons for research, industry and medicine and is operated as a Corporate Research Center by the Technical University of Munich (TUM). Scientific use of the FRM II, with around 1,200 user visits per year, is organised within the Heinz Maier-Leibnitz Zentrum (MLZ).

The chart below shows the overall network comprising the Neutron Source FRM II and the MLZ, as well as the funding bodies and the scientific users that perform experiments at the MLZ, addressing the major challenges facing present-day society.

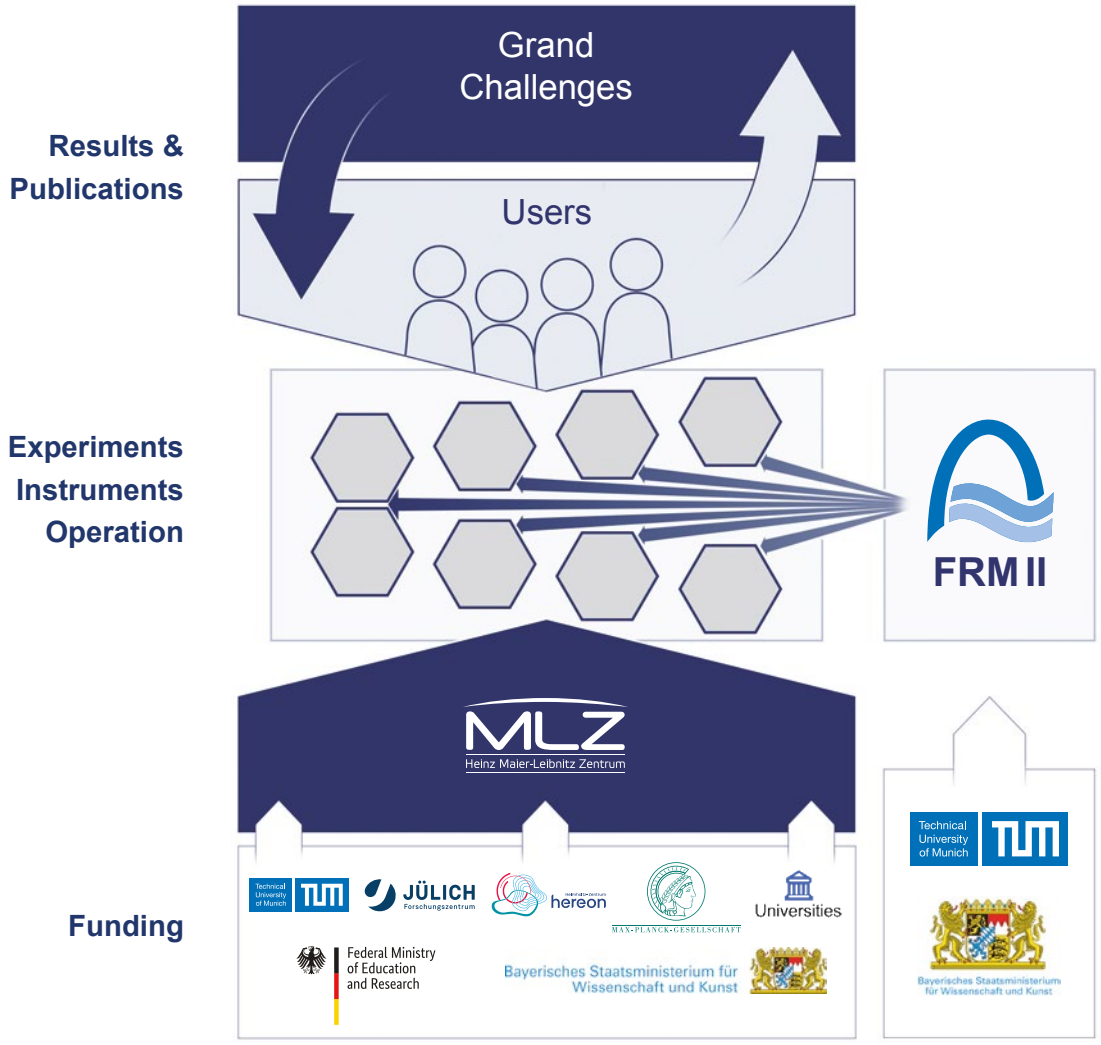

Figure 1: The neutron source FRM II and the user facility MLZ.

Scientific Director MLZ, FRM II
Prof. Dr. Christian Pfleiderer

Technical Director FRM II
Dr. Axel Pichlmaier

Scientific Director MLZ, HGF
Prof. Dr. Martin Müller

Administrative Director FRM II
Dr. Jürgen Neuhaus
Robert Rieck (until August, 2024)

Scientific cooperation at the Heinz Maier-Leibnitz Zentrum (MLZ)

The Heinz Maier-Leibnitz Zentrum with its cooperating partners, the Technical University of Munich (TUM), Forschungszentrum Jülich GmbH (FZJ) and Helmholtz-Zentrum hereon GmbH is rooted in a network of strong partners including the Max Planck Society (MPG) and numerous university groups that benefit from scientific use of the Forschungs-Neutronenquelle Heinz Maier-Leibnitz. The organisational chart of the MLZ is shown below.

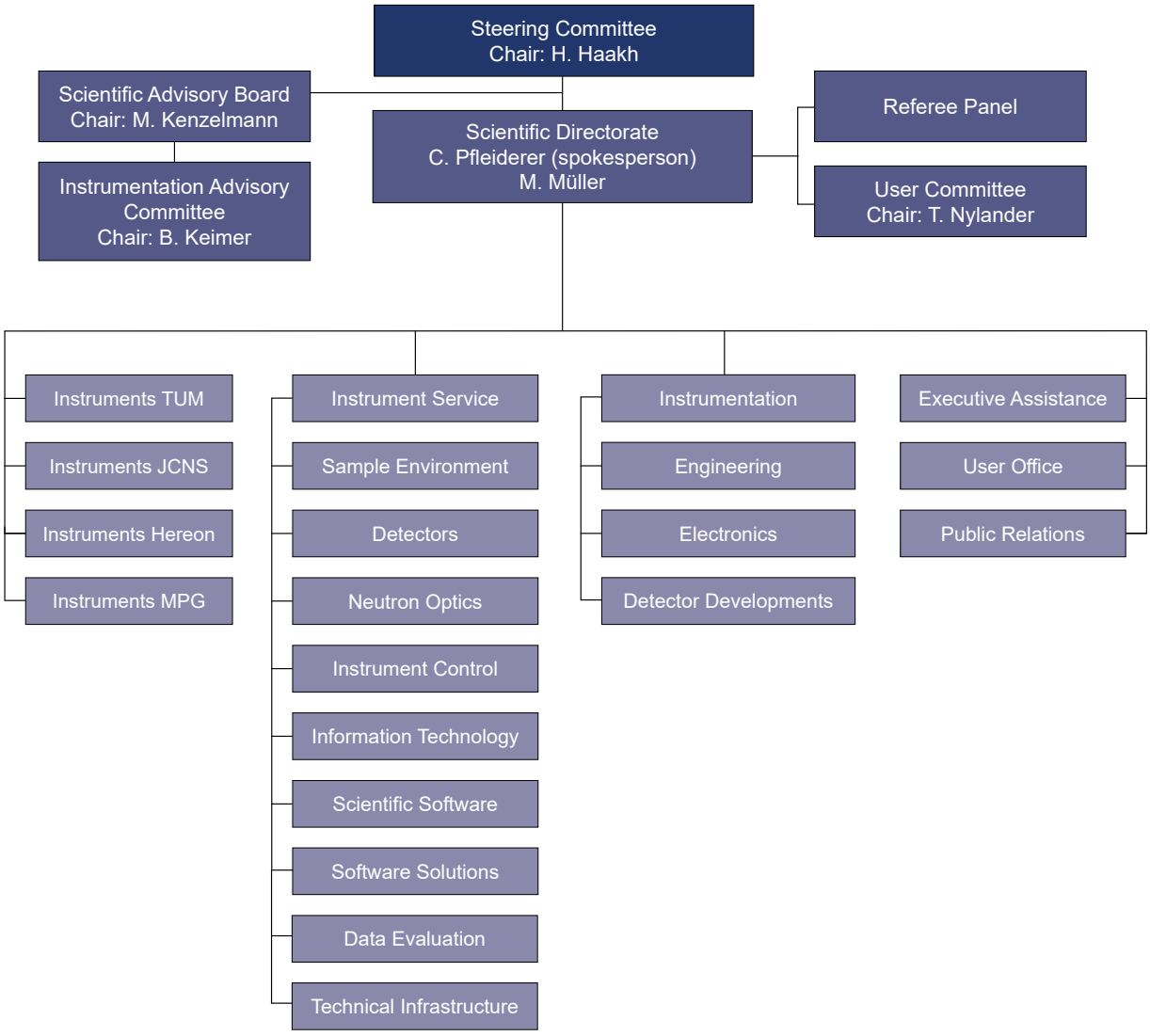

Figure 2: Organisational chart MLZ (2024).

Staff

The charts below show the staff of MLZ and FRM II. The staff of MLZ, as per their share among the partners with a detailed break-down of their function within the MLZ is also depicted.

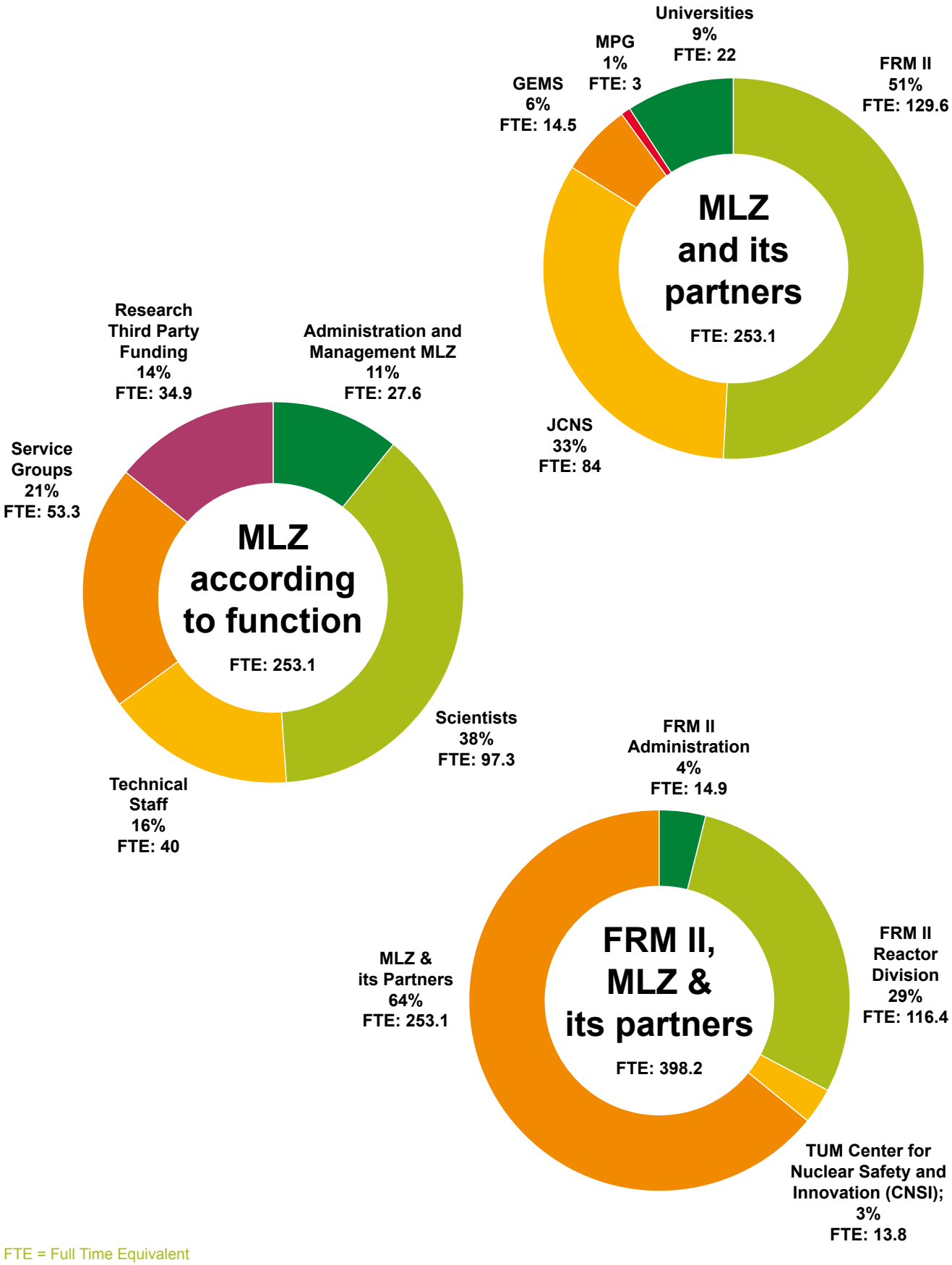

FTE = Full Time Equivalent

Budget

The tables and charts below show the revenue and expenses for 2024.

Revenue 2024

Federal Funding	16.700.000 €
Bavarian Funding	35.010.000 €
Contribution TUM (Planstellen)	10.189.308 €
Contribution FZJ	11.864.000 €
Contribution Hereon	1.320.000 €
Total	**75.083.308 €**

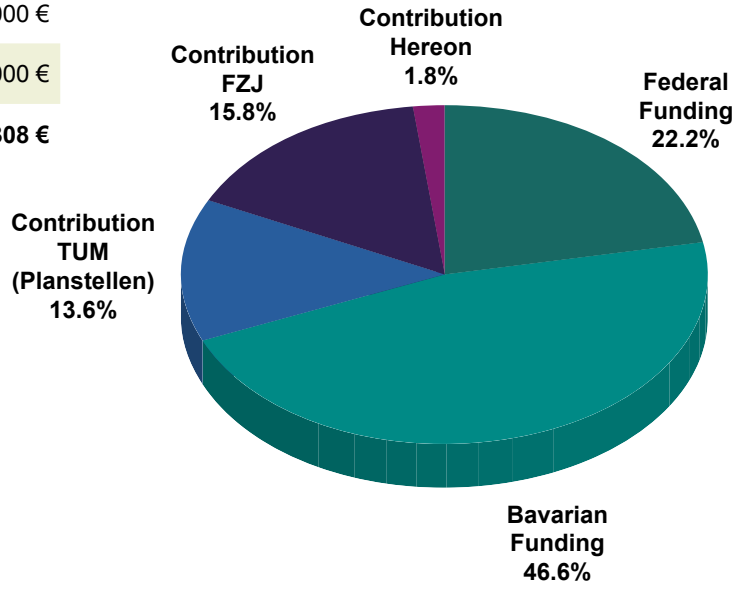

Expenses 2024

	TUM	FZJ	Hereon	**Total**
Personnel costs	20.170.897 €	8.450.000 €	1.789.627 €	**30.410.524 €**
Consumables	32.810.206 €	4.549.000 €	714.601 €	**38.073.807 €**
Investment	9.268.497 €	3.570.000 €	295.770 €	**13.134.267 €**
Total	**62.249.600 €**	**16.569.000 €**	**2.799.998 €**	**81.618.598 €**

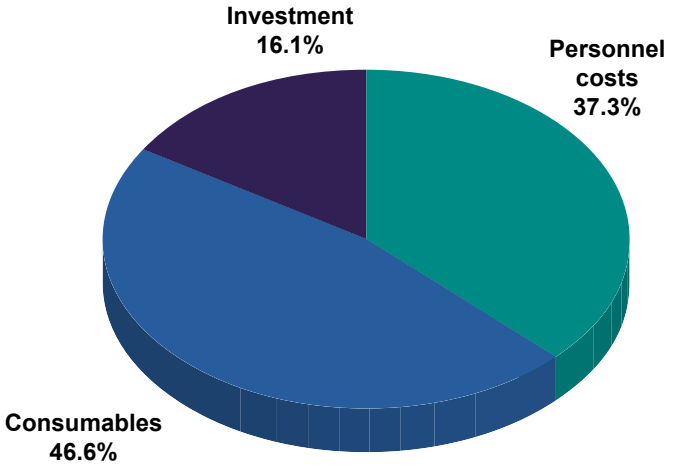

Publications & Theses

In 2024, we received notice of a total of 210 scientific publications, including journal articles, contributions to books and conference proceedings (https://impulse.mlz-garching.de and figure below). Furthermore, in total 54 theses supervised by staff of the MLZ and its partner institutions were completed in 2024.

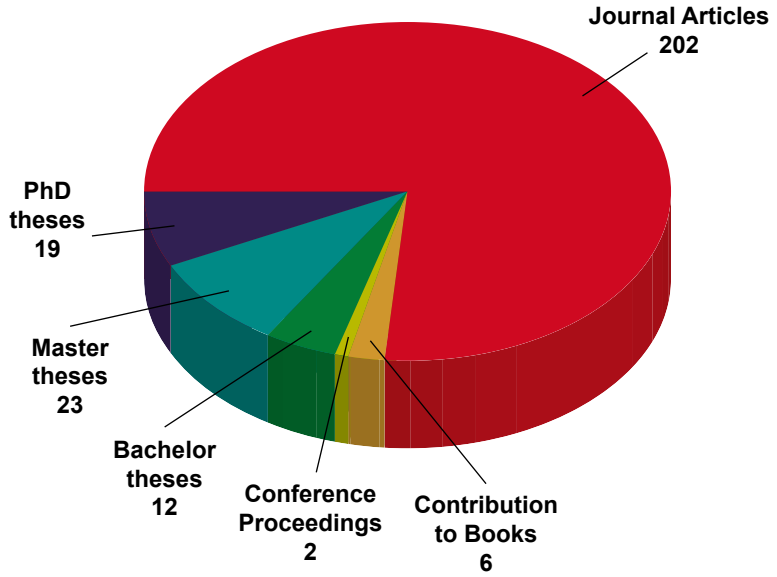

In 2024, 92 PhD theses, based on experiments at the MLZ or method and instrument developments for the MLZ, were either ongoing or completed. Of these, 79 are under the direct supervision of staff at the MLZ and its collaboration partners while the others involve external users. In total, 21 of the 92 PhD theses have been completed in 2024, including external users. Of all the doctoral students, around 96% come from German universities, around 4% from other universities in Europe.

The next figure shows the classification of the journal articles by Scientific Area (several tags per journal article are possible):

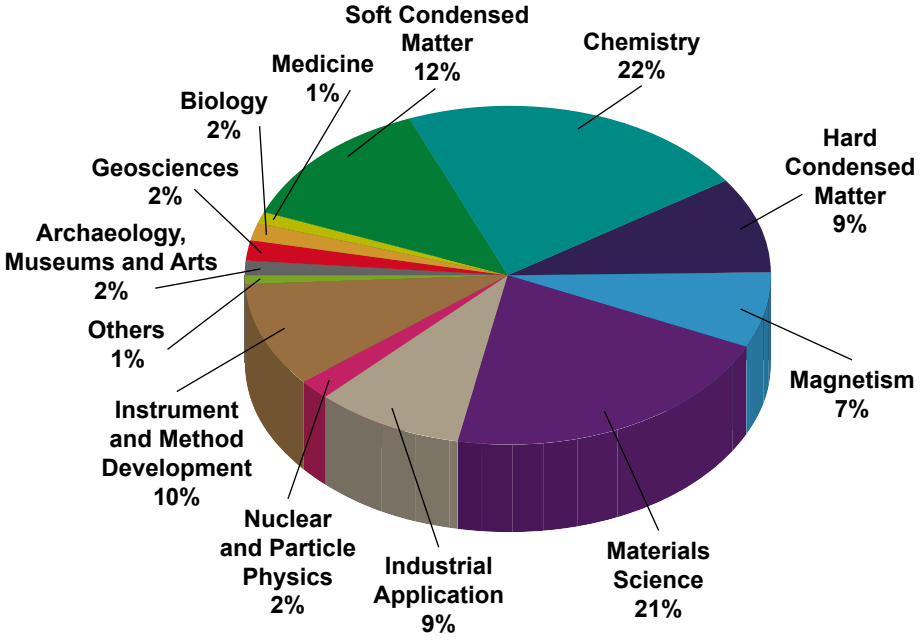

The journal articles at the MLZ can be pictured as a pyramid: Basic Research & Methods (17%) required to tackle the Key Technologies (48%) and articles that address directly the Grand Challenges of our society today (35%). The circular charts represent the individual subjects being dealt with within these three categories.

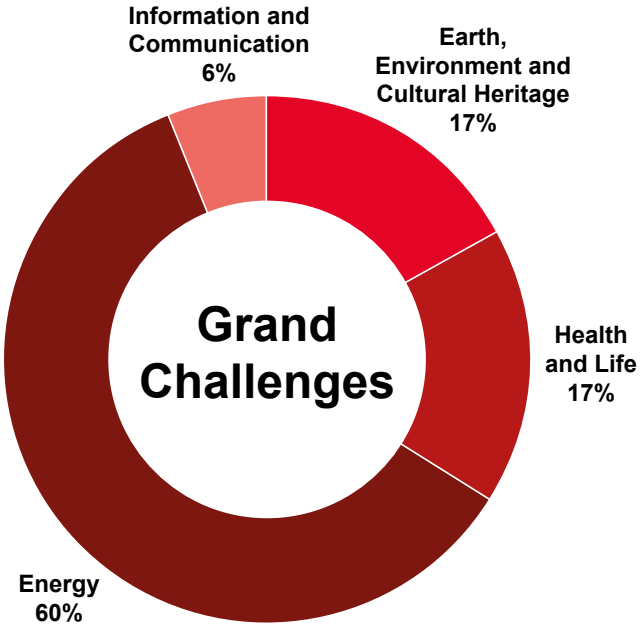

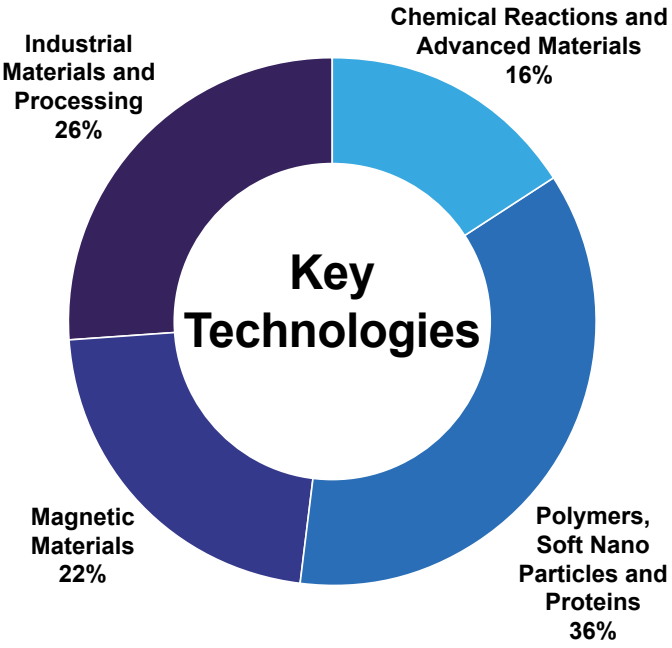

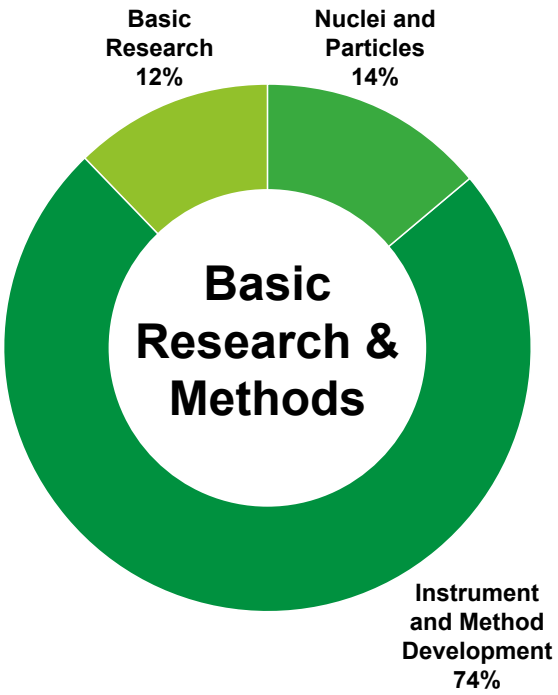

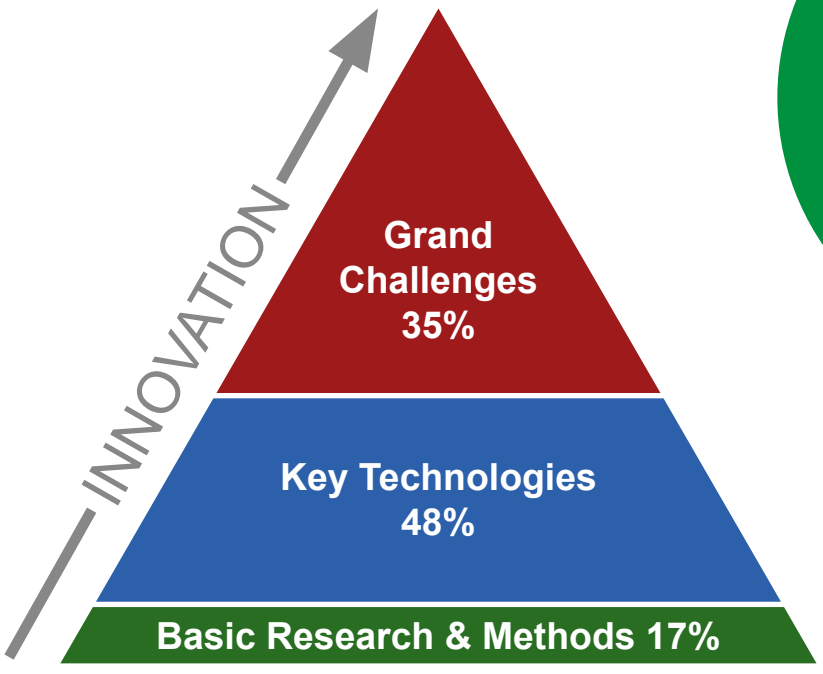

Cover pages

Research by MLZ scientists and at the FRM II made it to the cover pages of several journals in 2024 (see selection below).

A. Mutschke et al.,
The Non-Centrosymmetric Borate Hydride $Sr_4Ba_3(BO_3)_{3.83}H_{2.5}$, Chem. Eur. J. 30(63), e202403048 (2024)
DOI: 10.1002/chem.202403048

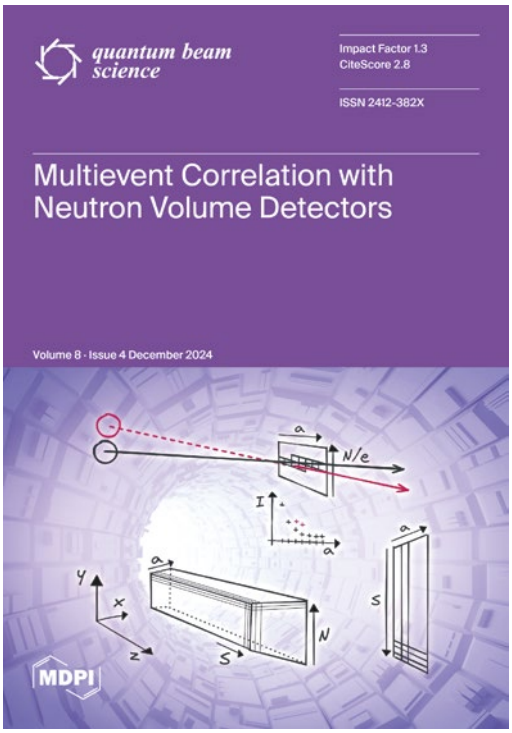

N. Nachtigall et al.,
Multievent Correlation with Neutron Volume Detectors, Quantum Beam Sci. 8(4), 30 (2024)
DOI: 10.3390/qubs8040030

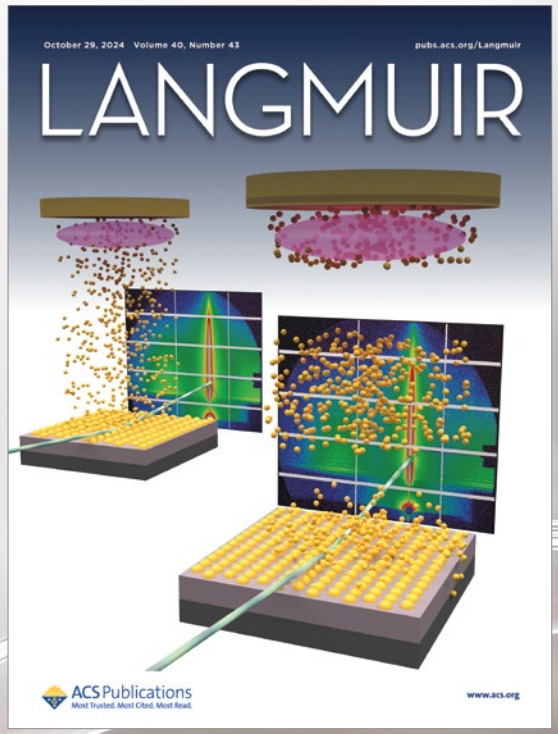

Y. Bulut et al.,
Investigating Gold Deposition with High-Power Impulse Magnetron Sputtering and Direct-Current Magnetron Sputtering on Polystyrene, Poly-4-vinylpyridine, and Polystyrene Sulfonic Acid, Langmuir 40(43), 22591 (2024)
DOI: 10.1021/acs.langmuir.4c02344

Committees

Steering Committee

Chair
Dr. Harald Haakh
Jochen Leyendecker (until autumn, 2024)
Federal Ministry for Education and Research

Members
Albert Berger
Technical University of Munich

Prof. Dr. sc. techn. Gerhard Kramer
Technical University of Munich

Prof. Dr. Astrid Lambrecht
Forschungszentrum Jülich GmbH

Dr. Albert Schmid
Bavarian State Ministry of Science and the Arts

Prof. Dr. Regine Willumeit-Römer
Prof. Dr. Matthias Rehahn (until August, 2024)
Helmholtz-Zentrum hereon GmbH

Guests
Prof. Dr. Christian Pfleiderer
FRM II, Technical University of Munich

Prof. Dr. Martin Müller
Helmholtz-Zentrum hereon GmbH

Prof. Dr. Stephan Förster
Forschungszentrum Jülich GmbH

Dr. Axel Pichlmaier
FRM II, Technical University of Munich

Dr. Jürgen Neuhaus
Robert Rieck (until August, 2024)
FRM II, Technical University of Munich

Dirk Schlotmann
Forschungszentrum Jülich GmbH

Figure 1: Steering Committee meeting in December 2024 with M. Müller, R. Willumeit-Römer, J. Neuhaus, K. Hess, S. Förster, H. Haakh, A. Schmid, A. Berger, C. Pfleiderer, A. Pichlmaier, and G. Kramer (from left to right).

Scientific Advisory Board

Chair
Prof. Dr. Michel Kenzelmann
Paul Scherrer Institute, Villigen

Members
Dr. Ken Andersen
Institut Laue-Langevin, Grenoble

Prof. Dr. Lise Arleth
University of Copenhagen

Prof. Dr. Giovanni Bruno
Bundesanstalt für Materialforschung und -prüfung (BAM)

Prof. Dr. Martin Fertl
Johannes Gutenberg University, Mainz

Dr. Jens Gibmeier
Karlsruhe Institute of Technology (KIT)

Prof. Dr. Thomas Hellweg
Bielefeld University

Prof. Dr. Bernhard Keimer
Max Planck Institute for Solid State Research, Stuttgart

Prof. Dr. Rainer Niewa
University of Stuttgart

Prof. Dr. Julian Oberdisse
Université de Montpellier

Dr. Victoria Garcia Sakai
ISIS Neutron and Muon Source, Didcot

Prof. Dr. Regine v. Klitzing
Technical University of Darmstadt

Figure 2: Scientific Advisory Board meeting in April 2024 with J. Gibmeier, B. Keimer, G. Bruno, J. Oberdisse, L. Arleth, T. Hellweg, V. Garcia Sakai, K. Andersen, M. Müller, and C. Pfleiderer (from left to right).

Figure 3: Instrumentation Advisory Committee meeting in March 2024 with W. Lohstroh, S. Mattauch, H. Rønnow, C. Pappas, B. Keimer, C. Niedermayer, U. Köster, J. Neuhaus, C. Pfleiderer, M. Meven, A. Senyshyn, and F. Ott (from left to right and from bottom to top).

Instrumentation Advisory Committee

Chair
Prof. Dr. Bernhard Keimer
Max Planck Institute for Solid State Research, Stuttgart

Members
Dr. Maria Teresa Fernández-Díaz
Institut Laue-Langevin, Grenoble

Prof. Dr. Ulli Köster
Institut Laue-Langevin, Grenoble

Prof. Dr. Christof Niedermayer
Paul Scherrer Institute, Villigen

Dr. Frédéric Ott
Laboratoire Léon Brillouin, Saclay

Prof. Dr. Catherine Pappas
Delft University of Technology

Prof. Dr. Henrik Rønnow
Ecole Polytechnique Fédérale de Lausanne

Dr. Robin Woracek
European Spallation Source, Lund

MLZ User Committee

Chair
Prof. Dr. Tommy Nylander
Lund University

Members
Dr. Andrea Scotti
RWTH Aachen University

Dr. Jens Gibmeier
Karlsruhe Institute of Technology

Dr. Ana Brás Würschig
University of Cologne

Dr. Sandra Cabeza
Institut Laue-Langevin, Grenoble

Prof. Dr. Holger Kohlmann (Observer on behalf of the KFN)
Leipzig University

Evaluation of beam time proposals: Members of the Review Panels

Dr. Markus Appel
Institut Laue-Langevin, Grenoble

Prof. Dr. Lise Arleth
Niels Bohr Institute
University of Copenhagen

Dr. Mikhail Avdeev
Frank Laboratory of Neutron Physics
Joint Institute for Nuclear Research, Dubna

Prof. Dr. Piero Baglioni
University of Florence

Dr. Luis Fernández Barquín
University of Cantabria, Santander

Prof. Dr. Peter Battle
University of Oxford

Dr. Matthew Blakeley
Institut Laue-Langevin, Grenoble

Dr. Johann Bouchet
Commissariat à l'énergie atomique et
aux énergies alternatives, Arpajon

Dr. Philippe Bourges
Laboratoire Léon Brillouin, Saclay

Prof. Dr. William Brant
Uppsala University

Prof. Dr. Richard Campell
University of Manchester

Dr. Petr Čermák
Charles University, Prague

Dr. Robert Cubitt
Institut Laue-Langevin, Grenoble

Dr. Sabrina Disch
University of Cologne

Dr. Stephan Eijt
Delft University of Technology

Prof. Dr. Ulli Englert
RWTH Aachen University

Prof. Dr. Björn Fåk
Institut Laue-Langevin, Grenoble

Dr. Bela Farago
Institut Laue-Langevin, Grenoble

Prof. Dr. Rafael Omar Ferragut
L-NESS, Como

Dr. Anne-Caroline Genix
Laboratoire Charles Coulomb
Université Montpellier

Dr. Francesco Grazzi
National Research Council of Italy,
Florence Research Area

Dr. Christian Grünzweig
Paul Scherrer Institute, Villigen

Dr. Klaus Habicht
Helmholtz-Zentrum Berlin für
Materialien und Energie

Prof. Dr. Thomas Hellweg
Bielefeld University

Prof. Dr. Paul Henry
ISIS Neutron and Muon Source, Didcot

Dr. Ingo Hoffmann
Institut Laue-Langevin, Grenoble

Dr. Dirk Honecker
ISIS Neutron and Muon Source, Didcot

Dr. Christy Kinane
ISIS Neutron and Muon Source, Didcot

Dr. Joachim Kohlbrecher
Paul Scherrer Institute, Villigen

Dr. Reinhard Kremer
Max Planck Institute for
Solid State Research, Stuttgart

Prof. Dr. Christian Krempaszky
Technical University of Munich, Garching

Prof. Dr. Jeremy Lakey
University of Newcastle

Dr. Reidar Lund
Oslo University

Dr. Sandrine Lyonnard
Commissariat à l'énergie atomique et
aux énergies alternatives, Grenoble

Dr. Nicolas Martin
Laboratoire Léon Brillouin, Saclay

Dr. Gwilherm Nénert
PANalytical B.V., Almelo

Dr. Thomas Nitschke-Pagel
TU Braunschweig

Dr. Esko Oksanen
European Spallation Source, Lund

Prof. Dr. Andrea Orecchini
Università degli Studi di Perugia

Dr. Alessandro Paciaroni
Università degli Studi di Perugia

Prof. Dr. Christine Papadakis
Technical University of Munich, Garching

Dr. Oleg Petrenko
University of Warwick

Dr. Thilo Pirling
Institut Laue-Langevin, Grenoble

Prof. Dr. Radosław Przeniosło
University of Warsaw

Prof. Dr. Diana Lucia Quintero Castro
University of Stavanger

Dr. Navid Qureshi
Institut Laue-Langevin, Grenoble

Dr. Florin Radu
Helmholtz-Zentrum Berlin für
Materialien und Energie

Dr. Sarah Rogers
ISIS Neutron and Muon Source, Didcot

Dr. Emmanuel Schneck
Max Planck Institute of
Colloids and Interfaces, Potsdam

Prof. Dr. Roland Schwab
University of Tübingen

Dr. Romain Sibille
Paul Scherrer Institute, Villigen

Dr. Thorsten Soldner
Institut Laue-Langevin, Grenoble

Prof. Dr. Thomas Sottmann
University of Stuttgart

Dr. Andreas Stark
Helmholtz-Zentrum hereon GmbH

Dr. Johannes Sterba
Atominstitut Wien, TU Wien

Dr. Christopher Stock
University of Edinburgh

Dr. Pavel Strunz
Nuclear Physics Institute, Réz near Prague

Dr. Anne Stunault
Institut Laue-Langevin, Grenoble

Dr. László Szentmiklósi
Hungarian Academy of Sciences, Budapest

Dr. Kristiaan Temst
KU Leuven

Dr. Alexander Tsirlin
Augsburg University

Prof. Dr. Regine von Klitzing
Technical University of Darmstadt

Dr. Oksana Zaharko
Paul Scherer Institut, Villigen

Prof. Dr. Hongbin Zhang
Technical University of Darmstadt

Partner institutions

Bavarian Research Institute of
Experimental Geochemistry and Geophysics
University of Bayreuth
www.bgi.uni-bayreuth.de

Georg-August-Universität Göttingen

- Geoscience Center
  www.uni-goettingen.de/de/125309.html

German Engineering Materials Science Centre GEMS
Helmholtz-Zentrum hereon GmbH
www.hereon.de/central_units/gems/index.php.de

Jülich Centre for Neutron Science JCNS
Forschungszentrum Jülich GmbH
www.fz-juelich.de/de/jcns

Karlsruhe Institute of Technology

- Institute for Applied Materials – Energy Storage Systems (IAM-ESS)
  www.iam.kit.edu/ess/
- KIT Institute for Quantum Materials and Technologies (IQMT)
  www.iqmt.kit.edu/index.php

Ludwig-Maximilians-University

- Faculty of Physics
  www.physik.lmu.de

Max Planck Institute for Solid State Research Stuttgart
www.fkf.mpg.de

RWTH Aachen University

- Institute of Crystallography
  www.ifk.rwth-aachen.de
- Institute of Inorganic Chemistry
  www.iac.rwth-aachen.de

Technische Universität Dresden

- Institute of Solid State and Materials Physics
  www.tu-dresden.de/mn/physik/ifp

Technical University of Munich

TUM School of Natural Sciences

- Chair for Functional Materials
  www.ph.nat.tum.de/functmat/ueber-uns/
- Institute for Hadronic Structure and Fundamental Symmetries
  www.ph.nat.tum.de/e18/home
- Chair of Experimental Physics on the Topology of Correlated Systems
  www.ph.nat.tum.de/en/tcs/home/
- Chair of Precision Measurements at Extreme Conditions
  www.ph.nat.tum.de/e66/home
- Particle Physics at Low Energies
  www.ph.nat.tum.de/ene/home
- Chair of Biomedical Physics
  www.ph.nat.tum.de/en/e17/home

Central Scientific Institution

- RCM – Radiochemie München
  www.rcm.tum.de

Technical University of Munich

- MRI – Klinikum rechts der Isar
  www.mri.tum.de

TECHNISCHE UNIVERSITÄT WIEN
Vienna University of Technology

Vienna University of Technology

- Neutron- and Quantum Physics
  Research area at the Atominstitut Vienna
  Abele Group
  www.tuwien.at/en/phy/ati/neutron-and-quantum-physics

der Bundeswehr Universität München

Universität der Bundeswehr München

- Institute of Applied Physics and Measurement Technology
  www.unibw.de/lrt2

Universität zu Köln

University of Cologne
Faculty of Mathematics and Natural Sciences

- Institute for Nuclear Physics
  https://ikp.uni-koeln.de/
- Institute of Physics II
  https://ph2.uni-koeln.de/

PHYSIKALISCHES INSTITUT
UNIVERSITÄT HEIDELBERG ZUKUNFT SEIT 1386

Universität Heidelberg

- Physikalisches Institut
  www.physi.uni-heidelberg.de/

Imprint

Publisher

Technische Universität München
Forschungs-Neutronenquelle
Heinz Maier-Leibnitz (FRM II)
Lichtenbergstr. 1
85747 Garching
Germany

Phone: +49.89.289.14965
Fax: +49.89.289.14995
Internet: www.mlz-garching.de
www.frm2.tum.de
E-Mail: jahresbericht@frm2.tum.de

Editorial Office, Design and typesetting

Connie Hesse
Simon Habold
Michael Hörmannsdorfer
Christoph Kreileder
Reiner Müller
Björn Pedersen
Robert Schulze (getyourdesign, Berlin)
Sergey Vagin
Andrea Voit

Editors

Henrich Frielinghaus
Robert Georgii
Francesco Guatieri
Markus Hölzel
Michael Hofmann
Olaf Holderer
Johanna Jochum
Martin Meven
Andreas Ostermann
Björn Pedersen
Zsolt Revay
Anatoliy Senyshyn
Nicolas Walte
Marcell Wolf

Photographic credits

Front cover and p. 17	Bernhard Ludewig Editing: Reiner Müller (FRM II)
p. 6	top Yannick Liessem (TUM) bottom left: Astrid Eckert (TUM) bottom 2nd left: Christian Schmid (hereon) bottom 2nd right: Alessandra Schellnegger bottom right: Andreas Heddergott (TUM)
p. 8/9	Bernhard Ludewig
p. 10, 11, 12, 13, 14, 20	created with AI, Chat GPT Editing: Reiner Müller (FRM II),
p. 15	background photo by author, foreground created with AI, Chat GPT
p. 16	Garnar/stock.adobe.com Editing: Reiner Müller (FRM II)
p. 18	Алексей Закиров/stock.adobe.com
p. 19	Foreground: aleciccotelli/stock.adobe.com background: Reiner Müller (FRM II)
p. 21	Sana Baleia/stock.adobe.com Editing: Reiner Müller (FRM II)
p. 22/23	Bernhard Ludewig
p. 60/61	Bernhard Ludewig
p. 67, 2nd from top and bottom right:	Bernhard Ludewig
p. 88, top:	Csengele Hajdu
bottom left:	Michael Hoelzle (Forschungszentrum Jülich)
bottom right:	Bernhard Ludewig
p. 89 top left and middle	Andreas Heddergott (TUM)
top right:	Michael Hoelzle (Forschungszentrum Jülich)
back cover:	Andreas Heddergott (TUM)
p. 104	background: temmuzcan/istockphoto.com

Editors, authors or FRM II/MLZ: other images

MLZ Instrument Suite

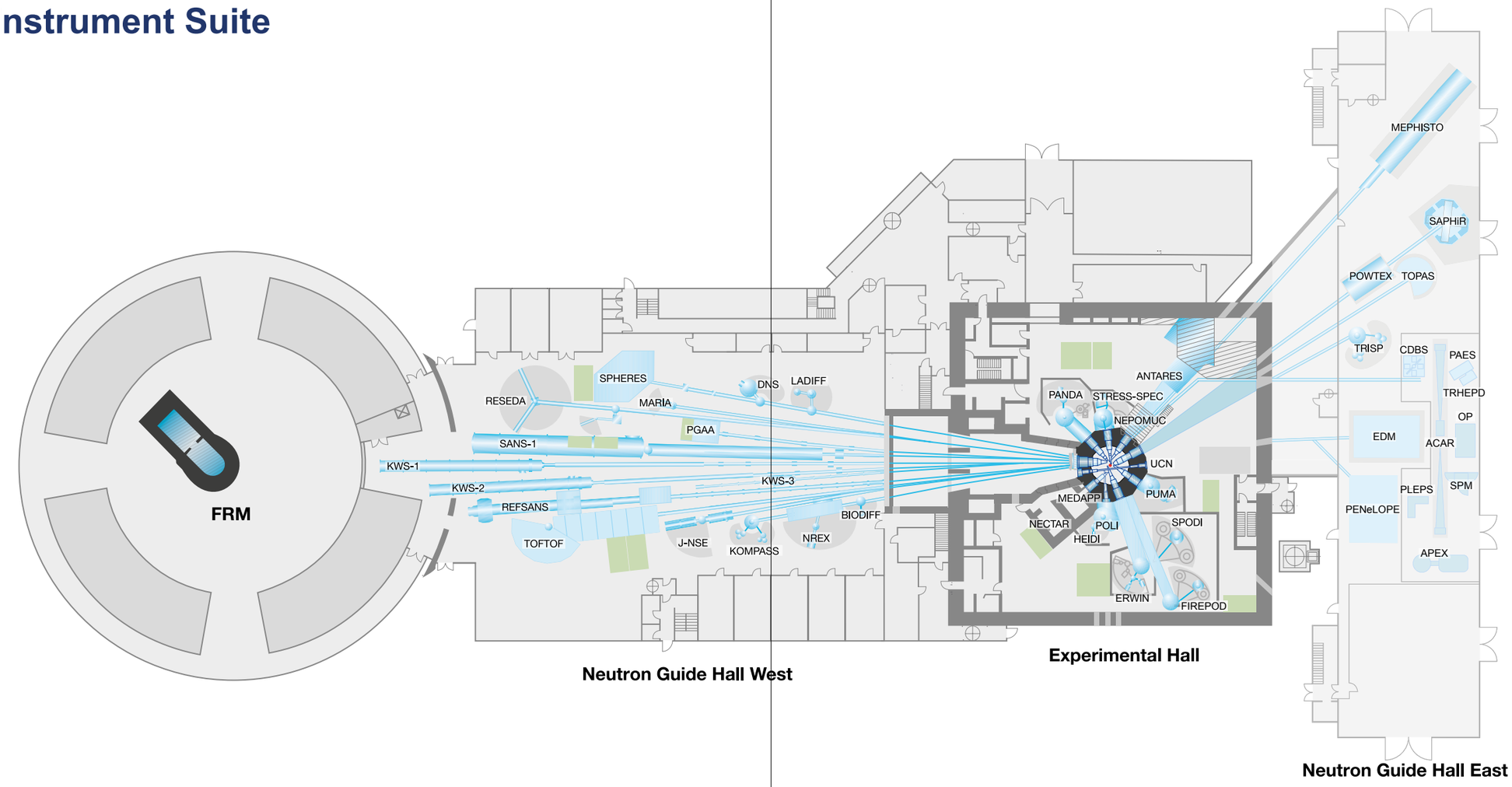

Instrument	Description	Neutrons	Operated by	Funding	Instrument group at MLZ
ANTARES	Radiography and tomography	cold	TUM	TUM	FRM II
BIODIFF	Diffractometer for large unit cells	cold	TUM, JCNS	TUM, FZJ	FRM II, JCNS
DNS	Diffuse scattering spectrometer	cold	JCNS	FZJ	JCNS
ERWIN	Powder diffractometer	thermal	TUM	TUM	FRM II
FIREPOD	Powder diffractometer	thermal	TUM	TUM	FRM II
HEIDI	Single crystal diffractometer	hot	RWTH Aachen	FZJ	JCNS
J-NSE	Spin-echo spectrometer	cold	JCNS	FZJ	JCNS
KOMPASS	Three axes spectrometer	cold	Uni Köln, TUM	ErUM, TUM	FRM II
KWS-1	Small angle scattering	cold	JCNS	FZJ	JCNS
KWS-2	Small angle scattering	cold	JCNS	FZJ	JCNS
KWS-3	Very small angle scattering	cold	JCNS	FZJ	JCNS
LADIFF	High resolution larmor diffraction and inelastic scattering	cold	TUM	TUM	FRM II
MARIA	Magnetic reflectometer	cold	JCNS	FZJ	JCNS
MEPHISTO	Instrument for particle physics, PERC	cold	TUM	TUM, DFG	FRM II
MEDAPP	Medical irradiation treatment	fast	TUM	TUM	FRM II
NECTAR	Radiography and tomography	fast	TUM, GEMS	TUM, Hereon	FRM II, GEMS
NEPOMUC	Positron source, CDBS, PAES, PLEPS, SPM, TRHEPD, OP, ACAR, APEX	-	TUM, UniBw München	TUM	FRM II

*construction
ErUM: instrument construction funded by ErUM-Pro (BMBF)

Instrument	Description	Neutrons	Operated by	Funding	Instrument group at MLZ
NREX	Reflectometer with X-ray option	cold	MPI Stuttgart	MPG	MPI Stuttgart
PANDA	Three axes spectrometer	cold	JCNS, TU Dresden	FZJ	JCNS
PGAA	Prompt gamma activation analysis, Neutron activation analysis (NAA), Neutron depth profiling (NDP)	cold	Uni Köln	TUM	FRM II
PUMA	Three axes spectrometer	thermal	KIT	TUM	FRM II
POLI	Single-crystal diffractometer polarised neutrons	hot	RWTH Aachen	FZJ	JCNS
POWTEX	Time-of-flight diffractometer	thermal	RWTH Aachen, Uni Göttingen, JCNS	ErUM, FZJ	JCNS
REFSANS	Reflectometer	cold	GEMS	Hereon	GEMS
RESEDA	Resonance spin-echo spectrometer	cold	TUM	TUM	FRM II
SANS-1	Small angle scattering	cold	TUM, GEMS	TUM, Hereon	FRM II, GEMS
SAPHIR	Six anvil press for radiography and diffraction	thermal	Uni Bayreuth	TUM	FRM II
SPHERES	Backscattering spectrometer	cold	JCNS	FZJ	JCNS
SPODI	Powder diffractometer	thermal	KIT	TUM	FRM II
STRESS-SPEC	Materials science diffractometer	thermal	TUM, GEMS	TUM, Hereon	FRM II, GEMS
TOFTOF	Time-of-flight spectrometer	cold	TUM	TUM	FRM II
TOPAS	Time-of-flight spectrometer	thermal	JCNS	FZJ	JCNS
TRISP	Three axes spin-echo spectrometer	thermal	MPI Stuttgart	MPG	MPI Stuttgart
UCN*	Ultra cold neutron source, EDM, PENeLOPE	ultra-cold	TUM	TUM, DFG	FRM II

Front page:
The entanglement of the spin and energy of a neutron was measured at the CG-4B polarised beamline at HFIR, USA following initial experiments at RESEDA, MLZ.

Back page:
The MLZ Team in summer 2024.

Heinz Maier-Leibnitz Zentrum (MLZ)
www.mlz-garching.de
DOI: 10.14459/2024md1763028